Addis Ababa University

Addis Ababa Institute of Technology

School of Mechanical and Industrial Engineering

Simulation of the Effect of Aerodynamics on Quadcopter UAV for Precision Agricultural Sowing

A Thesis Submitted to the School of Mechanical and Industrial Engineering of Graduate Studies of Addis Ababa Institute of Technology, Addis Ababa University in Partial Fulfillment for the Degree of Master of Science in Mechanical Engineering (Mechanical Design)

By: Anania Mulugeta

Advisor: Behailu Mamo Zewdie (PhD Candidate)

Addis Ababa, Ethiopia

October, 2023

Addis Ababa University
Addis Ababa Institute of Technology
School of Graduate Studies
School of Mechanical and Industrial Engineering

Simulation of the Effect of Aerodynamics on Quadcopter UAV for Precision Agricultural Sowing

By:
Anania Mulugeta

Approved by Board of Examiners:

Behailu Mamo Zewdie (PhD Candidate)	_____	_____
Advisor	Signature	Date
_____	_____	_____
Internal Examiner	Signature	Date
_____	_____	_____
External Examiner	Signature	Date
Dr. Araya Abera	_____	_____
School Dean	Signature	Date
Dr. Sosina Mengistu	_____	_____
Associate Director for PG Program	Signature	Date

DECLARATION

With all the university's regulations, ethical conducts followed, and all resources that are not original to this work duly acknowledged, I hereby declare that this thesis entitled ''Simulation of the Effect of Aerodynamics on Quadcopter UAV for Precision Agricultural Sowing'' has not been submitted for any of the requirement of master of science degree in mechanical engineering program.

Signature: _____ October, 2023

Name: Anania Mulugeta Date

This is to clarify that the above declaration made by the candidate is correct to the best of my knowledge.

Signature: _____ October, 2023

Advisor Date

Behailu Mamo Zewdie

(PhD Candidate)

ACKNOWLEDGEMENT

I would like to give Glory to God and the Virgin Mary for their permission to start & finish this work. I would like to express my deepest gratitude to my advisor Behailu Mamo Zewdie (PhD Candidate) for his professional guidance and support in preparing follow up and completing this thesis. I also would like to thank the school for collaboration as well. A great gratitude to the staff of AAiT railway excellence center. My supreme thanks also go to my families for their everyday support & prayer.

CONTENTS

ACKNOWLEDGEMENT ii

LIST of TABLES vi

LIST of FIGURES vii

LIST of ABBREVIATIONS x

NOMENCLATURE xii

ABSTRACT xiii

CHAPTER ONE 1

INTRODUCTION 1

1.1. Background 1

1.2. Statement of the problem 6

1.3. Objectives 7

1.3.1. General objective 7

1.3.2. Specific objectives 7

1.4. Scope and limitations of the study 8

1.5. Significance of the study 8

1.6. Organization of the thesis 8

CHAPTER TWO 9

LITERATURE REVIEW 9

2.1. PA and factors affecting PA technology 9

2.2. UAVs in PA & overall agriculture 10

2.3. Major typical seed sowing UAVs as an agricultural application 14

2.4. Flight aerodynamics of UAVs 17

2.5. Effects of weather conditions on the use of UAVs for agriculture 19

2.5.1. The categories of the wind fields 19

2.5.2. Effects of wind field and response stability on the structure of UAVs 20

2.6. Alteration of altitude with weather conditions & their effect on agricultural UAVs 24

2.7. CFD analysis of UAV models 28

CHAPTER THREE 32

MATERIALS AND METHODS 32

3.1. Materials 32

3.2. Methods 32

3.2.1. Conceptual frame work as a methodological procedure 33

3.2.2. Pre-set conditions of research analysis 34

3.2.3. Characterization 35

3.2.4. Data collected for modeling 37

3.2.5. Modeling 40

3.2.6. Hovering stability analysis……...43

3.2.7. Numerical CFD simulation 44

3.2.7.1. Wind flow field axis identification……...45

3.2.7.2. Transient turbulence CFD simulation……..45

3.2.7.3. Dimensions of the flow domain……...46

3.2.7.4. Boundary conditions……48

3.2.7.5. Mesh independent analysis (Mesh optimization)……48

3.2.7.6. Computational model setup mesh generation……..50

3.2.7.7. Simulation……51

CHAPTER FOUR 53

RESULTS AND DISCUSSION 53

4.1. Downwash flow at 0.5 m hovering height and with alteration of altitude 53

4.1.1. Velocity magnitude 53
4.1.2. Pressure distribution 57
4.1.3. Drag coefficients and forces 60
4.1.4. Pressure contour & stability effect 61
4.2. Horizontal wind field at 0.5 m hovering height with alteration of altitude 67
4.2.1. Velocity magnitude 67
4.2.2. Pressure distribution 69
4.2.3. Drag coefficients and forces 71
4.2.4. Pressure contour & stability effect 72
CHAPTER FIVE 79
CONCLUSION AND RECOMMENDATIONS 79
5.1. Conclusion 79
5.2. Recommendations 80
5.3. Future work 80
REFERENCES 81
APPENDICES 88
Appendix A. Plane of symmetry 88
Appendix B. Model for validation 88
Appendix C. Mesh independence 89
Appendix D. Graphics reports 90
Appendix E. Velocity data points 94
Appendix F. Data points of impulse response 101

LIST OF TABLES

Table 1. Feature-based specifications of UAVs. 22

Table 2. Weather conditions recorded during the field trials. 22

Table 3. Weather conditions & aerodynamic parameters of environmental locations. ... 24

Table 4. Spray test and environmental parameters measured. 26

Table 5. Review of wind speed variation with altitude. 27

Table 6. Selection matrix of concept screening. 40

Table 7. Simulation type identification for model 2-A. 45

Table 8. Simulation type identification for model 2-B. 46

Table 9. Simulation type identification for model 2-C. 46

Table D-10. Plot of velocity contour for M2-A & M2-B along downwash wind flow. .. 90

Table D-11. Plot of velocity contour for M2-C along downwash flow 91

Table D-12. Plot of velocity contour for M2-A & M2-B along horizontal wind flow. ... 92

Table D-13. Plot of velocity contour for M2-C along horizontal wind flow 93

Table E-14. Data point of velocity vs position along with wind speeds. 94

Table F-15. Values of time domain rolling moment on M2-C during downwash..... 101

LIST OF FIGURES

Figure 1. Leading drone-related research countries/organizations 1

Figure 2. Expected reach of UAVs in various applications. 2

Figure 3. Typical applications of UAVs in agriculture. 2

Figure 4. 2D representation of the overall research idea. 5

Figure 5. Precision agriculture branched tasks. 10

Figure 6. Typical specific applications of drones. 10

Figure 7. Periodic transitional change of UAVs agricultural applications. 11

Figure 8. Percentage of research on crop production..... 12

Figure 9. Schematic diagram of nozzle installation. 13

Figure 10. Schematic of implemented UAV flight modes..... 13

Figure 11. Overall structure of an aerial seeding system for rapeseed based on a multi-rotor UAV and an air-assisted spray. 14

Figure 12. 3D view of overall assembly of seed sowing octa copter & accepted seeds of various size groups. 15

Figure 13. 3D representation of sowing UAVs..... 16

Figure 14. Potshot seeding drone. 16

Figure 15. Manufactured seed sowing UAVs. 17

Figure 16. Rotary-wing UAVs. 17

Figure 17. The reference frames and momentum principle. 18

Figure 18. Schematics of multi-copter flight mechanism and aerodynamic parameter... 18

Figure 19. Multi-copter flight mechanism. 19

Figure 20. Airspeed definition and wind triangle. 20

Figure 21. Forces acting on a hovering drone in wind..... 20

Figure 22. Wind field distribution along x, y, & z direction for sampling points. 23

Figure 23. Exploited view of sowing UAV research. 25

Figure 24. Image of distribution of droplets under different elevations. 25

Figure 25. Wind speed ranges and variation with altitude. 26

Figure 26. Graph showing linear relation height has with wind velocity. 27

Figure 27. Flow domain boundary condition of wind analysis on UAV in buildings. 28

Figure 28. Mesh and downwash CFD view of UAVs. 28

Figure 29. A UAV model aerodynamically analyzed at 0^0 29

Figure 30. Velocity distribution locations of downwash flow. 30

Figure 31. Research flow chart. 33

Figure 32. Representation of an environment. 34

Figure 33. 2D Illustration of the assumed wind analysis on UAV. 34

Figure 34. Tasks clarified for the concepts to be selected. 36

Figure 35. Representation of sample sown area. 37

Figure 36. Measurement of the 100 grains at AAiT chemical laboratory. 38

Figure 37. Schematic representation of rectangular solid frame with elliptical hopper. . 41

Figure 38. Schematic representation of crossed helical frame with elliptical hopper. 41

Figure 39. Schematic representation of mobius ring frame with elliptical hopper. 42

Figure 40. Representation of moment coefficients alteration due to wind flow. 43

Figure 41. CFD analysis flowchart 44

Figure 42. Fluid domain axis and symmetry plane identification. 45

Figure 43. Fluid domain boundary condition along horizontal & downwash flow. 47

Figure 44. Mesh metrics graph in terms of number of elements for M2-A. 49

Figure 45. Mesh metrics graph in terms of number of elements for M2-B. 49

Figure 46. Mesh metrics graph in terms of number of elements for M2-C. 50

Figure 47. Fluid domain mesh generated image of variants along horizontal and downwash flow axis. 51

Figure 48. Velocity magnitude with respect to position for all models. 55

Figure 49. Models compiled plot of velocity magnitude vs position at variable wind speeds. 56

Figure 50. Pressure with respect to position for all models. 58

Figure 51. Models compiled plot of pressure vs position at variable wind speeds. 59

Figure 52. Drag force and coefficients with respect to variable wind speed. 60

Figure 53. Contour plot and impulse response of model 2-A along downwash flow..... 62

Figure 54. Contour plot and impulse response of model 2-B along downwash flow..... 64

Figure 55. Contour plot and impulse response of model 2-C along downwash flow..... 66

Figure 56. Plots of velocity magnitude for three models along horizontal wind flow. ... 68

Figure 57. Plots of pressure magnitude for three models along horizontal wind flow. ... 70

Figure 58. Drag force and coefficient relative to wind speed variation. 71

Figure 59. Contour plot and impulse response of model 2-A along horizontal flow. 73

Figure 60. Contour plot and impulse response of model 2-B along horizontal flow..... 75

Figure 61. Contour plot and impulse response of model 2-C along Horizontal flow..... 77

Figure A 62. Representation of symmetries of the models in terms of planes. 88

Figure B 63. Schematic representation of external model. 88

Figure C 64. Captured images of skewness metrics of all models. 89

LIST OF ABBREVIATIONS

2D	A Two Dimensional
3D CAD	A Tridimensional Computer Aided Design
A/R	Afforestation and Reforestation
AAiT	Addis Ababa Institute of Technology
ADLI	Agricultural Development Led Industrialization
ANRC	American National Research Council
API	Application Programming Interface
AVT-161	A computational method determining a task group in NATO
CA	Controlled Agriculture
CAD	Computer Aided Design
CFD	Computational Fluid Dynamics
DJI	Da-Jiang Innovations
EIAR	Ethiopian Institute of Agricultural Research
GIS	Geographic Information System
IMU	Inertial Measure Unit
KPI	Key Parameter Indicator
PA	Precision Agriculture
PAM-20	Unique name of large range UAV type
PEEK	Poly-Ether-Ether-Ketone
PID	Process Identifier
PWM	Pulse Width Modulation
RANS	Rynolds Average Navier Stock
SACCON	Name derived from Floriano Saccon’s
SDGs	Sustainable Development Goals
TTA	TT Aviation Technology Co. Ltd of Beijing
UAM	Unmanned Aerial Mobility
UAV	Unmanned Aerial/Automated Airborne Vehicle
UAVs	Unmanned Aerial/Automated Airborne Vehicles
UAVsSS	Unmanned Aerial Vehicles Supported Seed Sowing

USA	United States of America
UCAV	Unmanned Configured Aerial Vehicle
VTOLs	Vertical Take-off & Landings
WDM	Unique Name of Granular Carrier and Seeder Drone

NOMENCLATURE

R_c	Characteristic length
M2-B	Crossed helical frame with elliptical hopper
$\underline{\rho}$	Density of air
ρ_p	Density of payload
Cd	Drag coefficient
F_d	Drag force
μ	Dynamic viscosity of air
M2-C	Mobius ring frame with elliptical hopper
m	Payload total mass
cm	Pitch moment coefficient
M2-A	Rectangular solid frame with elliptical hopper
R_e	Reynolds number
$\underline{\Omega}$	Rotor angular velocity
cl	Rolling moment coefficient
${v_w}^2$	Square of wind speed
A	Surface area of the object
v	Total volume
X	Unknown variable in grams
W_{frame}	Weight of the frame
W_p	Weight of the payload
v_w	Wind speed
cn	Yaw moment coefficient

ABSTRACT

Nowadays, agricultural aerial vehicles are being broadly applied at the focal point of the farming development. Where crop damage rate raised by 1 % without mechanization at sown area, wind was one of the negative factors to utilization of UAVs for this purpose. This research was directed with the objective of characterizing three quadcopter UAV models and numerical CFD analysis of the models to study the aerodynamic behavior and stability analysis for precise agricultural sowing application. Implementing the finite volumetric analysis using Rynolds Average Navier Stock method, Ansys was used to simulate the fluid flow simulation along the identified horizontal and downwash wind fields for wind speed ranges of 0.3 m/s, 0.6 m/s, 0.9 m/s, and 1.2 m/s, 2.5 m/s considered in case of altitude increase. The objective parameters were velocity magnitude, pressure distribution, drag force, drag coefficient and moment coefficients. Findings of drag coefficients of rectangular solid, crossed helical, mobius ring all with elliptical hopper were 0.274, 1.29, 2.5 respectively, for downwash flow and 1.5, 2.6, 3.7 respectively, for horizontal flow during 2.5 m/s wind flow. Instability in terms of impulse response were more pronounced on mobius ring with elliptical hopper at 2.5 m/s wind gust while rectangular solid with elliptical hopper had revealed a desirable minimum drag coefficient and stability condition on moment coefficients for both flow cases as compared to the other models. In conclusion, shape effects had been observed on the variation of drag and stability values particularly on mobius ring with elliptical hopper.

Key Words: Aerodynamic, Precise agriculture, Sowing, Quadcopter UAV, Wind gust

CHAPTER ONE

INTRODUCTION

1.1. Background

Agriculture is an extensive area which plays a significant role in humans' life. It comprises of wide area sectors under it to increase productivity while reducing initial production costs. It is a reality that there is a replacement of huge and environmentally emissive land and air vehicles with unmanned aerial vehicles (UAVs). Agricultural aerial vehicles are being broadly applied at the focal point of the farming development. Productivity i.e., obtaining an optimal product from a well-controlled agricultural input process is a valuable issue in our day-to-day life. Noticeably, 1, 2, 3 & 15 of the 17 sustainable development goals (SDGs) promote the precision agriculture and productivity (Mondejar et al., 2021). Ever since mankind's evolvement in using tools to smoothen their lifestyle, there has been lots of innovations to advance the agricultural sector. The mechanization includes modification or innovation of agricultural machineries. When it comes to country specific researches, agricultural mechanization through the use of UAVs has been widely studied and implemented in USA, China, India and Italy among top lists (Rejeb et al., 2022) in response to the growth of the agricultural sector.

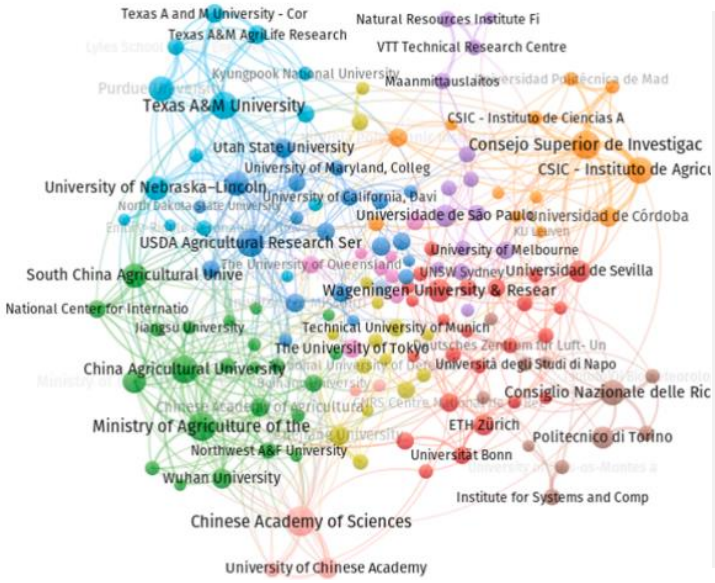

Rank	Countries
1	USA
2	China
3	India
4	Italy
5	Spain
6	Germany
7	Brazil
8	Australia
9	Japan
10	United Kingdom
Rank	**Organizations**
1	Chinese Academy of Sciences
2	Ministry of Agriculture of China
3	Consejo Superior de Investigaciones Científicas
4	Texas A&M University
5	China Agricultural University
6	USDA Agricultural Research Service
7	CSIC - Instituto de Agricultura Sostenible IAS
8	Purdue University
9	Consiglio Nazionale dell Ricerche
10	South China Agricultural University

Figure 1. Leading drone-related research countries/organizations (Rejeb et al., 2022)

.

In definition, Unmanned aerial vehicles (UAVs), also known as drones, refer to flying objects that can be operated through a remote control or can perform autonomous flight without a pilot (Lee et al., 2021). There are varieties of UAVs implemented for varieties of applications including agriculture as summarized in a pie chart below(Ahmed et al., 2022).

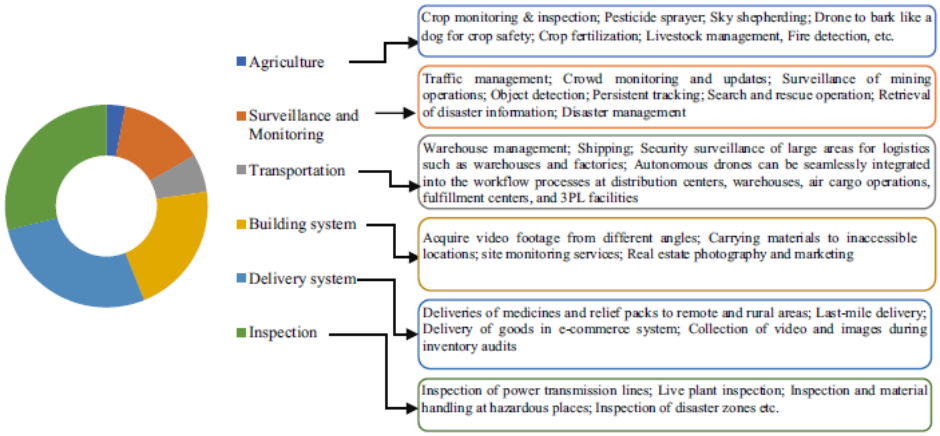

Figure 2. Expected reach of UAVs in various applications (Ahmed et al., 2022).

A compilation of branches of applications implemented under agriculture as a whole is shown in the figure below. It can be seen that usage of latest technologies and devices is making the sector more interactive. one of the contributions is from unmanned aerial vehicles.

Figure 3. Typical applications of UAVs in agriculture (Zhang & Kovacs, 2012).

.

As per the outline of (Mohan et al., 2021) if done properly, unmanned aerial vehicle-supported seed sowing (UAVsSS) can aid to afforestation in naturally friendly, swift and in a safe way including in unsafe territories and can support overall manual planting efforts.

From (Gezahegn, 2019)'s paper it was found that, as plant thinness increases, the side competition between plants becomes serious, affecting the growth and development of every single plant. Furthermore, the way that by widening their roots, number of their branch's lowers. This is on the base that there are more closeness & supplies for vegetative development near to branches, which energizes precise cultivation. According to (Delavarpour et al., 2021), with awareness, preferable options, the appropriate expenses and opportunities, precision will add value in agriculture.

According to (Kim et al., 2019), agricultural robots particularly, unmanned aerial vehicles have been and will be highly decreasing the working hours, increasing productivity, stability and measurement precisions, which makes them lie at the hub of smart agriculture.

According to (Chamola et al., 2021) survey result, it is being visible that UAVs are nowadays practically applied in agriculture faster. Besides, due to their lower investment costs, environmentally friendly, optimized size and smartness, they are now preferable as compared to conventional agricultural machineries. Tasks of seed, pesticide, fertilizer spraying weed mapping, crop monitoring are more preferably performed by UAVs which indirectly reduces human resources (Felismina et al., 2017a).

To use UAVs for a certain application, knowing their attributes and configuration is important. Apart from that, the user should have a clear picture of energy utilization, simplicity of flying, wind security and topographies to pick the finest UAV for that purpose. More importantly, prior notice of unpredictable elements like temperature (T^0) and wind disturbances is necessary (Delavarpour et al., 2021).

Imperatively aerial spraying is affected by wind field (Chen et al., 2017). The compiled review of the scientists was to measure wake propagation that the wind creates underneath a uniaxial single-rotor automatic helicopter. Meaning that the uncovered wake propagation may have a certain effect on droplet depositions.

Wind fields can suddenly and unexpectedly change, making control more challenging and compromising flight safety. An energy transfer occurs when the wind affects a drone's flight path and transfers energy to the drone (Gianfelice et al., 2022). A quadrotor faces wind drag when it is hovering at an area in space, which causes the quadrotor to shift (Abichandani et al., 2020).

As stated by (Diaz & Yoon, 2018), for strong wind velocities, it becomes difficult to manage vehicle flights. This study also highlighted the implication of measuring the effects of weather on small quadcopters as well as on large aerial vehicles like Urban Air Mobility. In order for UAM to be practicable, the vehicles must be vigorous enough to be able to safely hover over our environment.

Widening the scope, in extremely inconsistent wind conditions, insects can fly (Olejnik et al., 2022). A study on CFD models of fruit flies was done by the researchers, which then confirmed their findings with free flight tests of a small air vehicle. Due to the insect's low inertia and high wind gusts, the animal can experience linear and angular accelerations (Engels et al., 2019). Many insects continue to fly in windy circumstances, despite the negative impact of winds on their ability to control their flight (Leitch et al., 2021).

More importantly, multi-copters can hover, which makes them preferable for doing a particular jobs while remaining stationary which permits them to maintain a constant altitude in the air (Lee et al., 2021). Therefore, hover mode aerodynamic stability is essential for the safety and overall functionality of the drone, particularly when precise operations such as drop deposition or delivery is needed. Empathetic to these, a numerical study was conducted for examining and identifying three model variants of quadcopter type drone frame structure with corresponding parameters when exposed to a certain level of wind gust on operation during hovering. A firm characterization & modeling procedures such as; a concept screening with leveling and selection matrix or

trade of study was exercised to find out the suitable combination to be exported for a numerical CFD stability analysis and standard input parameters. It then followed a stability numerical CFD with simulation type of fluid flow (fluent) with wind/an air flow over the body from (x, y) axis (sideways, downwash). There are out put variables such as longitudinal and lateral stability in terms of pitch, yaw and roll angles for the stability analysis, pressure distribution, velocity contour, drag coefficient (Cd) and drag force (Fd) that are recorded from the CFD simulation to specify the spot necessary for interpretation.

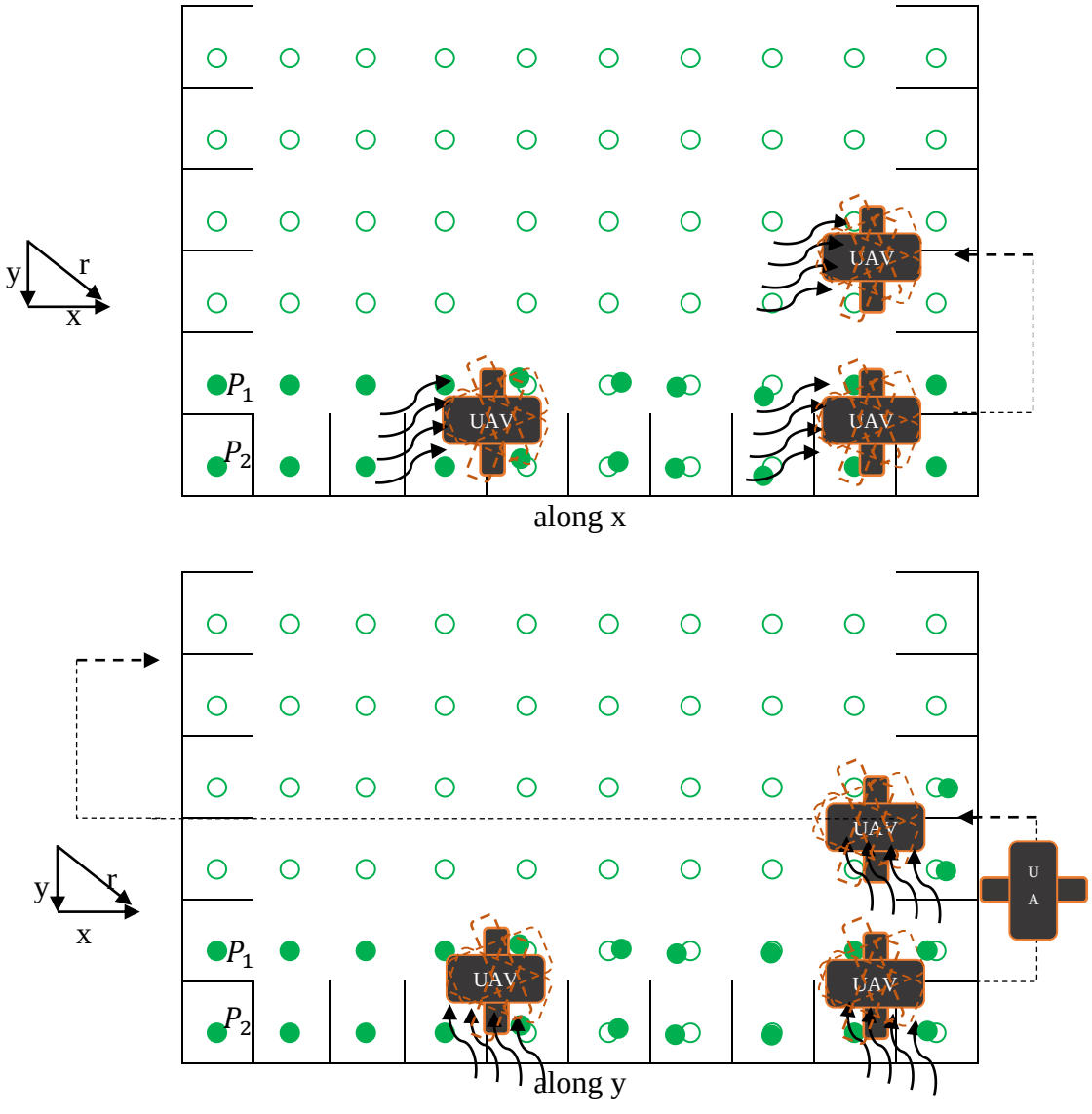

[P1, P2- crop droplet points] [(x), (y)- Wind gusts] [- - - Motion path of UAV]

Figure 4. 2D representation of the overall research idea.

This all-research design is then conducted with the purpose of brightening the possibility of enhancing an unmanned aerial vehicle for precision sowing efficient product to be used in agricultural technologies when the world is striving for advanced technology for fastest growing in the areas of agricultural technology, in particular, use of UAVs for agricultural productivity.

1.2. Statement of the problem

Crop productivity is a core point in lives beyond agricultural aspects. As per Technology Multiplication & Seed Research and Agricultural Mechanization Research under EIAR, Ethiopia, doing research in increasing crop production through mechanizing agriculture is an asset. In variable scale production, these missed droplets will lead to lose of productivity and economic decline (seed economics) (Brar et al., 2017).

In relation to agricultural mechanization researches, (X. Liu & Li, 2023) magnified the effects of utilization of mechanized machinery for grain crop production of rice, wheat and maize. As per the scholars' findings, the influence rate of machinery service utilization on the three-grain crop productivity is by 0.0059, 0.0148 and 0.0607 respectively. While without utilization, where farmers/labor use, crop damage rate rises by 1 %. On the scholars' paper, crop damage is indicated as grain affected area/grain sown area.

Seeds to be sown using row crop vegetation need precision to drop the seeds to the ground to efficiently perform, reduce input cost and hence reduce loss of productivity (Brar et al., 2017). One of the factors which is expected to affect a UAV developed for this purpose (hinders to keep precision) is wind disturbance.

UAVs are typically more vulnerable to wind disturbance (Delavarpour et al., 2021) although they are flying at low altitude, considerably small payload, optimum size and leisurelier soaring speeds than manned air vehicles (Diwate et al., 2018). All types of wind disturbance, from minor turbulence to typhoons, will impact UAVs to varying degrees. This case control is difficult and potentially puts flight safety at risk due to air movement disruption (Wang et al., 2019) during both hovering or forward flight (Lei & Wang, 2020).

Considering untouched work on the study of UAVs for row crop sowing & weather impact on it that hinders to achieve PA. Researches made by three researchers (Felismina et al., 2017a, 2017b; Lysych et al., 2021) however, made a close research on the effect of aerodynamics on the body of a UAV without touching the wind guest the assembly might have with the environment, the geometry variants and wind speed ranges with orientation.

It is significant that analyzing varieties of geometries with parameters and studying the effect with varying wind speed is expected to bring an acceptable result. While in operation, the body is subjected to wind disturbance resulting in missing the target to drop the seed in the specific hole which results in decrease of productivity.

This problem identified is expected to affect the areas where seeds such as maize, wheat, beans, peas, soybeans…etc. crops grow. This instability case was parametrized by effects or changes in pressure distribution, drag force, drag coefficients and moment coefficients.

1.3. Objectives

1.3.1. General objective

The main objective of the study is to simulate the effect of aerodynamics on quadcopter UAV for precision agricultural sowing

1.3.2. Specific objectives

The subsequent specific objectives are set to answer the research questions & achieve the main objective.

- Study shape contribution of geometric variants.
- Simulation of horizontal and downwash wind flow of model variants for five variable wind speeds and plot pressure distribution, velocity magnitude, drag force, drag coefficient and moment coefficients.
- Interpret the optimum UAV profile based on numerical analysis result.

1.4. Scope and limitations of the study

Concept development, characterization, modeling, conducting CFD simulation along x and y flow field & investigating the pressure distribution, velocity magnitude, the drag force & coefficients, and moment coefficients were under the scope. The rotor & analytical aerodynamic analysis, structural mechanics and wind field along z were not studied. There also was a limit in studying particle flow simulation and the deposition drift. A limitation on analysis of weight of seeds by variable mass system.

1.5. Significance of the study

Significantly, it is an addition to agricultural sectors as an input source for agricultural technology development, multiplication, seed and agricultural mechanization research under EIAR, Ethiopia. It is an addition to the farmers to use the product for their productivity, to researchers including alumni's of AAiT who are interested in this area. And to a great extent, the author will be upgraded with a knew knowledge of research development. A paper with an area under ADLI being made in AAiT will also be an asset for the university.

1.6. Organization of the thesis

Chapter one describes the base background/introduction of the research with the inclusion of the problem that led to define this research and objectives set with some sort of scope & limitations. Under chapter two, the compilation of peer reviewed articles and references in relation with this research area has been presented. Chapter three depicts the materials used for the research and the wide methodologies such as characterization, modeling and numerical simulations implemented. Chapter four is comprised of results and discussion. This chapter outlines the findings from the previous chapter analysis and a brief discussion of the results obtained. The final chapter is conclusion and recommendations, which explains the compiled statement of the output of the paper from authors finding relating with previous references and the authors recommendations for the readers. Finally, the references and supplementary appendices has been included.

CHAPTER TWO

LITERATURE REVIEW

2.1. PA and factors affecting PA technology

As (EIAR, 2003) explained these days, the developed world is on precision agriculture, where site-specific agricultural conditions are monitored and inputs like seeds, fertilizer, herbicide and other amendments are metered and delivered on the spot. The agricultural mechanization, food science and post-harvest research program generate technologies, which create the environment for the biological inputs to perform to their optimum potential.

Although there is a decreased number of educated and knowledgeable farmers, (Teklewold et al., 2012) claims that adopting technologies by farmers still results in extremely significant improvements. When it comes to maize yield, the national average is around 25 q/ha, whereas farmers that use enhanced varieties and mechanization typically receive above 50 q/ha.

From (Results of Agricultural Machinery and Post-Harvest Engineering Research, 2018), the lack of appropriate implements to seed at the right depth with minimum soil disturbance is recognized as one of the major constraints faced by African smallholders on adopting controlled agriculture (CA). According to the research, cereal crops are seeded through broadcasting, which is one of the factors restricting on-farm productivity and when regarded nationwide, requires more seed.

This time, multirotor and fixed-wing UAVs are increasingly being used for precision agriculture. Particularly, multi-rotor UAVs are used for extremely precise tasks, such as precision regulator (Kim et al., 2019).

A recent study conducted by (Nowak, 2021) boldly described precision agriculture (PA) as an all-inclusive administrative concept which relies on dedicated material/data collection input and processing to enhance sustainability, efficiency and productivity of agricultural operations with battered activities.

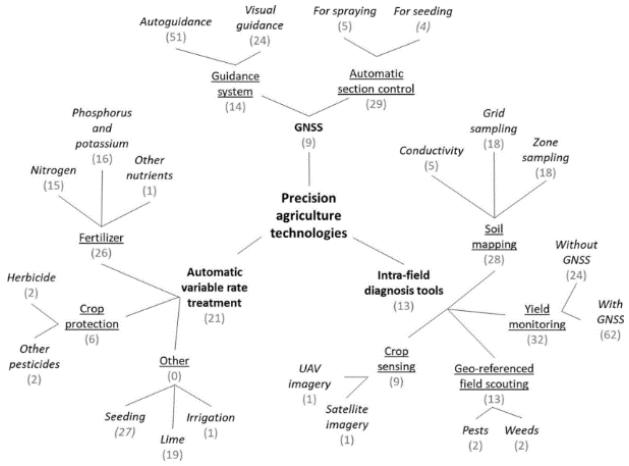

Figure 5. Precision agriculture branched tasks (Nowak, 2021).

2.2. UAVs in PA & overall agriculture

Some of the major agricultural activities that can be performed by UAVs includes crop monitoring, crop planting, livestock management, crop spraying, irrigation, and mapping. Among agricultural specific applications, recent researchers (Hafeez et al., 2023; Tewari, 2023) compiled and presented classifications of them into actions in an image.

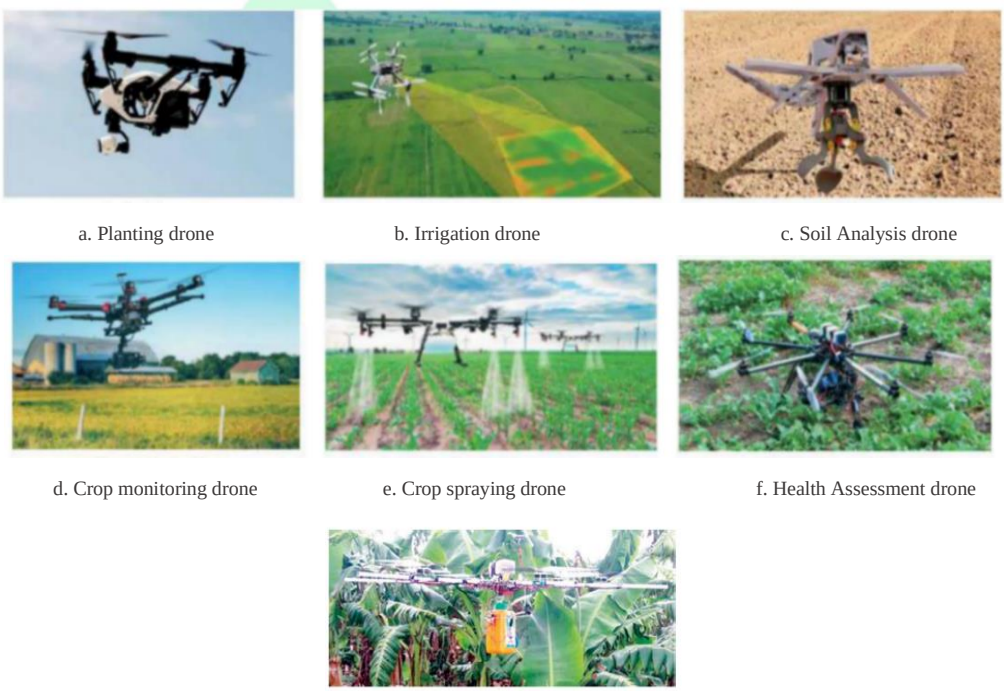

a. Planting drone b. Irrigation drone c. Soil Analysis drone

d. Crop monitoring drone e. Crop spraying drone f. Health Assessment drone

g. Pesticide spraying drone

Figure 6. Typical specific applications of drones (Hafeez et al., 2023; Tewari, 2023).

Some of the biggest problems in farming include ineffective crop monitoring systems and the unpredictable weather conditions make monitoring more difficult, increase risk of production. The farmer can resolve some of these obstacles with the aid of an agricultural UAV. One benefit of UAVs in agriculture is the indicated shorter trip path, as well as time and labor savings. Additionally, the information gathered by UAVs is helpful for planning seed planting patterns and early soil analyses (Yinka-Banjo & Ajayi, 2020).

As (Rejeb et al., 2022) presented, the evolution of UAVs for precision agriculture was seen in two periods. The fact that it rose from 5th to 2nd place in the 2nd period shows how crucial drones are to achieving precision agriculture as a whole. They can make monitoring, detection, and estimation practices faster, cheaper, and easier in comparison with other remote-sensing and ground-based systems.

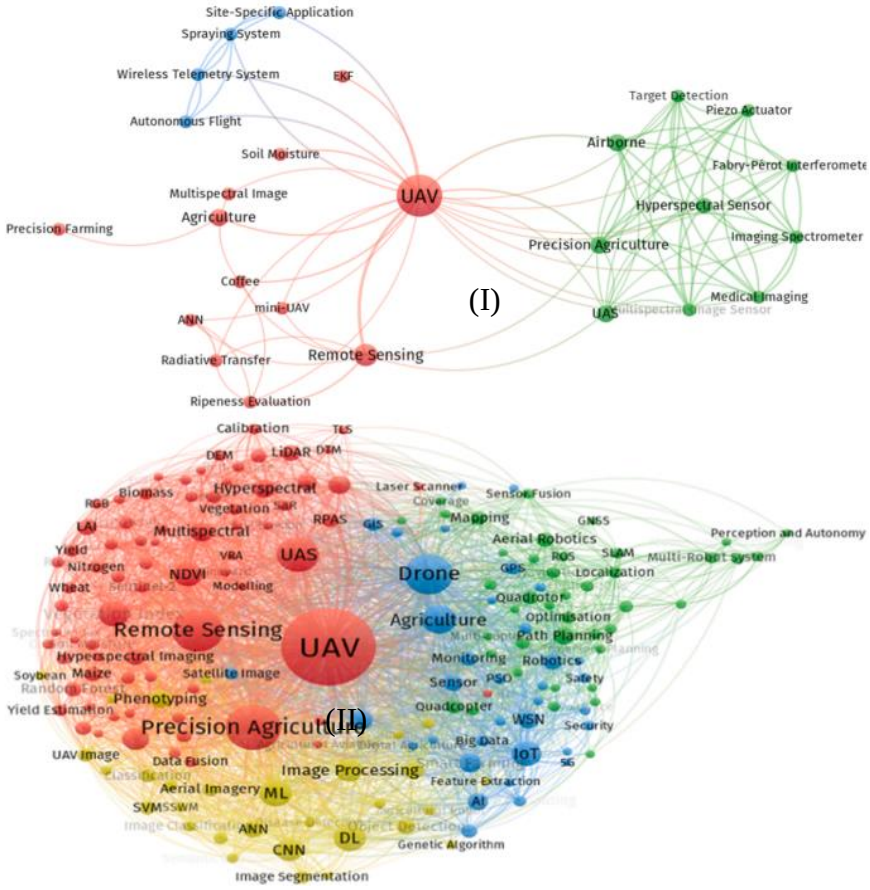

Figure 7. Periodic transitional change of UAVs agricultural applications.
(a). Keyword co-occurrence networks for the period 1990–2010. (b). Keyword co-occurrence networks for the period 2011–2021 (Rejeb et al., 2022).

Drones have discovered a number of useful applications in agriculture, including farm analysis, time savings, greater agricultural productivity, Geographic Information System (GIS) mapping integration, and imaging of crop health status (Zhang & Kovacs, 2012). According to the scholars, in the future, farmers will be able to plant their crops utilizing drone-planting systems thanks to the development of agriculture technology for crop handling and monitoring. As it will be simple to directly implant the seed into the chosen soil region in a field, this will lower the labor cost.

The study of (Yatribi, 2020) included a section on using UAVs in agriculture. More than 150 peer-reviewed articles have been written about its use throughout more than six different application sectors, including agriculture. According to research by (Atiqah BADALUDDIN et al., 2020), the numbers gathered, shown as a pie chart, support the research's decision to focus on the bigger percentage, or roughly 60%, of agricultural activities that involve spraying.

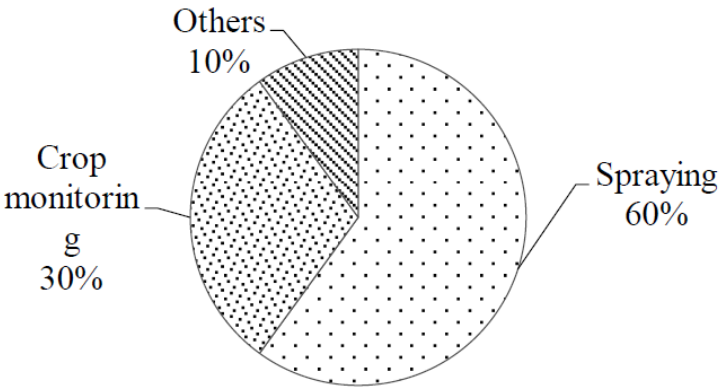

Figure 8. Percentage of research on crop production (Atiqah BADALUDDIN et al., 2020).

In a 40 m × 60 m experimental field with mature rice chosen as the test crop, (Wen et al., 2018) conducted research on UAVs for variable spray systems using PWM & PID controls. The target area was cut into 10 m × 10 m-sized pieces. The drone was constructed with a PWM control system to droplet pesticides on to the chosen test crops in accordance with a path and orientation as shown in the picture below. The dose was set to five different levels, and the flight speed of the drone was stabilized with 5 m/s.

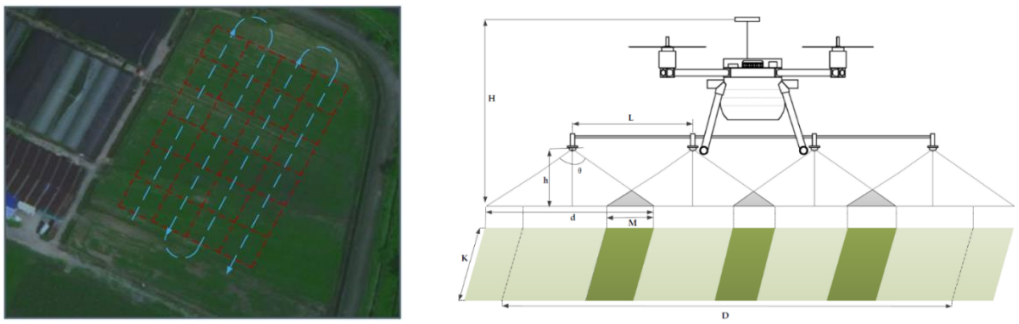

h - height of the nozzle from the top of the crop in m; M - width of the overlap area of the adjacent nozzles in m; D - effective spray width of the drone in m.

Figure 9. Schematic diagram of nozzle installation (Wen et al., 2018).

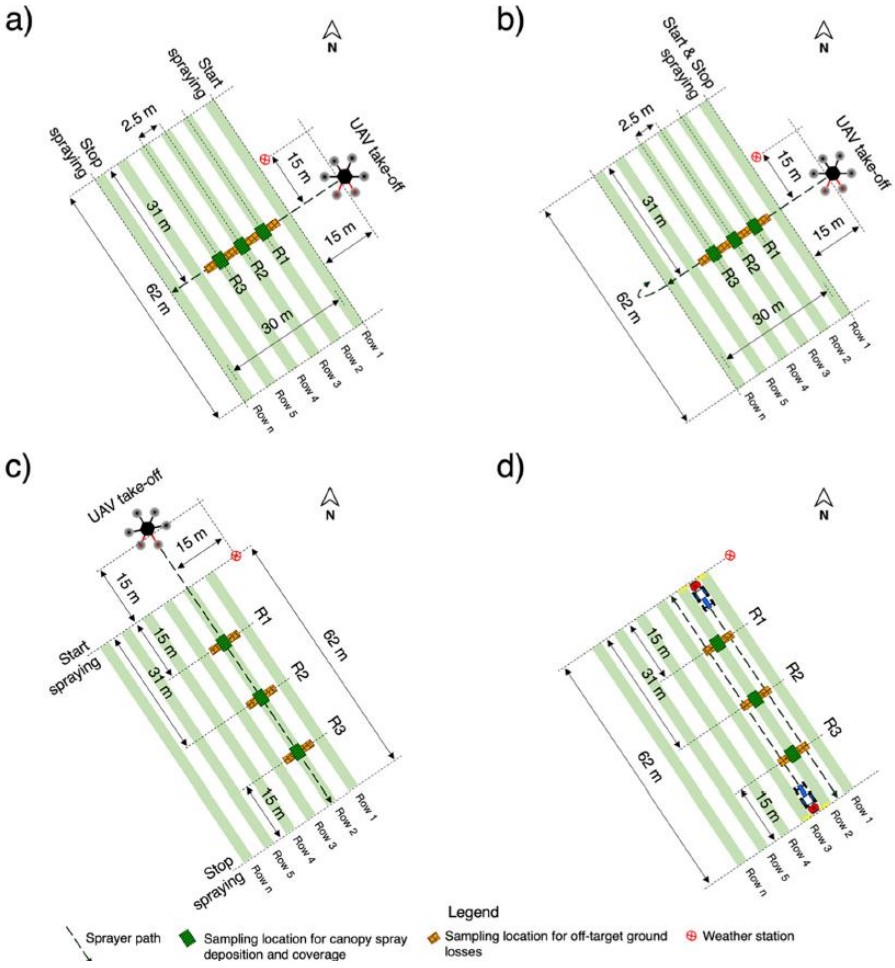

a) 1way broadcast), b) 2-way broadcast, c) 1-way band, d) reference spray technique.

Figure 10. Schematic of implemented UAV flight modes (Biglia et al., 2022).

A supportive study by (Biglia et al., 2022) in figure 10 depicted the optimum path to be followed for spraying operation of a UAV on a vineyard. The adopted spraying nozzles were selected according to the three planned flight modes, and six different types of nozzles were used. The 1-way band and 2-way broadcast trials were respectively used to target the spray.

Before and after the operation of seeding, the soil should be cultivated by automatic machines such as tractors and the seed holes need to be top covered (top dressed) respectively. For this, in order to assist the operating time, labor & farming management as a whole, (Qi et al., 2022) proposed the top-dressing system as a UAV broadcast's feeding port, the caliber was installed to do the dressing. A grasping mechanism such as designed by (Deployable et al., 2017) which can be mounted on to the drone so that the top dressing can be performed.

2.3. Major typical seed sowing UAVs as an agricultural application

(Huang et al., 2020) used a commercial six-rotor agricultural UAV model for seed sowing agricultural application. The whole system was composed of three main modules: aircraft, seed supply module, seed distributing and guiding module. The seeds accelerated under the airflow and divided into several rows by the distributor. The seeds continue to go through the hose and hard tube in each row before falling from the seeding tube and landing on the field.

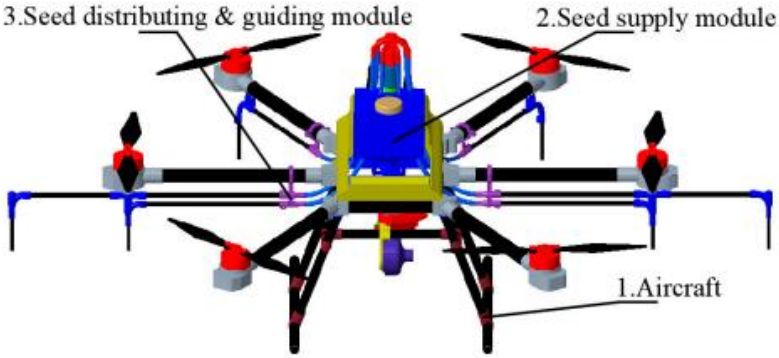

Figure 11. Overall structure of an aerial seeding system for rapeseed based on a multi-rotor UAV and an air-assisted spray (Huang et al., 2020).

(Lysych et al., 2021) also developed a set of sowing devices intended for use with UAVs. It can sow bulk seeds such as maize & beans having a mass of 0.127 - 0.280 kg. in parallel with this research concept, (Zhou et al., 2020) has proposed five different shapes of maize from the nine varieties on different wide locations and the particles are modeled and analyzed numerically using the discrete element method to study the interaction between the seed and sowing machine. (Zdancevic, 2015) also studied the shape of the actual maize seed and analyzed the discrete element method. Both the later scholars tried to model the seed particle shape using software with the extent of accuracy.

(a)- small sized (b)- medium sized (c)- large sized seeds

Figure 12. 3D view of overall assembly of seed sowing octa copter & accepted seeds of various size groups (Lysych et al., 2021).

(Berner, 2020) presented two types of UAVs applied for agricultural sowing applications. One was the Chinese company TTA Aviation in Beijing, which had equipment for seeding and distributing granular fertilizer that worked with drones. The second, grain Flyer 3 WDM 8-20, was a rotor-based machine that was designed to carry out many tasks along with the additional replacement equipment that was to be mounted on it in the field figure 13. The granulated sowing operation having a size of $\leq$ 8 mm is done at a variable height as needed.

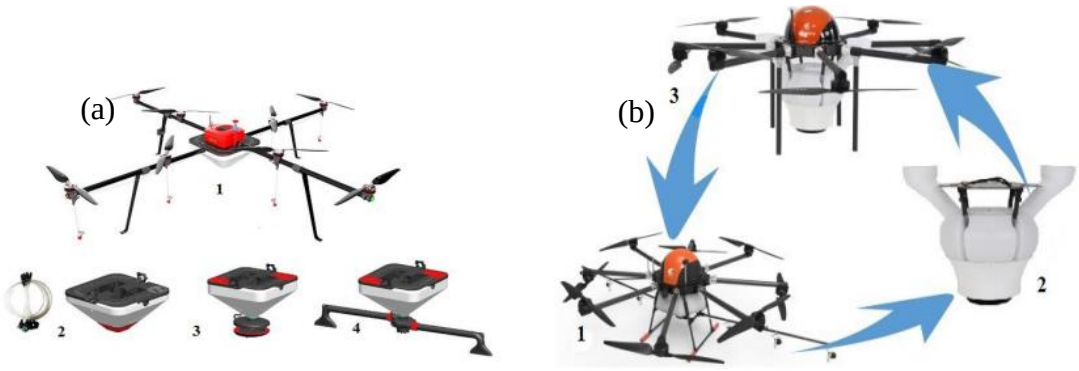

(a): named seed Flyer 3 WDM 8 -20, 3 - reservoir for spreading, 4 - reservoir for nozzle (b) drone of TTA company serving for spraying, sowing and spreading of fertilizers: 2 - device for sowing and spreading of fertilizers.

Figure 13. 3D representation of sowing UAVs (Berner, 2020).

In order to obtain the distribution characteristics of the seeds, (W. Liu et al., 2022) conducted a field test by organizing a self-made mud trough (2.5 m×2.0 m, 5 cm in depth). A hexacopter shot seeding UAV test was carried out at a working height of 1.5 m. it was designed for five row crop sowing.

Figure 14. Potshot seeding drone (W. Liu et al., 2022).

A compilation of UAVs to support the agricultural sector was presented by (Mohan et al., 2021). It comprises sowing & planting drones few of the captured. It has been understood from the scholar's paper that, the geometry profile varies as per the desired operation such as seed distribution, sowing, and planting. Some of these models were modeled in 3D CAD software and printed out by additive manufacturing, shown in figure 15-c. others were manufactured with classical production process.

a b c

(a)- automatic seed coater, (b)-seed spreader, (c) -coated seeds to perform aerial sowings

Figure 15. Manufactured seed sowing UAVs (Mohan et al., 2021).

2.4. Flight aerodynamics of UAVs

Based on the aerodynamic features by (Radoglou-grammatikis et al., 2020), UAV can be classified into three types: fixed-wing, rotary-wing and hybrid. As per the researchers' discussion, the airflow of the rotary-wing is composed of several rotors that generate the appropriate power necessary for lifting which does not need a forward airspeed for lifting. Depending on the number of rotors, a rotary-wing UAV can also be classified into; tri-, quad-, hexa- and octocopters. They indicated that a rotary-wing UAV possesses easier control and are able to carry desired payload compared to the fixed-wing type.

Figure 16. Rotary-wing UAVs (Radoglou-grammatikis et al., 2020).

Like other bodies which can be represented by reference frames, drones which are a six degree of freedom rigid bodies is represented in terms of local (x_b, y_b, z_b) and global (x_e, y_e, z_e) coordinates by (Jayakrishnan, 2016).

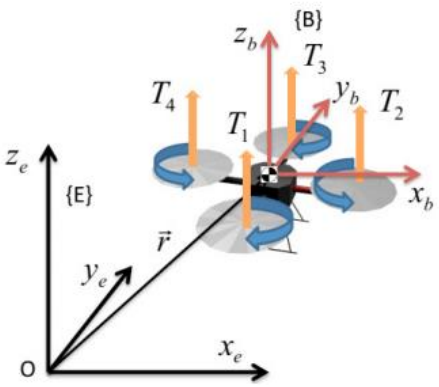

Figure 17. The reference frames and momentum principle (Jayakrishnan, 2016).

A research conducted by (Lee et al., 2021) as per flight aerodynamics of UAVs claims that, multirotor UAVs use the vertical take-off and landing technology, which indirectly generate lifting force from the forward thrust via the geometry of aerodynamically designed frame. Additionally, having flexible wings gives them the ability to do hovering, allowing them to maintain a constant airborne altitude without the need for path generation to move in any direction.

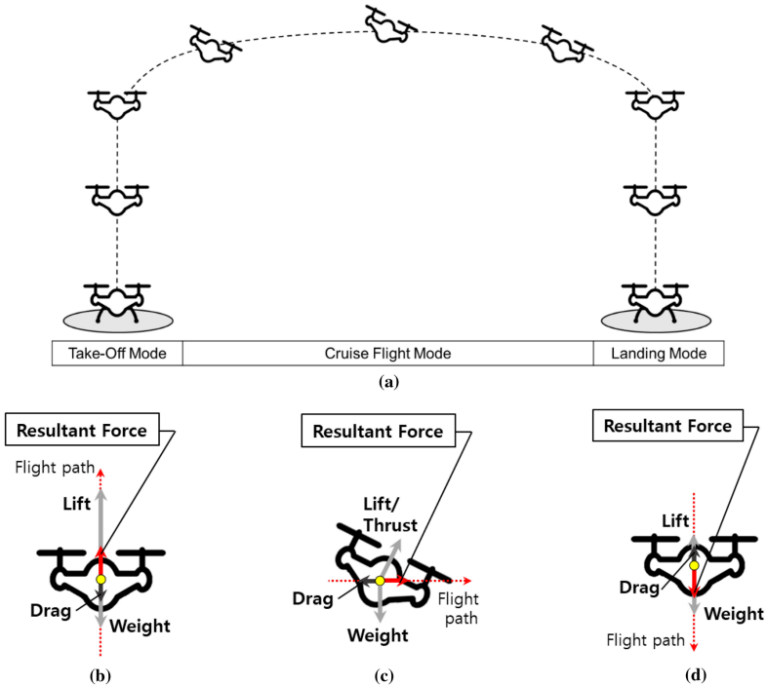

(a) flight trajectory, (b) take-of mode, (c) cruise flight mode, (d) landing mode.

Figure 18. Schematics of multi-copter flight mechanism and aerodynamic parameter (Lee et al., 2021).

(Lee et al., 2021) also described the fight mechanism of a multi-copter. According to the scholars, if the quadcopter is to fly to the right, the rotational velocities of the two rear rotors are increased, as shown in Figure 19. This tilts the body forward and creates drag backward.

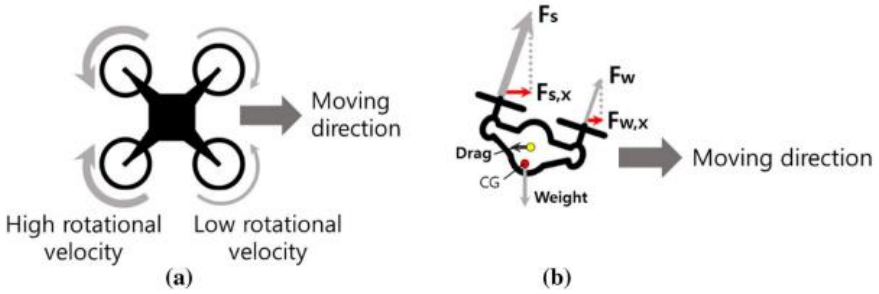

(a) Top view (b) Side view

Figure 19. Multi-copter flight mechanism (Lee et al., 2021).

2.5. Effects of weather conditions on the use of UAVs for agriculture

2.5.1. The categories of the wind fields

(Wang et al., 2019) outlined types of wind and summarized the sorts, qualities, and numerical models of the wind, which have extraordinary effect on automated aeronautical vehicle in the low-elevation climate. The categories are;

Constant wind is the typical wind speed in a certain environment, which varies with time and space. Because it is merely the reference value for wind speed in a particular environment, the constant wind does not actually exist in nature.

Turbulent flow is a continuous random fluctuation, which is always accompanied by the constant wind. Vortices, topography and wind shear has been considered to be the causes of turbulence.

The steady wind that varies over time or in space is referred to as wind shear. The change of two wind vectors at two points in space divided by the gap of those two points is how the American National Research Council (ANRC) defines the degree of wind shear. In terms of the UAV, a propeller vortex wind forms when the compressed air pass through the interval of the rotating blades and form a vortex field.

2.5.2. Effects of wind field and response stability on the structure of UAVs

A picture presented by (Ariante et al., 2021) in figure 20 describes the kinematic model of a quadcopter UAV in terms of the relation among the wind field, and stability along x-axis with the local reference frames (x, y, z) of the drone body. The scholars in detail presented the relation among the airspeed (velocity with respect to the surrounding air) and the ground speed (velocity with respect to the Earth frame).

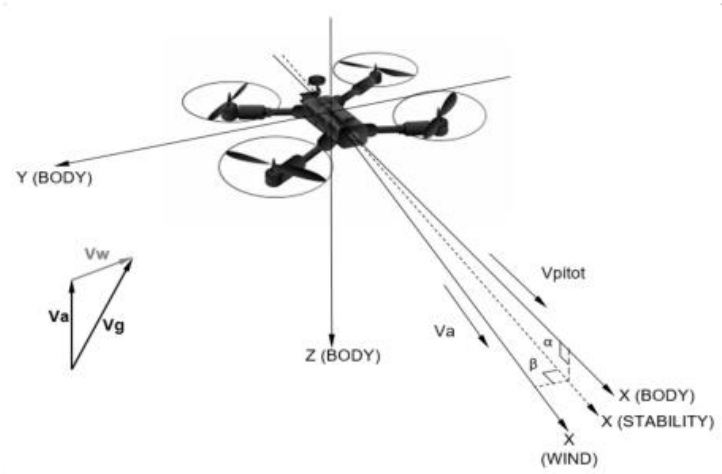

Figure 20. Airspeed definition and wind triangle (Ariante et al., 2021).

A related research made by (Meier et al., 2022) also represented the wind flow field over the body of the drone during hovering in horizontal airflow.

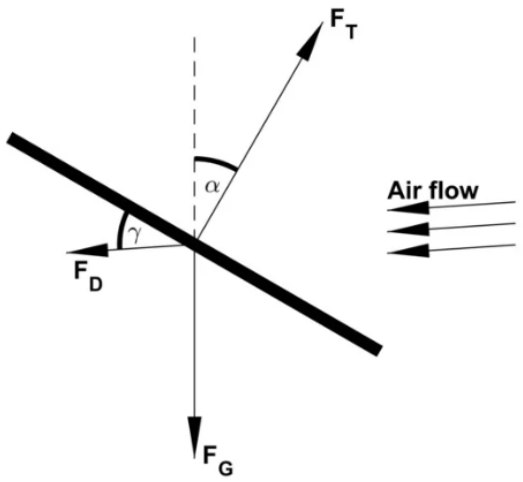

F_G - gravity force, F_T - thrust, F_D - drag, γ – incidence and α - tilt angles

Figure 21. Forces acting on a hovering drone in wind (Meier et al., 2022).

Static response is the response of the UAV to gusts and atmospheric disturbances. It is characterized as the propensity of the UAV to get back to a state of balance when exposed to an unsettling influence. Theoretical bases for setting stability assurance was presented by (Sugandi et al., 2018). On the saying of the scholars, there are longitudinal (pitch moment coefficient) and lateral (roll & yaw moment coefficient) stability criteria to decide whether an object is statically or dynamically stable. According to the scholars, values of plotted vs phase angle should be roll (cl<0), pitch (cm<0) and yaw (cn>0). In another way in terms of impulse response, the frequency or amplitude response should damp and converge constantly to almost zero after a certain air disturbance.

Drones are typically approved to fly at wind speeds of 4–14 m/s. Wind speeds exceeding 15 m/s are not recommended to fly in (Gianfelice et al., 2022). They also elaborated in addition to high wind speeds, turbulence is considered more challenging due to the rapid change in the speed and direction of the wind leading to risk scenario for drone flight.

A constructive finding from (Paz et al., 2020) stated, in a multi-rotor at 5 m/s, the interaction with the drag force displaces these structures backwards, even though they are still recognizable to keep their counter-rotating movement.

According to (Diwate et al., 2018), a drone follows only the dedicated path if there is no obstacle in the path. But climatic condition, such as the intensity and direction of the wind while seed sowing add further complexity to the control problem. They evaluated an algorithm to adjust the UAV route under changes in wind intensity and direction.

In the case of (Diaz & Yoon, 2018), small multi-rotor UAVs have poor stability in gusts due to the generation of a strong pitching moment when a sudden wind impacts the UAV. In their study, the complete DJI Phantom 3 during hover had been simulated with wind gusts at different wind velocities (V_{wind}).

Numerous research works by (Yinka-Banjo & Ajayi, 2020) have been done in determining the efficiency of UAVs for spot spraying (similar to crop spraying). Some factors considered were balancing UAV altitude and speed with spraying height and accuracy as well as droplet sizes, spray pressure and the possible effects of the UAVs'. table 3 below summarizes their type & properties.

Table 1. Feature-based specifications of UAVs.

UAV type	Altitude (km)	Avg. control range (km)	Avg. airspeed (m/s)
Multi-rotor UAVs (DJI Agras MG-1P)	2	3–5	7
Fixed-wing UAVs (AgEagle RX60)	0.125	2	18.8
Single-rotor (Alpha 800)	3	30	15.2
Fixed-wing-multi-rotor hybrid UAVs (Jump 20)	4	500–1000	30

Source: (Yinka-Banjo & Ajayi, 2020)

A field study conducted by (Biglia et al., 2022) presented a supportive data record of 13 agricultural UAVs investigating the effects on the canopy spray deposition and coverage due to different UAV-spray system configurations in operation. A detail of their record was presented in the table below.

Table 2. Weather conditions recorded during the field trials.

Configuration	Temperature		RH [%]		Wind speed			Wind direction	
	Mean	Δ h1-h2	Mean	Δ h1-h2	Min	Max	Mean	Dominant	Mean [°]
T1	12.1	−0.36	71.1	0.54	0.45	1.80	1.02	SE	127
T2	20.0	−0.35	30.1	0.22	0.70	2.06	1.17	S	185
T3	21.8	0.05	56.6	0.26	0.05	1.88	0.73	NNW	334
T4	20.9	−0.06	54.1	0.53	0.03	0.70	0.36	NNE	11
T5	20.4	0.04	54.9	0.16	0.08	1.48	0.85	NE	54
T6	21.3	−0.16	23.6	0.47	1.02	1.91	1.53	ESE	111
T7	15.9	−0.28	49.7	0.18	0.51	2.36	1.32	S	172
T8	19.4	0.04	67.1	0.40	0.09	1.89	0.95	NNW	340
T9	21.6	0.59	60.9	−2.53	0.24	1.22	0.56	NW	297
T10	23.5	0.07	53.1	0.11	0.37	0.94	0.71	ENE	83
T11	21.2	−0.03	23.9	0.03	0.59	2.22	1.36	ESE	100
T12	25.0	−0.04	48.8	0.38	0.36	1.64	0.95	S	165
T13	19.7	0.16	28.5	−0.71	0.28	1.13	0.64	N	1

Source: (Biglia et al., 2022)

Another experimental study conducted by (Chen et al., 2017) has revealed the effect of wind field on droplet deposition in effective spray area using HY-B-15L type UAV. They tested spray deposition of pesticides on selected rice plants six times with variable flight speed. The scholars measured the wind effect with three dimensions (x, y, z). A plot of charts showing the wind field distribution with the sampling points taken was captured as shown in figure 22.

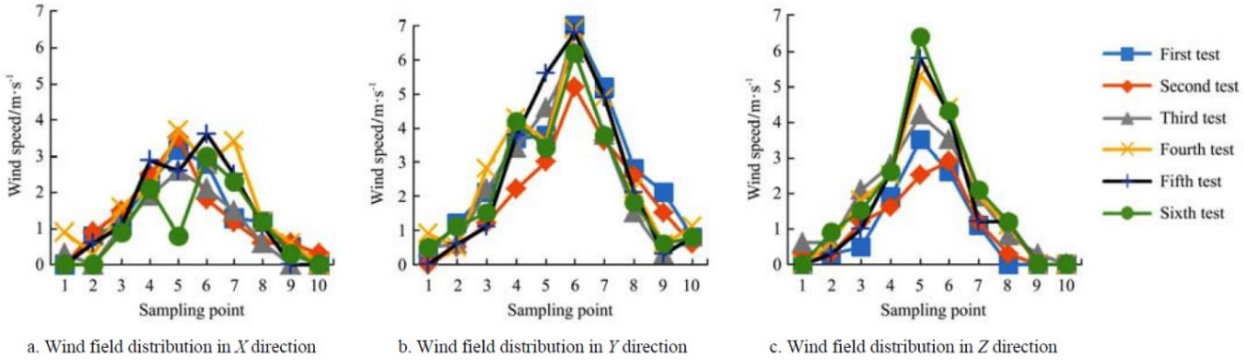

Figure 22. Wind field distribution along x, y, & z direction for sampling points (Chen et al., 2017).

An important factor to consider for drone path planning is the potential for navigating under extreme weather conditions. Although there are many improvements being made in the design of drones to make them more durable for such conditions, environments with precipitation, fog, and severe wind can have an adverse effect on a drone's endurance, visibility, and sensors for navigation and collision avoidance (Gugan & Haque, 2023). Recently, there have been a few studies that have proposed solutions for such weather conditions. Some studies have proposed solutions where drones can evaluate risk and avoid regions that may have severe weather conditions when generating a path.

(Diwate et al., 2018) designed a path control system for a seed sowing UAV using Arduino Atmega2560 microcontroller. As per their notation, the drone will follow only the dedicated path if there is no obstacle in the path. Climatic condition, such as the intensity and direction of the wind while seed sowing add further complexity to the control problem, the researchers assessed an algorithm to adjust the UAV route under changes in wind intensity and direction to minimize the waste of seed.

With the numerical value of volume being obtained, necessary survey data to support the numerical analysis was executed. As indicated by (Kumar et al., 2021) in Table 5, to perform numerical recreation on a demonstrated body, especially for CFD examination, some reference/base upsides of wind speeds are fundamental. Following this, recording wind particular and later on C_d&C_l, they demonstrated drone and examined the CFD in Ansys.

Table 3. Weather conditions & aerodynamic parameters of environmental locations.

Location	Wind speed (km/hr)	Temperature (^{O}C)	C_d	C_L
Desert	34.3	46	0.37012	−0.036
Desert	10.5	46	0.036	−0.004
Desert	34.3	35	0.37	−0.037
Desert	10.5	35	0.0368	−0.0043
Desert	13.7	25	0.061	−0.0067
Desert	4.3	25	0.00665	−0.0005
Desert	13.7	14	0.0617	−0.0067
Desert	4.3	14	0.0066	−0.00051
Grasslands	30	25	0.2846	−0.028
Grasslands	7	25	0.01689	−0.00179
Beach	55	31.2	0.931	−0.0085
Beach	55	23.5	0.912	−0.0836

Source: (Kumar et al., 2021).

2.6. Alteration of altitude with weather conditions & their effect on agricultural UAVs

In real situations, elevation is directly related with weather conditions. In particular, wind flows. As elevation increases, the amount of wind flow over the surfaces of a certain lifting particles also increases.

(Gianfelice et al., 2022) magnified to obtain historical, real-time, or forecast data, use of a publicly available Application Programming Interface (API) was necessary. This API generates meteorological data including wind bearing and wind speed at a 10 m height. It is important to note that this API data can be swapped for real-time data taken from a drone as long as the elevation, latitude, longitude, wind speed, and wind bearing can be measured. They also showed the necessity of measuring at multiple elevations.

A lab trial made by (Berner, 2020) showed a record for two variable heights of elevation of a seed sowing drone. The drone moving on two heights: 1.0 m and 0.5 m over the groove path, had a significant influence on the transverse distribution of the falling rye seeds. The air blow changed the flight path of the seeds, spread with the use of rotating disc, and abbreviated their way of flight.

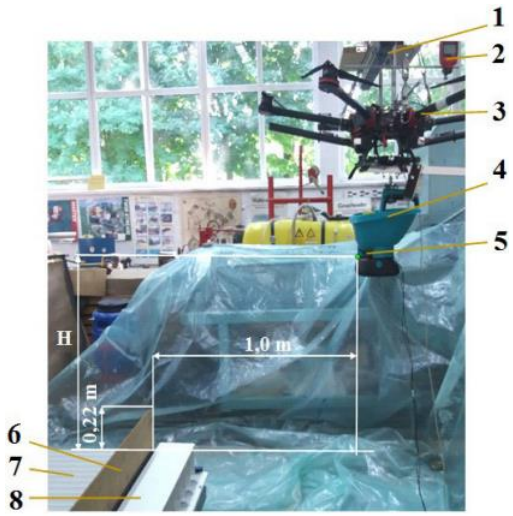

1 – the holder, 2- tachometer, 3 – drone, 4 – seed spreader, 5 – spreading disc, 6 – vertical cover, 7 – groove.

Figure 23. Exploited view of sowing UAV research (Berner, 2020).

Using the parameters of 1 m/s airflow speed, sampling height of 0.5 m and 0° nozzle spray angle as samples, (Ling et al., 2018) examined the impact of various spray heights on the deposition rules. According to the researchers', less atomized particles were discovered as the sampling height grew figure 24. This occurred because atomized particles diffuse more quickly at greater sampling heights.

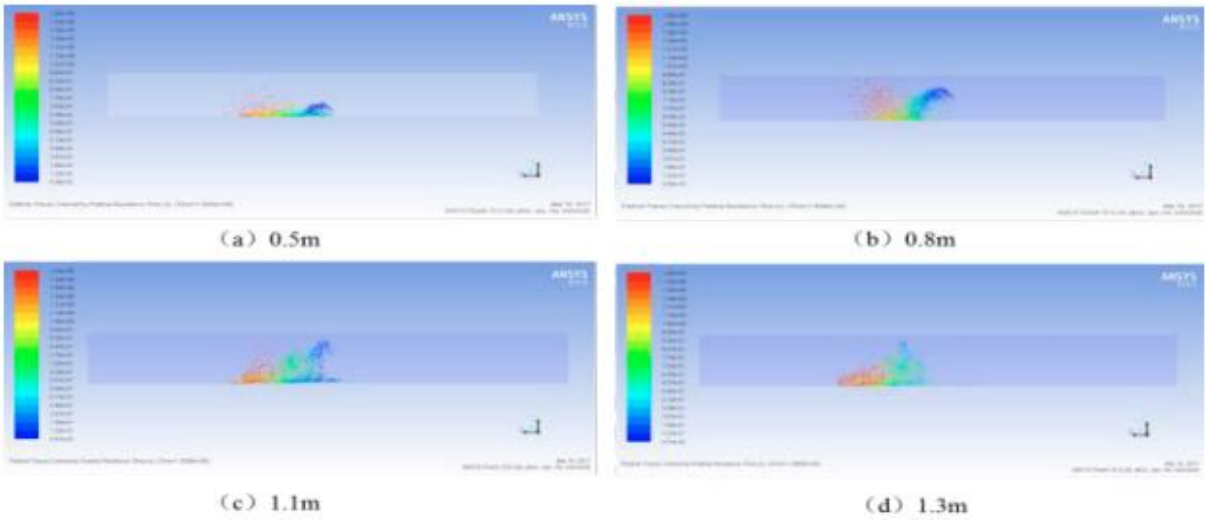

Figure 24. Image of distribution of droplets under different elevations (Ling et al., 2018).

Consistent with aerodynamic principles of multi rotors, (Lei & Lin, 2019) presented the effect of wind speed with the alteration of altitude. On their representation, it ranged from 0.3-1.5 m/s at heights <2 m which is low altitude proximate to the ground. As stated by their outline, a working height of 0.5 m lays in the average range of 0.3-1.5 m/s.

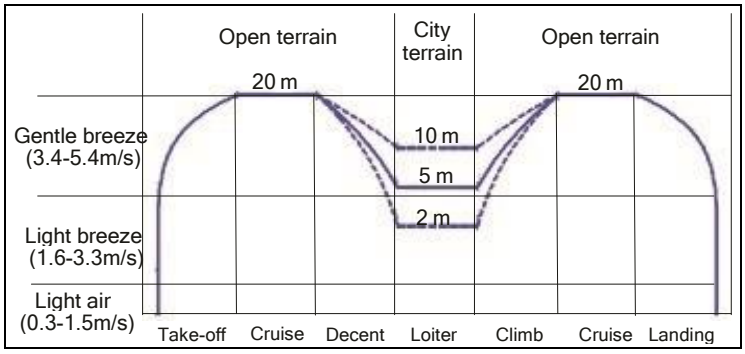

Figure 25. Wind speed ranges and variation with altitude (Lei & Lin, 2019).

According to (Qi et al., 2022), when the multirotor UAV was flying at a height of 1 m, the downwash airflow's intensity was at its highest and most unsteady. This raised the notion that, in order to equally disperse the deposition, the downwash air velocity should be less than 5 m/s. the researchers also overstated the variation of air velocity for variable flight heights of 1, 2, 3, 4, 5, & 6 m of a quadcopter.

Table 4. Spray test and environmental parameters measured.

Test number	Flight height (m)	Flight speed (m s ^{1})	Wind speed (m s ^{1})	Temperature (^{o}C)
1	1.0	6.0	2.7	34.6
2	2.0	6.0	2.5	32.5
3	3.0	6.0	2.2	31.2
4	3.0	4.0	2.6	30.4
5	3.0	5.0	2.7	32.7
6	4.0	6.0	1.7	30.5

Source: (Qi et al., 2022)

(Zhu et al., 2019) also studied horizontal wind effect simulation on droplet drift and of particles by UAV using CFD. The scholars simulated the wind effect on the deposition of the particles at 0.8, 1 and 1.5 m of operating heights with wind speed of 0, 1, 3 & 5 m/s. as per their analysis, the drift deposition visibly affected by wind at a speed of 3 m/s.

A compilation of reviews on the relation between the alteration of altitude with wind speed. There are good supportive papers concentrating on measurement of wind gusts by multirotor UAVs specifically quadcopters at hover, tilting and forward flights. Some used measurement sensors, anemometers & vane sensors. They measured vertical and horizontal speeds alternatively.

Table 5. Review of wind speed variation with altitude.

Author	Data type	Flight type	Altitude (m)	Wind speed (m/s)	
(Meier et al., 2022)	Simulation & field	Hover and moving	20	4.1	
(Qi et al., 2022)	Simulation & field	Hover and moving	1 – 4	1.7 – 2.7	
(Lei & Lin, 2019)	Simulation & experimental	Hovering	$\leq$1	Light air	0.3-1.5
			1 $\leq$ h < 4	Light breeze	1.6-3.3
			5, 10, 20	Gentle breeze	3.4-5.4
(Ling et al., 2018)	Simulation	Hovering	0.5	1	
			0.8	2	
			1.1	3	
			1.3	4	
(Lei & Wang, 2020)	Simulation	Hovering	20	$\leq$ 5	

A very constructive experimental research made (Prudden et al., 2018) the relationship wind speed has with alteration of flight height ranging from 0-7 m/s of wind speed with 0-60 m height respectively. The scholars also presented the alteration of wind speed with hour variation per a day which shows how wind speed even varies with time.

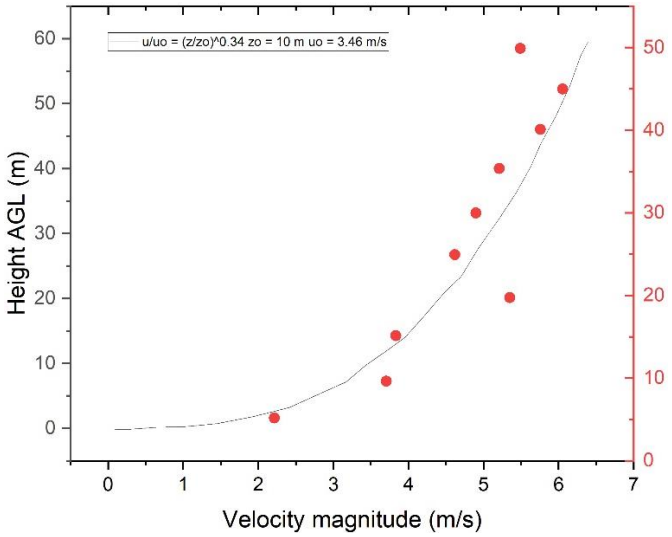

Figure 26. Graph showing linear relation height has with wind velocity (Prudden et al., 2018).

2.7. CFD analysis of UAV models

A real time wind prediction for a safe drone flight in city numerical study conducted by (Gianfelice et al., 2022) shows a stepwise CFD simulation taking a real-time geometrical data in Toronto. The study was directed in simulating the wind effect along South and North, 50G S, 50G N with 0, 180, 300 and 350^0 wind bearing. To simulate the drone and building model the researchers used Ansys fluent with cylindrical flow domain.

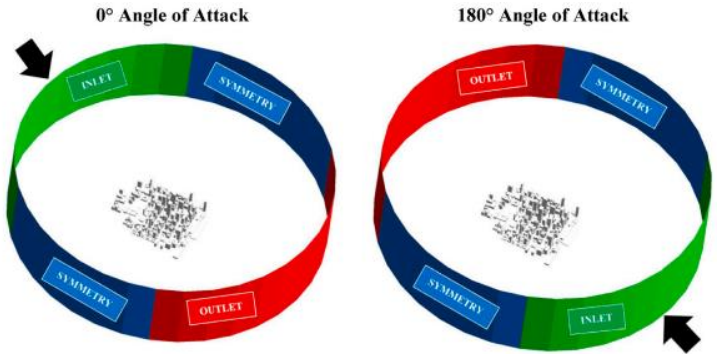

Figure 27. Flow domain boundary condition of wind analysis on UAV in buildings (Gianfelice et al., 2022).

(Atmaca et al., 2019) performed a CFD under finite volumetric analysis using the k-ε turbulence model on two models of drones consecutively in motion. Their aim was to make aerodynamic analyzes of UAVs swarming behavior and to identify reliable zones for vehicles. Then they recorded turbulence, pressure, and velocity changes.

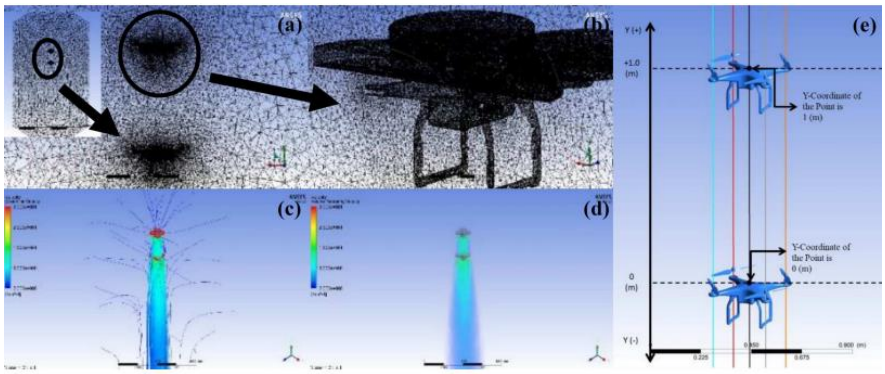

(c) streamline velocity (d) velocity rendering (e) locations of consecutive drones.

Figure 28. Mesh and downwash CFD view of UAVs (Atmaca et al., 2019).

A sample of randomly modeled agricultural UAV and the aerodynamic effect on the body/airframe at $0^0 - 30^0$ orientation was studied using CFD Fluent by (Felismina et al., 2017). They recorded pressure & velocity contours. As per researcher's notation, the pressure contour effect on the edge position is high which indicates that there is high pressure force. The 0^0 orientation and its CFD-Post result plot for pressure contour is shown figure 29.

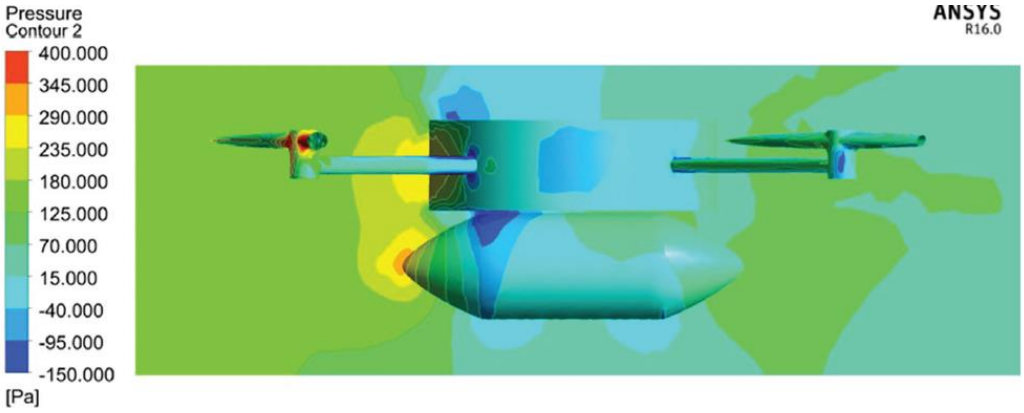

Figure 29. A UAV model aerodynamically analyzed at 0^0 (Felismina et al., 2017b).

(Yael & Arias-montano, 2020) used three different software packages to study the aerodynamic properties of the prototype. For every one of them, the scholars selected a speed of V = 25 m/s. On their study, the researchers stated that since flow is incompressible, dependency of the aerodynamic coefficients on speed is insignificant and they omitted the corresponding terms. The researcher's aim was to computationally estimate the aerodynamic derivatives for a Dual-System as a mean to use them in the mathematical model and control system design for flight simulation. The scholars then conducted numerical CFD simulations with ANSYS Fluent®, XFLR5 & X-foil programs.

(Lei & Lin, 2019) demonstrated CFD analysis in a wind tunnel. The scholars also attested a numerical simulation of fluid flow fluent. The scholars directed their study on the coaxial rotors & the rotor carrying arms. The scholars set the wind speed to be analyzed along x and y axis components.

As stated by (Cummings et al., 2018) modern CFD techniques have a relatively high level of fidelity and have successfully modeled the nonlinear aerodynamic behavior of aircraft at full-scale Reynolds numbers. This method reduces some of the major uncertainties associated with sufficiently modeling physical space.

A result from (Polivanov & Sidorenko, 2021)'s numerical study showed the extent of interference propeller with the arm of the quadcopter and how the elements of the quadcopter frame can be used to destroy the vortex, which leads to a significant increase of thrust on the propeller and instability on the assembly due to frame imbalance.

(Li et al., 2022) numerically studied an agricultural UAV when used for spray deposition which is useful for agricultural plant protection. The scholars studied the downwash wind effect at variable wind speeds that has on droplet deposition drift of sprayed particles i.e., they simulated how wind disturbs and displaces the particles carrying bodies using CFD. The scholars plotted velocity distribution effect.

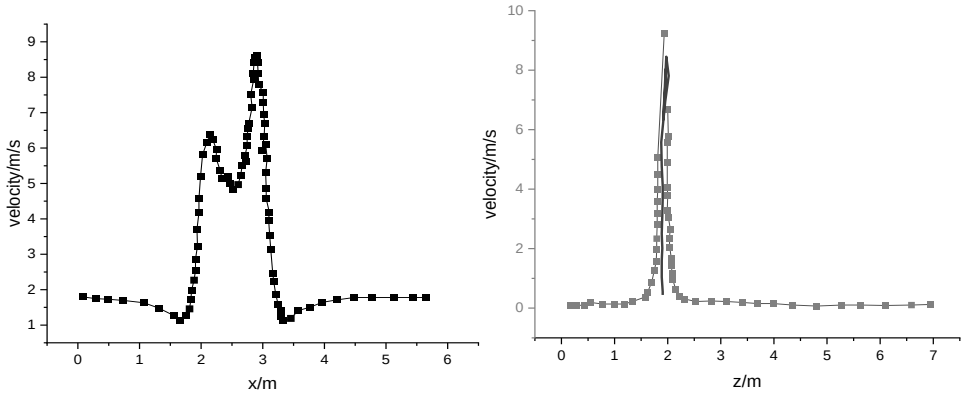

Figure 30. Velocity distribution locations of downwash flow (Li et al., 2022).

Tons of researches on sections under literature revised have been conducted by many researchers. Evaluation of altitude sensors for a crop spraying drone, drone technology for agriculture purposes, corn height estimation using UAV for yield prediction, CFD analysis of the aerodynamic effects on the stability of the flight of a quadcopter UAV in the proximity of walls and ground, influence of aerodynamics and proximity effects in quadrotor flight are some of the researches made on UAV, agriculture and environmental interaction. All the works are duly acknowledged.

Researches made by three researchers however showed a seed metering mechanism implement for sowing varieties of seeds designed and integrated with UAVs (Lysych et al., 2021) without touching the wind guest the assembly might have with the environment, a universal seeder system which can be applied for seeds to be accurately deposited at pre-established distances between plants developed by (Felismina et al., 2017a) with untouched section of wind disturbance on the body during operation, and although (Felismina et al., 2017b) made a close research on the effect of aerodynamics (wind disturbance) on the body of a UAV, the geometry variants and wind speed ranges has not been touched in relation to this aspect. According to the extent of the researchers review, in common including the above authors, particularly stability in terms of impulse response under CFD analysis of review section were not touched.

As per the understanding of the researcher stated under problems section after a deep review in the literature, there was a need to study the effect of aerodynamic shape, parameters and variable wind speed gusts effect on stability that hinders to achieving precision by UAVs implemented in agricultural sowing by a method of numerical computational fluid dynamics analysis.

CHAPTER THREE

MATERIALS AND METHODS

This section explains the research tools necessary and the methods implemented to execute and finalize the research.

3.1. Materials

In this section the materials to be used to conduct the research will be discussed. Following this, the materials; surveyed data, a 3D modeling software (Particularly Solid Works 2021), a simulation (Particularly Ansys 2020/R1 academics - CFD) and data analysis software origin lab was necessarily crosslinked to execute the study.

3.2. Methods

Basic characterization and modeling method of determining its profile is seen crucial to implement geometry variants on the body to conceptually model & simulate a typical quadcopter of multirotor UAV. The trade of study followed a screening out matrix by 6 leveling matrices to select three variants as a key parameter indicator (KPI) of shape, weight & dimension. Including a determinant survey from literatures on weight standard specifications of categorized UAV types, the geometry variants were screened out to the actual set. A numerical method of CFD simulation studying the significance of wind gust (disturbance) that may cause on the body at 0^0 orientation (hovering) was analyzed. For the numerical aerodynamic analysis, a particular simulation software – ANSYS fluid flow (fluent) was used particularly, with finite volumetric analysis using k-epsilon model under the simple Rynolds Average Navier Stock (RANS) method.

The pre-processing step to generate a mesh (after identifying the fluid domain) was given to Ansys Modeler, the solver step to Ansys Fluent® and the post-processing step was set to CFD-Post. The speed of the wind to be blown over the section of the body was set to range between v_w 0.3 m/s, 0.6 m/s, 0.9 m/s, 1.2 m/s & 2.5 m/s. Output variables such as pressure distribution, velocity flow line, C_d, F_d and moment coefficients were recorded from the simulation results in CFD-Post to specify the spot necessary.

3.2.1. Conceptual frame work as a methodological procedure

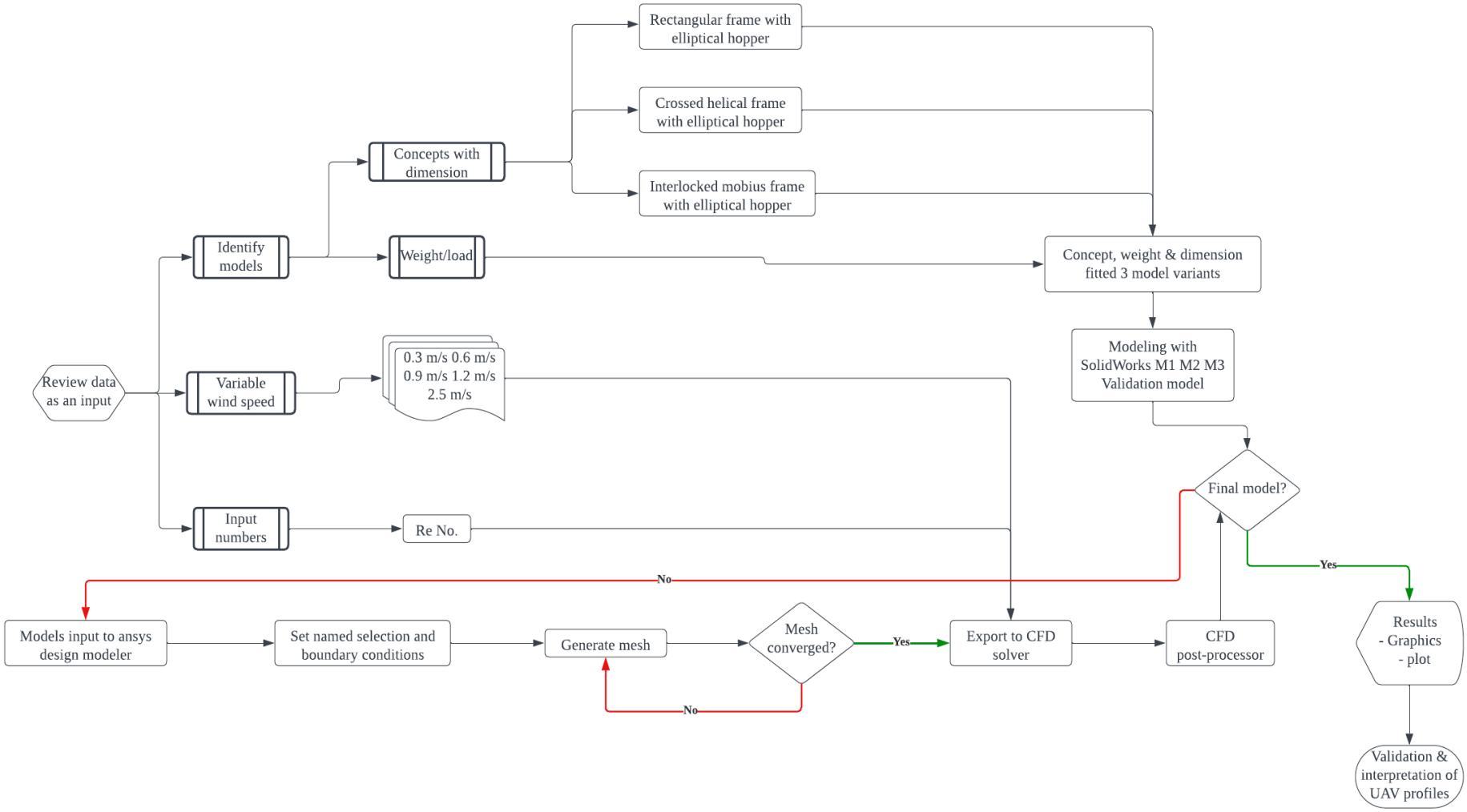

Figure 31. Research flow chart.

3.2.2. Pre-set conditions of research analysis

The key parameters that governed to settle this research are;

3.2.2.1. Wind & path

An environment can be divided into four with fixed-size cells to simplify the task of computing paths. Any cell containing a portion of an obstacle is marked as occluded, and without an obstacle is marked as free. Such lines can determine if there is a solution for any given input, but require a large amount of memory (Gugan & Haque, 2023).

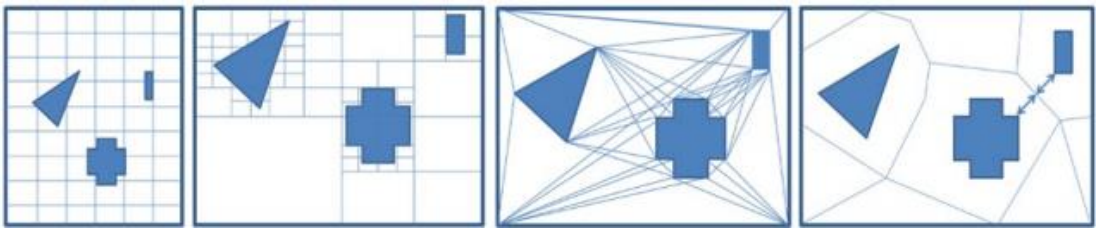

a. Uniform grid b. Quadtree c. Visibility graph c. Voronoi diagram

Figure 32. Representation of an environment (Gugan & Haque, 2023).

Following the findings of Gugan & Haque, this study has set a uniform grid/uniform path of working area, horizontal & downwash wind blow analysis over the bodies which aligns with the domain as well.

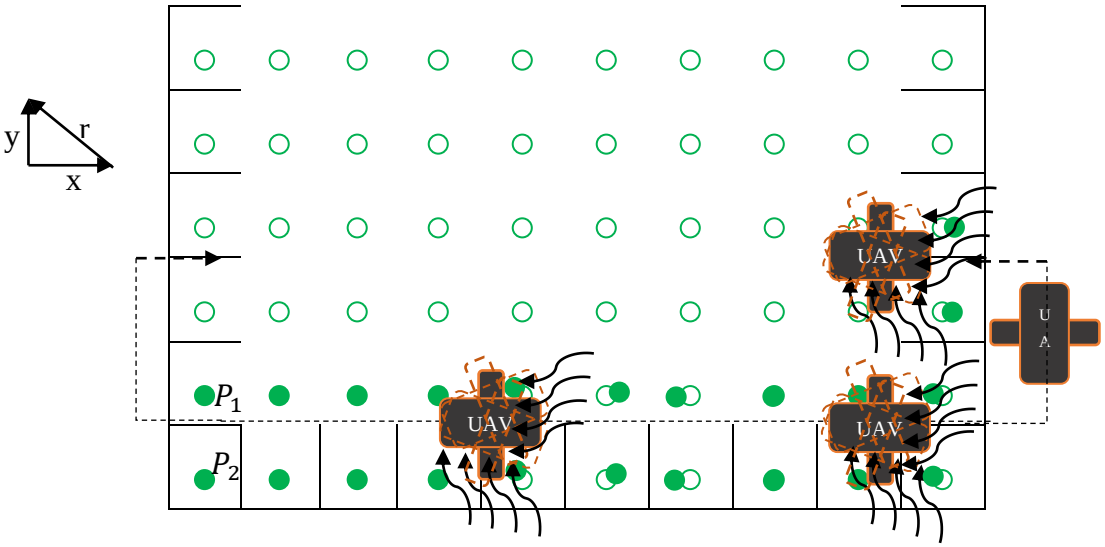

[(horizontal, downwash) (x, y) – wind flow directions]

Figure 33. 2D Illustration of the assumed wind analysis on UAV.

3.2.2.2. Wind effect with alteration of elevation

Compiling findings from (Ling et al., 2018) on the effect of varying elevations, particles of crops moved more readily with the airflow as the droplets left the nozzle. The researchers generalized that the affected region was larger and the accumulation was lower as the sampling height gets higher. (Gianfelice et al., 2022) magnified on the relation between altitude, wind bearing and flight including the extent of measuring at several elevations to serve as a reference for forecasting and extended researches.

(Berner, 2020) attested that for a seeding UAV made by TTA company, the height level of flight had a direct relationship with width of treatment (m) and yield. It showed that both width & yield increased from 10 – 18 m, 1 - 2 ha/flight respectively. Besides, the seeds' flight route was altered by the air blow, which spread using a rotating disc and condensed the trajectory of their flight. Since there exist linear proportionality, it is then implied that this study considers linear wind distribution of the drone along with alteration of elevation.

For this study, considering a hovering height of 0.5 m height from the ground, even for a slopy, a hill operation, it is scientifically considered that the altitude of hovering UAV from the ground still remains 0.5 m as the profile of the slopy & hill altitude increases above sea level. This rather creates an increase in wind speed. Hence this constant height is kept for a given operation and variation considered in this study as per the altitude not to be greater than 4 m with wind speed of 2.5 m/s.

3.2.3. Characterization

Geometry variants contribution as per shape/orientation parameters was examined considering the theoretical conceptual design procedures. The study was conducted by comparing 3 geometric variations. The scope of the geometry variants is narrowed to three for the technical reason of; the first geometry variant resembles the recent typical profile of UAVs for this application so, this concept is thought to represent it. The second and third geometry variants are new concept additions. For each, there was an integration and evaluation of the feasibility of parameters for the proceeding numerical analysis.

Corresponding to the selected geometry variant, another task is taken as shown in the flowchart below.

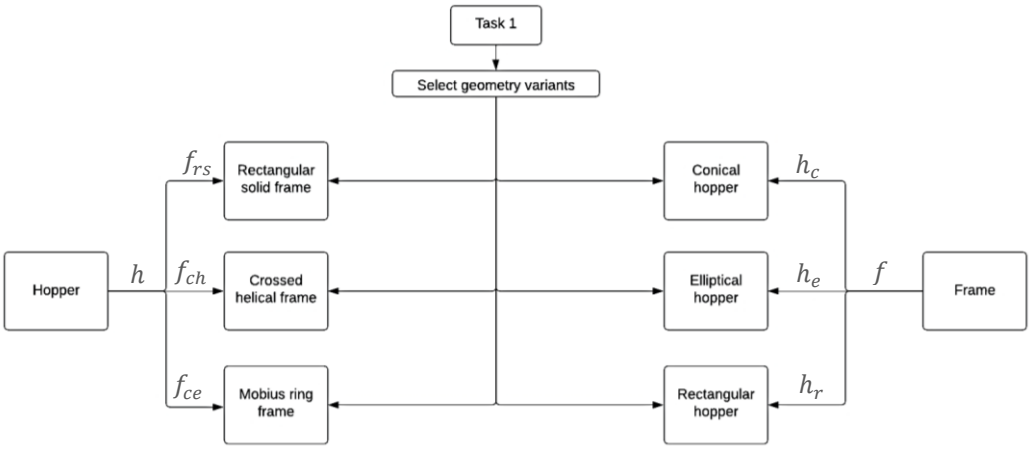

Matrix formation was identified to be more than 9 concepts. To export for task 2 selection, constant hopper with variable frame.

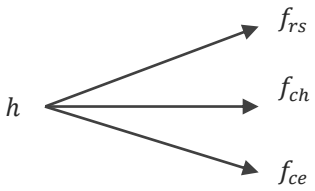

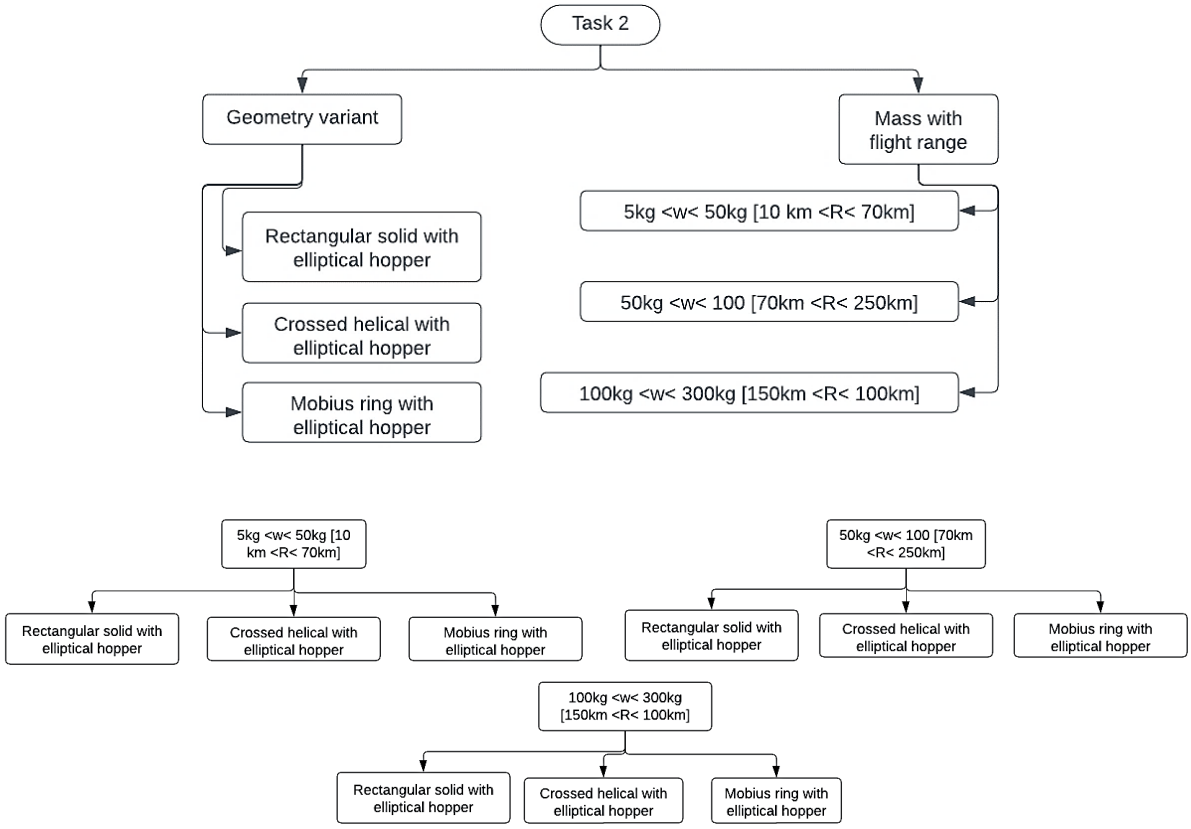

Figure 34. Tasks clarified for the concepts to be selected.

3.2.4. Data collected for modeling

A range has been taken an average from (Ababa et al., 2018; Belete, 2020; Edosa et al., 2019; Tesfaye et al., 2019) researches. In Ethiopia, the optimum maize plant density recommended by the research system varied from 44,444 plants per hectare (0.75 m × 0.30 m single seed per hill) to 53,333 plants per hectare (0.75 m × 0.25 m single seed per hill) depending on cultivar (Tesfaye et al., 2019). Following these, the length and width of the test bed is considered to be 1 hectare (100 m x 100 m) with single seed per hill of (0.7 m × 0.25 m). Below is illustrated a 6.94 m x 2.5 m sample area from the 1 hectare to sustenance the modeling.

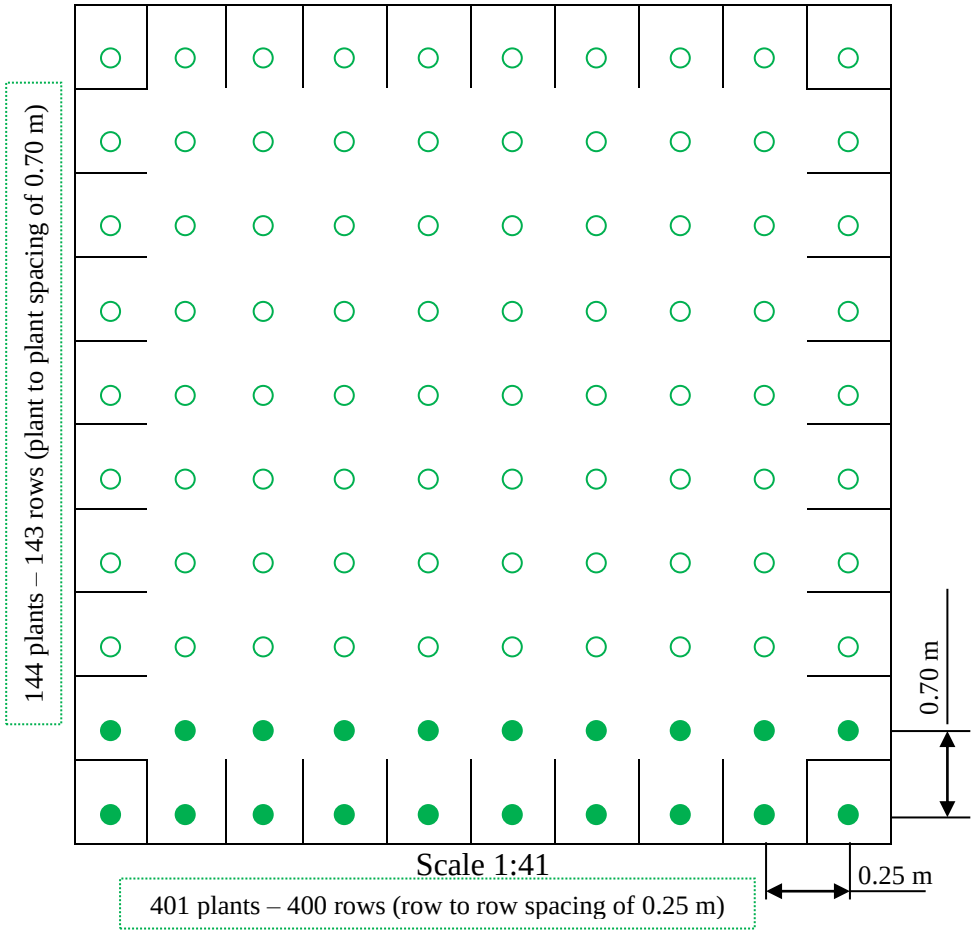

Figure 35. Representation of sample sown area.

The above analysis will lead us to set the dimensions and/or the position of seed dropping nozzle tips. Knowing the position is then important for setting the overall dimension (volume) of the multirotor drone. Mathematically,

$401\ x\ 144\ plants = 57744\ maize\ plants/seeds$ are expected to be sown in 1 hectare

A laboratory measurement of counted 100 corn grains at Addis Ababa Institute of Technology (AAiT) chemical laboratory has been carried out to assure the exact weight of the seeds. The test measurement was taken 3x3 for 3 different combinations of the seeds for accuracy.

a b c

a- dry, b- wet, c- mix.

Figure 36. Measurement of the 100 grains at AAiT chemical laboratory.

Following this, taking the ratio mathematically, X represents unknown gram of seed

$$\frac{100\ maize\ seeds = 37.3\ g}{1\ maize = \ X\ g?}$$

$\Rightarrow\ 1\ maize = 0.373\ g\ \therefore\ the\ 57744\ maize\ plants\ will\ weigh\ 21538.512\ g\ or\ 21.538512\ kg$

This explains that in one hectare, this much kgs can be planted with the corresponding geometry volume of UAV payload. While in comparison with the reviewed articles of (Ababa et al., 2018; Belete, 2020), up to 27.5 kg of maize in maximum can be planted. While the difference lies on at a time operation.

As (Hafeez et al., 2023) introduced on their paper, The idea of multi-splashing was set to connect two-spot planting planned for decreasing of working time which is one of the chief elements for efficiency. They outlined a robot named aero-drone for field checking to limit the hour of splashing.

Once more (Yinka-Banjo & Ajayi, 2020) expressed, with the utilization of UAVs, the quantity of additional workers required was chopped down in crop cultivating. As per the researchers outline, UAVs can shower crops around 40-60 times quicker than humans. For this, UAVs are the most preferable as they can fly straightforwardly in straight ways.

On the taking care of pace of payload i.e., the seed grains range, lots of investigations have been made. Payload for most UAV sprayers doesn't surpass 50 kg (Anand & R., 2019). furthermore, introduced a particular UAV type named PAM-20^0 which conveys a payload of 15 kg.

The trial testing process directed in Thailand by (Radoglou-grammatikis et al., 2020) incorporated a choice from different payloads (ranging from 0.2 kg – 2.5 kg) and elevation esteems. It was achieved in a 400x400 adjusted rectangular region made out of 8 predefined waypoints. In view of their trial results, the power utilization doesn't present a critical incentive for the payloads of 0.2 kg, 0.4 kg and 0.6 kg. Nonetheless, a minor augmentation was introduced for the payload with 0.8 kg. Concerning the elevation, the most extreme power utilization was introduced when an unsettling influence diminishes the height or velocity, stating the UAV needs to repay these qualities. (Felismina et al., 2017a) fostered a widespread seeder framework to convey a payload/feed pace of 5 kg of seeds all at once and broke down mathematically with an applied heap of 45 N.

The review led by (Huang et al., 2020) showed the air planting framework for rapeseed utilized wind current dispersion component which is a small scale variant of the wholesaler utilized in land seeders. The functioning width was 2.1 m and the greatest working rate was 8 m/s. The planting gadget weighted around 3 kg, and the payload was 5 kg of rapeseed.

Weighting these above studies ranging from 0.2 kg – 10 kg of payload feed intended for agricultural crops and tried to take the proportion, so at a time, the feeding rate/payload can be 4.3077024 kg with a routine cycle of 5 times for the complete 21.538512 kg of maize seeds to be planted. Therefore, now the mass of the seeds has been identified to be 4.3077024 kg. we require to get its volume. For that mathematically,

$$\rho = \frac{m}{v}, v = \frac{m}{\rho} \quad \text{..... (1)}$$

Where; m – Payload total mass

ρ_p – Density of payload

v – Total volume

Physical and mechanical properties of maize grains were determined as a function of moisture content in the range of 10-30 per cent using standard techniques. The average density ranged from 1219 to 886.470 kg/m^3 (Yenge et al., 2018). It has been seen from (Ababa et al., 2018)'s outline that, the grain yield (kg/ha) has direct relationship with moisture content. The scholars also showed the significant main effect of frequency and plant density ($P<0.05$) on harvest index and grain yield on maize production. This indirectly shows how moisture content has an effect on plant density.

With average moisture content as the temperature varies from the survey, the density is taken to be 890 kg/m^3, where total volume obtained also corresponds to the volume of the bucket payload.

$$v_{tot} = \frac{m_s}{\rho_s} \quad \text{..... (2)}$$

3.2.5. Modeling

To model the variants which are scoped out to this research, data collected were an input. Quadcopters can carry large payloads, have good flight time and cost effective (Radoglou-grammatikis et al., 2020). Following the survey, basic selection matrix were followed and the quadcopter UAV modeling was selected and designed by SolidWorks.

This leveling matrix was necessarily used to point out the scope of studying the CFD for 3 quadcopter UAV models. Basically, with six selected criterions, a trade of study was examined. The criterions set were factors which are thought to measure the variants.

Table 6. Selection matrix of concept screening.

Criterion	3D Concept								
	1	**2**	**3**	**4**	**5**	**6**	**7**	**8**	**9**
Precise sowing	+	+	+	+	+	+	+	+	+
Wind impact resistance ability	0	**+**	–	0	**+**	–	0	**+**	–
Accessibility	**+**	0	0	**-**	0	0	**+**	0	0
Flight time	-	+	–	+	0	–	+	0	–
Optimum payload	+	+	+	+	+	+	0	+	+
Dimensional stability	0	+	+	0	0	+	-	0	+

Notes: (–) — low value; (o) — moderate value; (+) — strong value.

→ Then using a selection matrix above, a trade of study was done to finally obtain a selected geometry variants with parameters for simulation. Following these, concept variant 2 is chosen. This selected model variant has a category of three 3D model concepts.

M2-A (Rectangular solid frame with elliptical hopper)

This is a rectangular solid geometry with elliptical hopper to weigh an average of 5 – 50 kg overall, a speed/flight range of 10 – 70 km/hr and overall dimension to depend on the geometry optimization drone with its components. It represents the x-type of geometry arrangement, an optimum profile for delivery purpose which was also supported by (Mohamedzain et al., 2022; Shukla & Komerath, 2018).

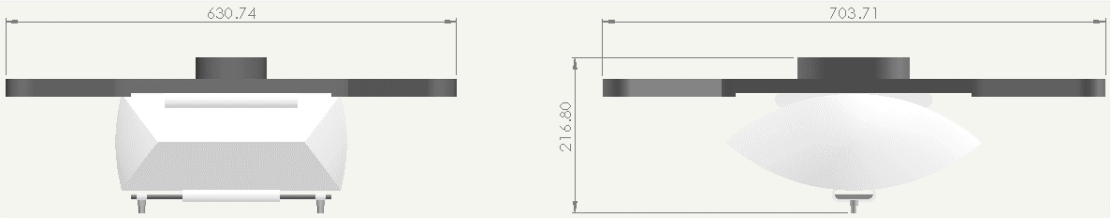

Figure 37. Schematic representation of rectangular solid frame with elliptical hopper.

M2-B (Crossed helical frame with elliptical hopper)

This is a crossed helical geometry with elliptical hopper to weigh an average of 5 – 50 kg overall, a speed/flight range of 10 – 70 km/hr with overall dimension to depend on the geometry optimization drone with its components. The whole assembly is assumed to have a close profile.

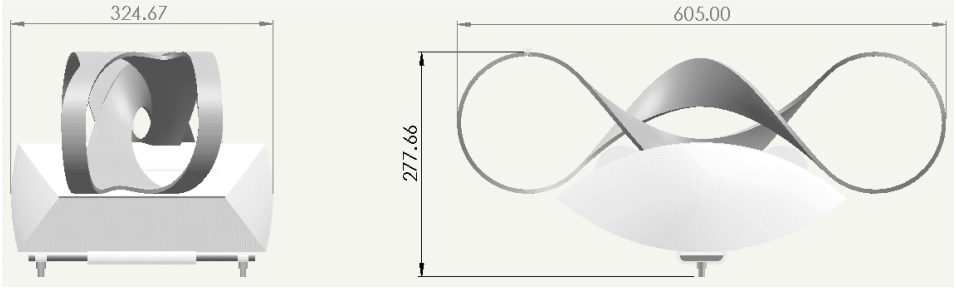

Figure 38. Schematic representation of crossed helical frame with elliptical hopper.

M2-C (Mobius ring frame with elliptical hopper)

This is a geometry with elliptical hopper to weigh an average of 5 – 50 kg overall, a speed/flight range of 10 – 70 km/hr and overall dimension to depend on the geometry optimization drone with its components. It is assumed to have a close profile.

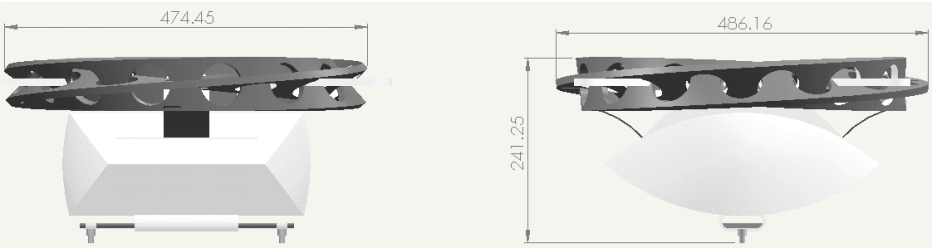

Figure 39. Schematic representation of mobius ring frame with elliptical hopper.

To a great extent, three models of rectangular solid configuration, crossed helical configuration, and mobius ring configuration all with elliptical hopper has been characterized and modeled for study in to CFD analysis. Correlating with reviewed research standards, the conceptually characterized & modeled variants fall under the category of light-weight type quadcopter multirotor UAV weighing 9.53, 5.141, 7.78 kg of total mass with a flight range of 10 – 70 km/hr respectively.

For the reference values, values such as the area, which corresponds to the projected frontal area of the UAV, dimensional stability, the air density, the temperature and velocity flow were imposed. From these values computing Reynolds number mathematically as an input helps to identify the flow type of wind.

$$Re = \frac{\rho \Omega R c}{\mu} \quad \text{..... (3)}$$

Obtaining one of the variables either drag coefficient or drag force initially can also lead us to determine the other with the equation below, where $v_w{}^2$ is UAV velocity, A - frontal area, C_d - drag coefficient and F_d - drag force. This equation and its principle have a direct relation with wind load and pressure drag. Reminding the two categories of drag, which are pressure drag and friction/viscous drag. Conceptually the corresponding terms indicates both.

$$C_d = \frac{F_d}{0.5 * \rho * v_w{}^2 * A} \quad \text{..... (4)}$$

3.2.6. Hovering stability analysis

Under this analysis, the static category during hovering is studied. The intended result is interpreted with regard to roll, yaw & pitch angles. during hovering at a height of 0.5 m, the direction of the flow of the wind as per (Ariante et al., 2021) is expected to have different profiles and may create stability disturbance deviation. The profiles are shown in the 3D figure below with their respective flow symmetrically. This profile representation works for the rest of the models.

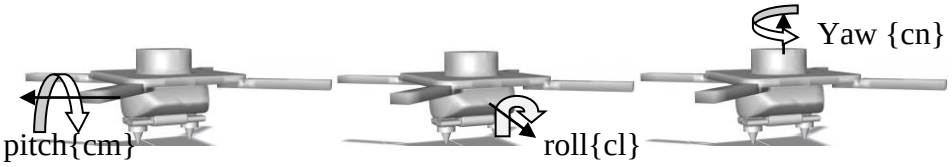

Figure 40. Representation of moment coefficients alteration due to wind flow.

It has to be noted that, the wind coming from any direction does creates alteration in yaw, pitch and roll moments of the body either in clockwise or anti-clockwise direction. It only differs on the extent of each alteration. A wind direction coming along horizontally either 0^0 or 180^0 in front surface area could significantly have a high rate of altering the body's pitch moment while still exist a certain percentage of alteration in the yaw and rolling moments.

The PID parameters termed as pitch, yaw and roll moment coefficients are one of the other necessary output parameters by analyzing in terms of phase angle (Sugandi et al., 2018) or impulse response (Paz et al., 2020). The phase angle determines its magnitude of either positive or negative for each of the three objective parameters. The pitch magnitude has to be less than 0 to stabilize the body due to longitudinal wind gust. The roll magnitude becomes negative (<0) as well in response to the lateral wind gust while yaw magnitude should be positive in response to lateral wind. And the impulse response determines convergence or sine wave.

Stability in terms of impulse response can be analyzed with step input response of either time or frequency domain. Both show the instance/magnitude of sudden continuous wind disturbance in terms of time and frequency. The amplitude of this domains should converge damp (damped wave) or undamped sinewave for static stability of an object.

3.2.7. Numerical CFD simulation

In this computational fluid dynamic simulation section, each system variant will be exported to Ansys® design modeler as geometry inputs to set named selection (the fluid domain), meshing, solver, solution and results interpretation. It was carried out three dimensionally for a single core serial processing option.

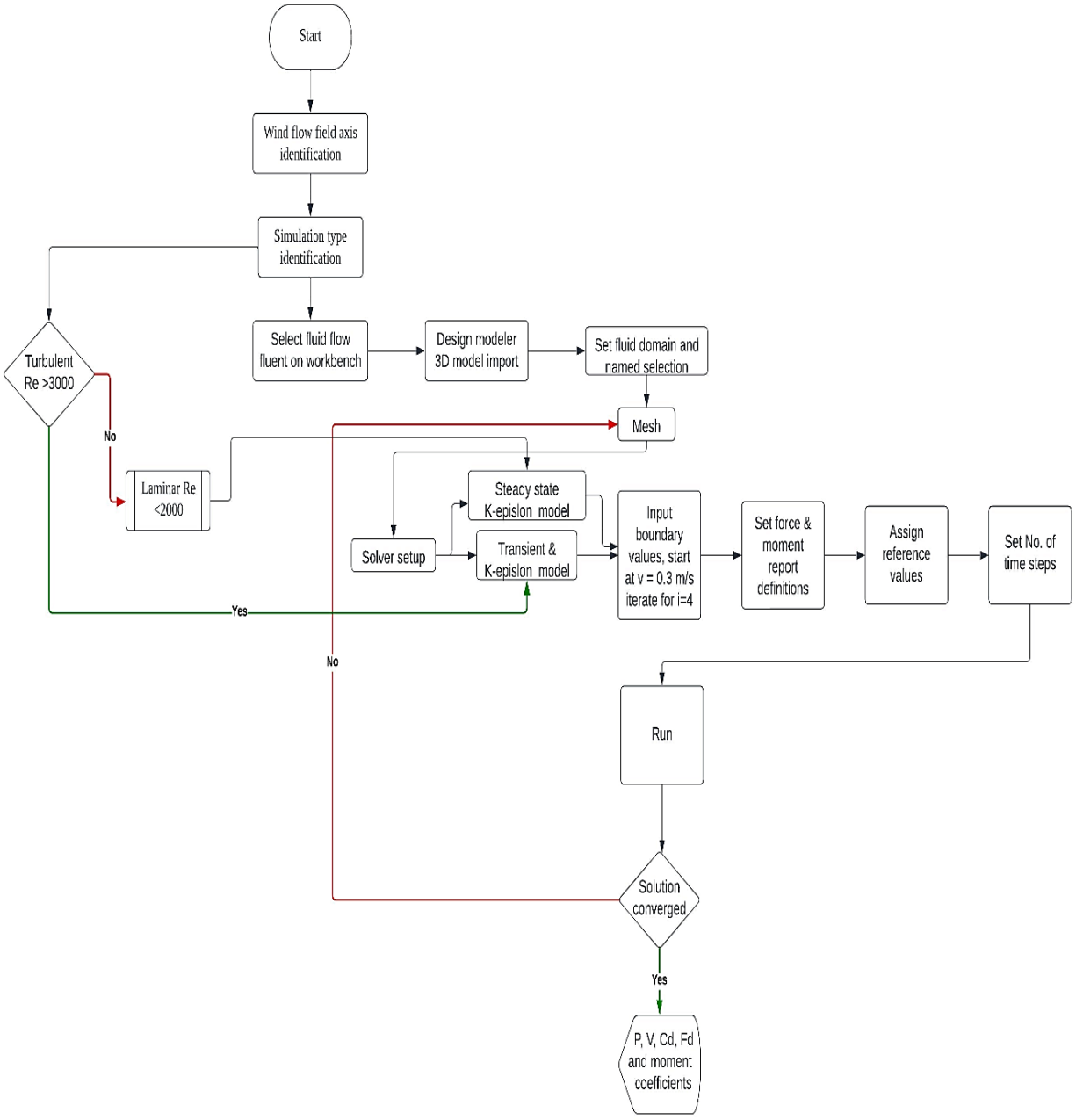

Figure 41. CFD analysis flowchart

3.2.7.1. Wind flow field axis identification

It is assumed in analyzing the wind effect along x and y axis. i.e., horizontal and downwash. The model is symmetry in x-y & y-z plane shown in figure A 62, appendix A. Implies, the quadra chunk represents the whole model. In a sense analyzing wind flow along an inlet axis of positive y-axis has an x-y symmetry plane. Analyzing wind flow along an inlet axis of positive x-axis has a y-z symmetry plane. For the two axis flows i.e., horizontal & downwash, a method of model transformation-rotation of 90^0 was implemented.

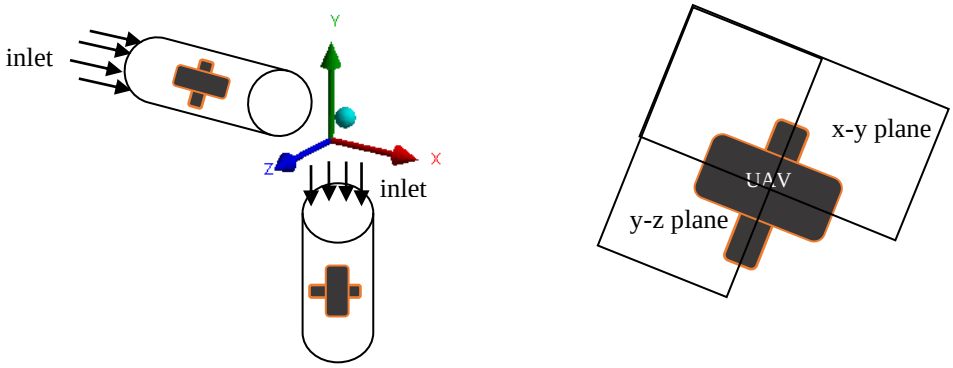

Figure 42. Fluid domain axis and symmetry plane identification.

3.2.7.2. Transient turbulence CFD simulation

After identifying certain steps such as the flow domain, steadiness, model approaches and flow parameters, the flow type with Reynold's number computation CFD simulation method was identified.

Table 7. Simulation type identification for model 2-A.

	Fluid velocity	C-dimension 0.77843 m	Substance Air (25 °C)	Fluid density 1.184 kg/m³	D. viscosity 0.000018 kg/(m·s)	K. viscosity 0.0000157 m²/s
Model 2-A	Fluid velocity 0.3 m/s	Reynolds number = 14864			- The flow is then turbulent.	
	Fluid velocity 0.6 m/s	Reynolds number = 24774				
	Fluid velocity 0.9 m/s	Reynolds number = 34683				
	Fluid velocity 1.2 m/s	Reynolds number = 49547				

Table 8. Simulation type identification for model 2-B.

M2-B with Characteristic dimension 0.20506 m	Fluid velocity 0.3 m/s	Reynolds number = 3916	- The flow is then turbulent.
	Fluid velocity 0.6 m/s	Reynolds number = 6526	
	Fluid velocity 0.9 m/s	Reynolds number = 9137	
	Fluid velocity 1.2 m/s	Reynolds number = 13052	

Table 9. Simulation type identification for model 2-C.

Model 2-C Characteristic dimension 0.48512 m	Fluid velocity 0.3 m/s	Reynolds number = 5046	- The flow is then turbulent.
	Fluid velocity 0.6 m/s	Reynolds number = 8411	
	Fluid velocity 0.9 m/s	Reynolds number = 11,775	
	Fluid velocity 1.2 m/s	Reynolds number = 16822	

Characteristic length is the only changing parameter while the other common parameters are used for the rest of the three models. All the three models fall under turbulence flow of air, since it varies with time without being constant (unsteady/transient), and the model approach which corresponds to this principle is k-ε method, Velocity and additional parameters are obtained using the RANS equation. It uses a discrete phase of k-ε model with one equation type. The transport equation (Hassan et al., 2022) is shown below.

$$\frac{\partial}{\partial t}(\rho u_i) + \frac{\partial}{\partial xj}(\rho u_i u_j) = -\frac{\partial p}{\partial xi} + \frac{\partial}{\partial xj}[(\mu + \mu_t)\left(\frac{\partial u_i}{\partial xj}\frac{\partial u_j}{\partial xi}\right)] \quad \text{..... (5)}$$

Where, p - pressure, ρ - density, μ - viscosity of the fluid, μ_t - turbulent viscosity of the fluid.

3.2.7.3. Dimensions of the flow domain

To execute the computational fluid dynamics analysis which also represents wind analysis and aerodynamic behavior, setting an appropriate flow domain dimension is crucial. it is significant to set an appropriate dimension as per the size of the geometries and standard references of (Zheng et al., 2020; Abu-Zidan et al., 2021). The dimension and named selections are shown in figure 43.

With heights of 216.8m, 277.6 m, 241.25 m for M2-A, M2-B and M2-C respectively, the distance from inlet to the body designated by H1 was set 5 times, 10 time to the outlet designated by H2 or total width designated by H3, and diameter designated by V1 was 5 times of heights of geometries. The ground to nozzle tip designated by V3 was 0.5 m high.

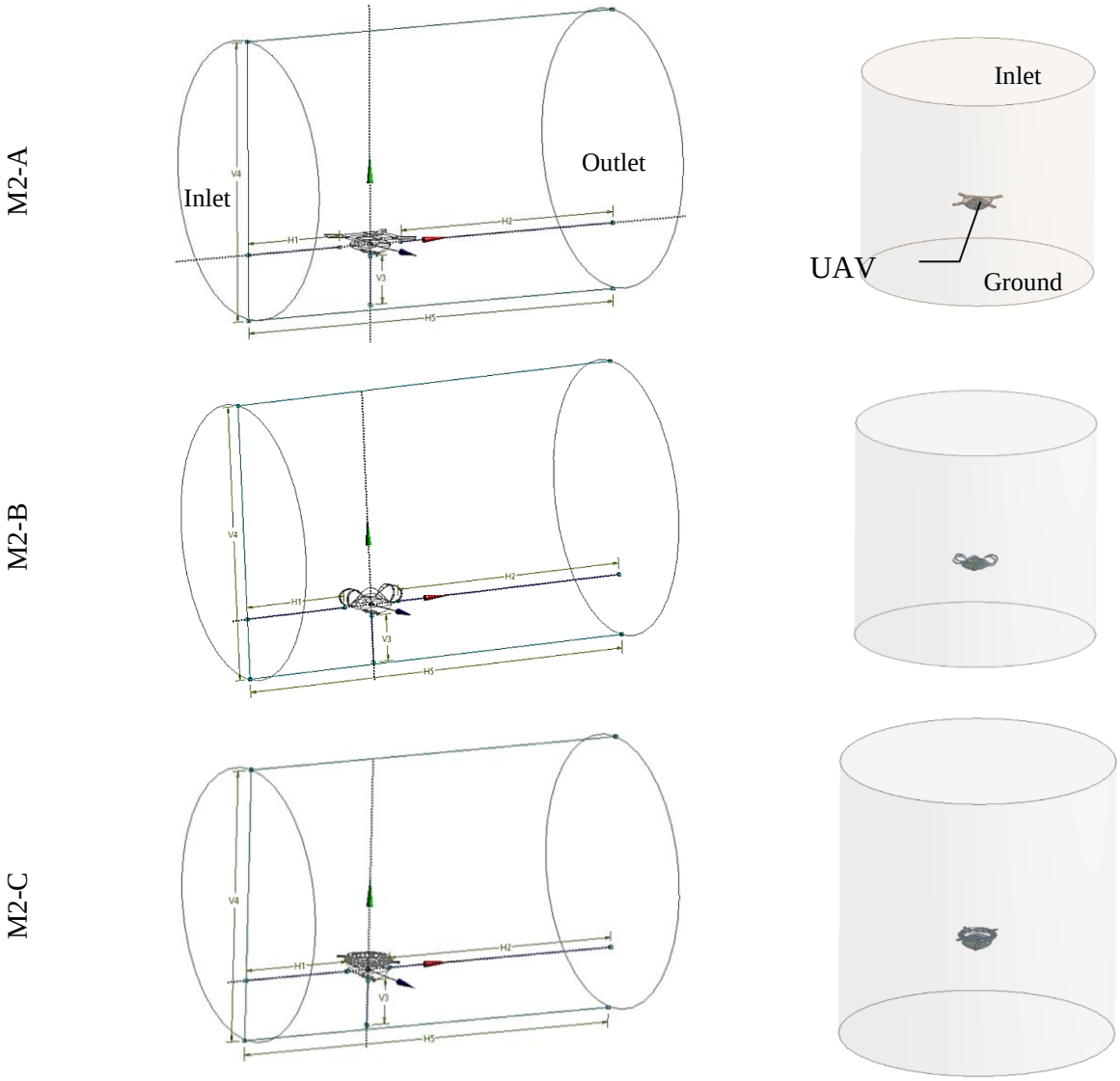

Figure 43. Fluid domain boundary condition along horizontal & downwash flow.

The fluid domain of both fields was identical followed by body transformation. A local axis was located at the center of each model which was necessarily a reference as an input and result interpretation as an output.

3.2.7.4. Boundary conditions

Boundary conditions or correspondingly flow domain is a set of primary criteria to analyze CFD. It consists of cell zones as a named selection which the software knows. The zones include inlet, outlet, walls, and symmetry. The zones were set as velocity inlet, pressure outlet, a geometry as a fixed wall, and a symmetrical exterior/interior wall.

Velocity Inlet boundary conditions are used at the inflow section of the channel in five ranges i.e., $v_w = 0.3\frac{m}{s}, 0.6\frac{m}{s}, 0.9\frac{m}{s}, 1.2\frac{m}{s}\ and\ 2.5\ \frac{m}{s}$.

The outflow boundary condition scheme was set to pressure outlet. As the default is the boundary atmospheric pressure.

To unbound fluid and solid regions at the vehicle and channel surfaces, symmetry boundary conditions were applied. State of the fluid boundary at the fluid zone, air was selected as the fluid substance.

3.2.7.5. Mesh independent analysis (Mesh optimization)

This is a section where the extent of improving the mesh quality is seen. In that, it takes minimum time to compute without compromising out the results and is at a stage where more refinement is impractical and useless.

In order to obtain a balance between a typical geometry at the same time as keeping a quality mesh, the quality of the elements compatible with the meshes was checked with the skewness and drag force Vs number of elements convergence quality standards. A mesh can be considered acceptable when the minimum aspect ratio on the domain is higher than 0.01 and the maximum skewness is lower than 0.98 (Kumar et al., 2021) or the graph of desired variable in this study, he graph of drag force Vs number of elements should approach constant curve showing no further deviations.

The grid independence of the three models showed that as the number of elements rises, the value of a result converges to the same value, as seen by the five, five & five different mesh numbers for the three models respectively. The mesh independence study was initiated with 0.3 m/s of wind speed for all the models.

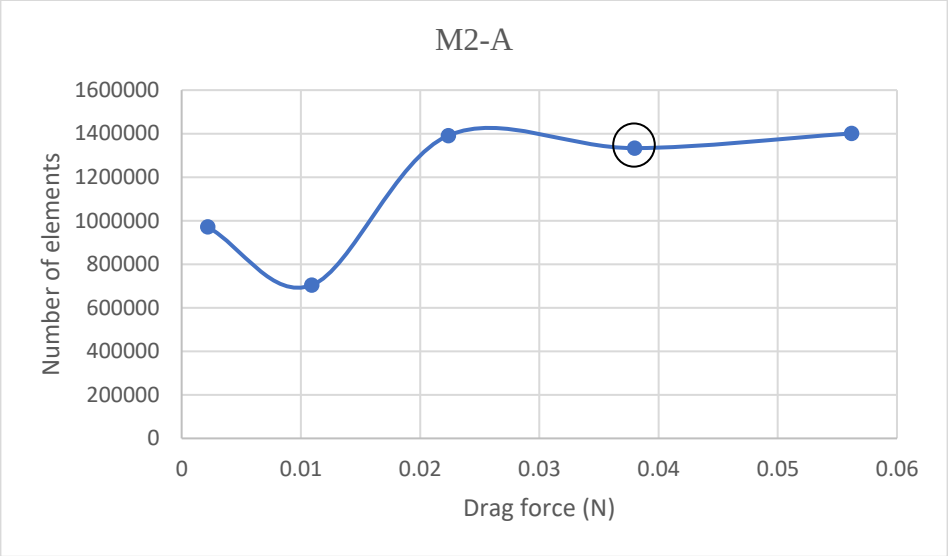

Figure 44. Mesh metrics graph in terms of number of elements for M2-A.

From the observed result in figure 44, the fourth mesh number selected for further analysis was quadratic tetrahedron shell with 1333584 number of elements at 100 mm element size. After the fourth mesh element, the result of drag force remains the same, indicating the mesh is enough for further simulation. The result will not depend on the element size.

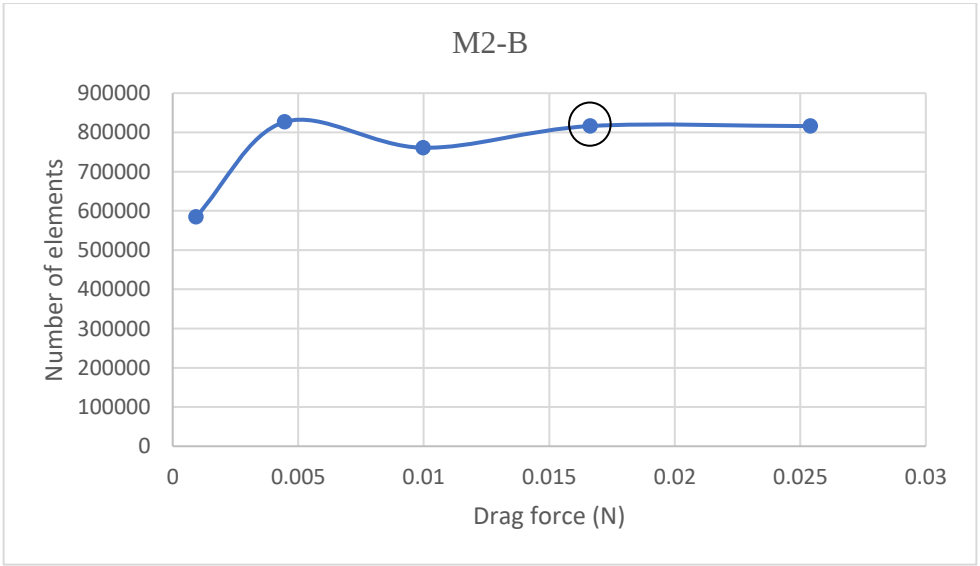

Figure 45. Mesh metrics graph in terms of number of elements for M2-B.

Metrics result in figure 45 shows, the fourth mesh number selected for further analysis was quadratic tetrahedron shell with 816208 number of elements at 132 mm element size. After the fourth mesh element, the result of drag force remains the same, indicating the mesh is enough for further simulation and the result will not depend on the element size.

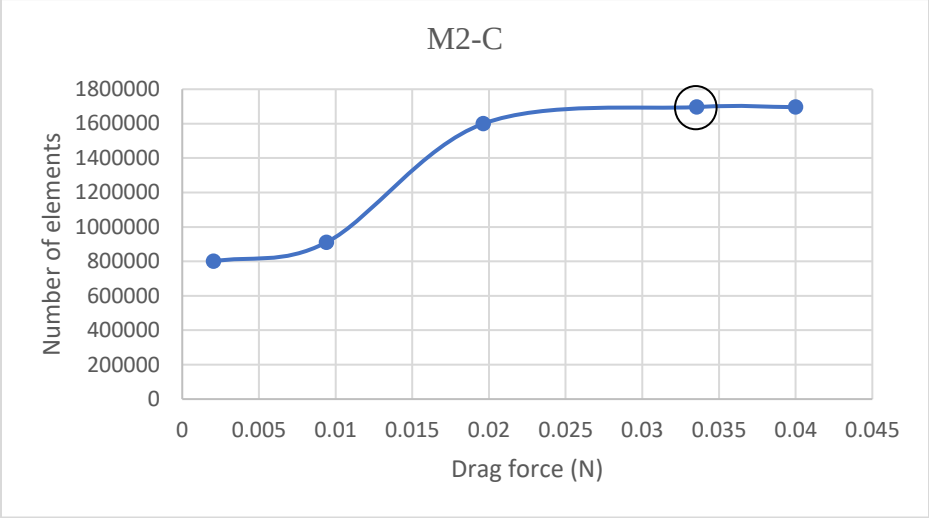

Figure 46. Mesh metrics graph in terms of number of elements for M2-C.

The fourth mesh number with 1696491 elements at 124.2 mm element size in figure 46 was selected for the solution. After the fourth mesh element, the result of drag force remains the same, indicating the mesh is enough for further simulation. The result will not depend on the element number.

3.2.7.6. Computational model setup mesh generation

After the grid independence analysis was studied and validated, the mesh was generated. It was generated with the model of quadratic tetrahedron mesh. Although the hexahedron mesh cell type gives accurate results for simpler geometries & CFD analysis, according to (Abbas, 2018), it has be seen that the higher order hexahedral and higher order tetrahedral elements are almost equally accurate for the same number of degrees of freedom & as per (Lei & Wang, 2020; Qi et al., 2022; Yang et al., 2017) cylindrical flow domain and tetrahedral mesh provide good result for CFD simulation. The flow domain mesh for both along horizontal and downwash flow axis are presented in the figure 47. The model and mesh metrics of validation model has been presented in appendix B, figure B 63 and appendix C, figure C 64 respectively.

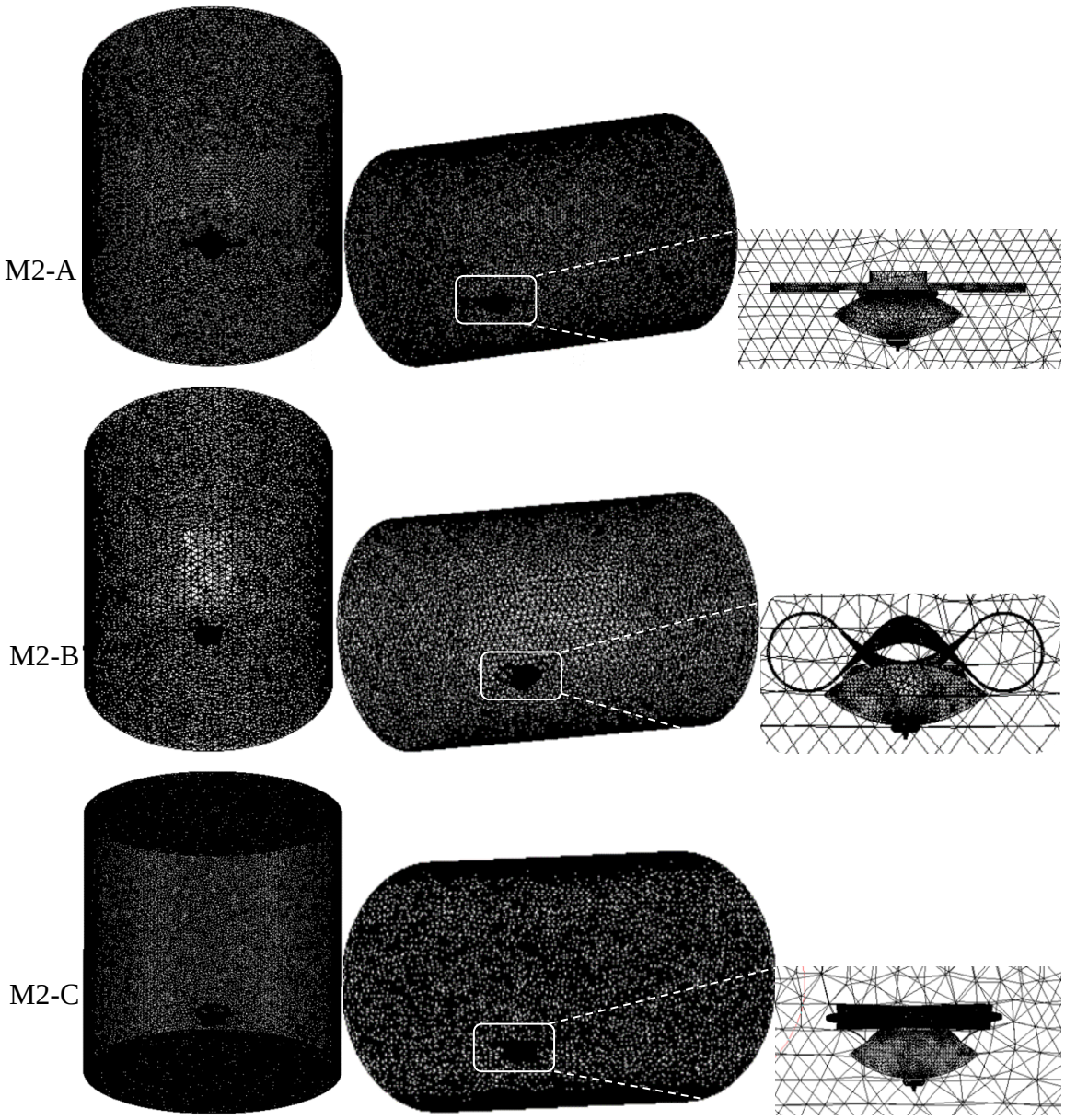

Figure 47. Fluid domain mesh generated image of variants along horizontal and downwash flow axis.

3.2.7.7. Simulation

The simulation has been carried out using Ansys 2020/R1 fluid flow (fluent) toolbox. After the models were designed, each were exported to workbench under geometry section of fluent tool box which was followed as one step for mesh optimization through skewness. After the independence/convergence study, each model was exported to solver setup where general transient, boundary conditions, schemes and methods are assigned.

Then it was initialized and run. After solution convergence, the solution section was updated and results were written in the FFT file directory. The simulation was to run at hovering with an altitude of 0.5 m from the ground. The wind gust velocities according to the researches at this working height is 1m/s (Ling et al., 2018) and 0.3 – 1.1 m/s as per (Lei & Lin, 2019). Basing these, the inlet air speed was set.

A supportive research findings by (Prudden et al., 2018) magnified the analysis for flow components of wind speed. The scholars actually used a field based experimental test using probe sensor mounted quadcopter UAV to estimate wind speeds at different elevations. According to the scholars, the probe's angle was taken into consideration while calculating the wind components because the Inertial Measure Unit (IMU) and probe axis were aligned. The probe's 90-degree cone of acceptance would therefore enable the capturing of off-axis flow vectors even though it would only be aligned with the flow at one wind speed. The probe's twin function of flow measurement and phased-advanced turbulence mitigation required that the forward-mounted position can adequately capture wind value. Following these, the simulation was directed to axis-oriented analysis. Then it was run with finite volumetric analysis using k-ε model under Reynolds navior stock method with a convergence criterion of 10^{-3}.

CHAPTER FOUR

RESULTS AND DISCUSSION

This is a section where detailed findings of the numerical simulation analysis with validation from the previous section are presented and discussed. Major findings namely the pressure distribution, wind velocity magnitude & its distribution over the surface, drag coefficient/force effect on the bodies, and moment coefficients that were created due to horizontal & downwash wind flow to alter the orientations of the bodies with their minor results has been discussed.

Results of the expected objective parameters for all the three models including validation model was obtained for wind speed ranges of 0.3, 0.6, 0.9, 1.2 and 2.5 m/s. According to (Qi et al., 2022), the findings of velocity magnitude distribution on UAV model for the downwash flow along y-axis for x distribution when the UAV located at 0.5 m above the ground for all wind gusts (m/s) showed a close result with this research finding. The difference lied on rotor effect inclusion. Specifically, according to the scientific findings of (Li et al., 2022), the profiles of velocity magnitude variation along horizontal axis and downwash axis has shown a similar scientific finding in that it increases at free streamline while decreases as it approaches a certain surface.

4.1. Downwash flow at 0.5 m hovering height and with alteration of altitude

4.1.1. Velocity magnitude

A result of the expected velocity magnitude for downwash analysis has been presented in figure 48. The velocity streamline/contour of each model at all wind speed ranges during downwash flow has been presented in appendix D, figure D-12 & D-14. The contours under the appendix depicted above clearly showed the fluid flow structural interaction where the magnitude of the wind rises and declines, where flow separation started, and maximum and minimum values of velocity developed.

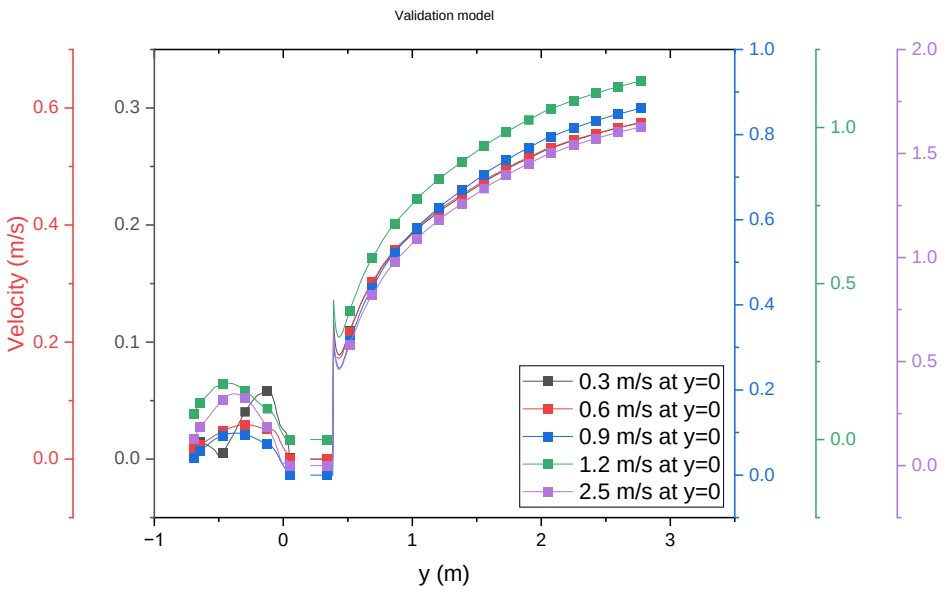

(a)

Plot of velocity distribution on external model for downwash flow shown above in figure 48 (a), describes the extent of velocity during inflow and outflow at all wind speeds.

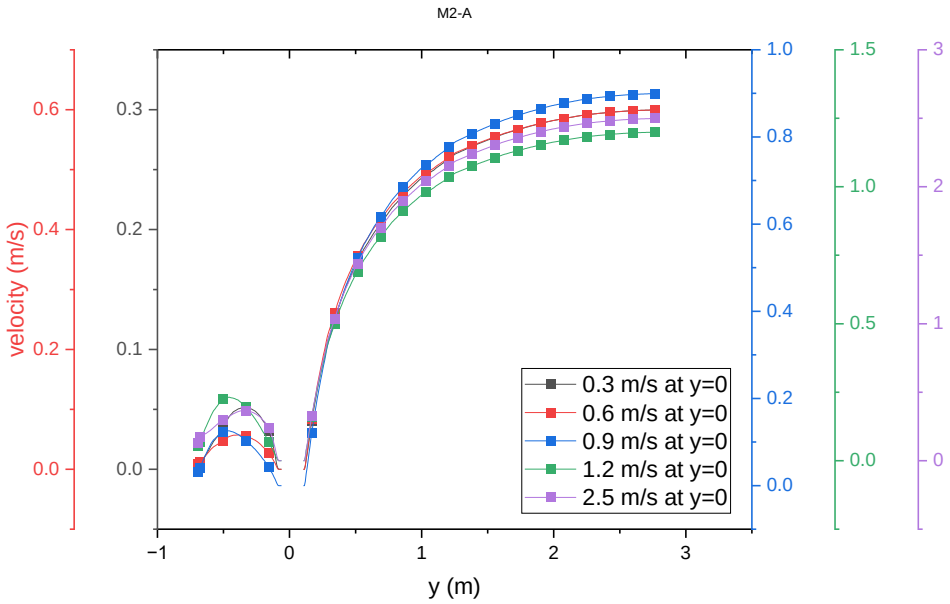

(b)

The amount of velocity during inflow and outflow at all wind speeds is described by the plot of velocity distribution on M2-A for downwash flow, which is depicted above in figure 48(b).

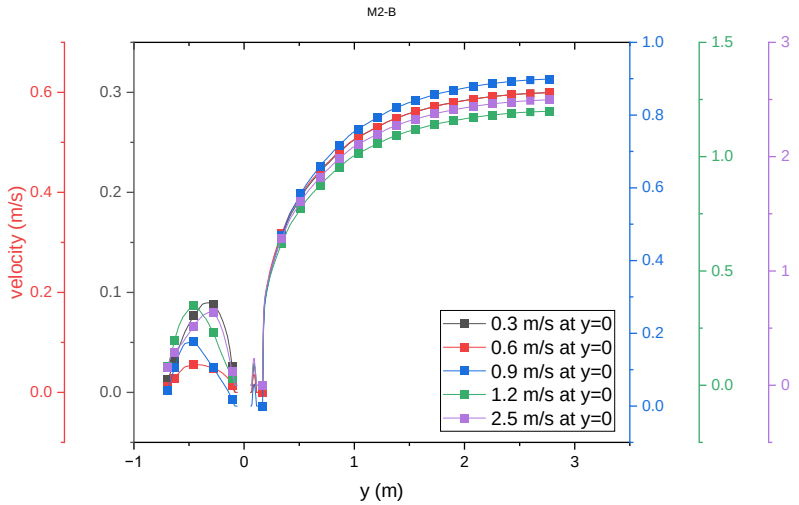

(c)

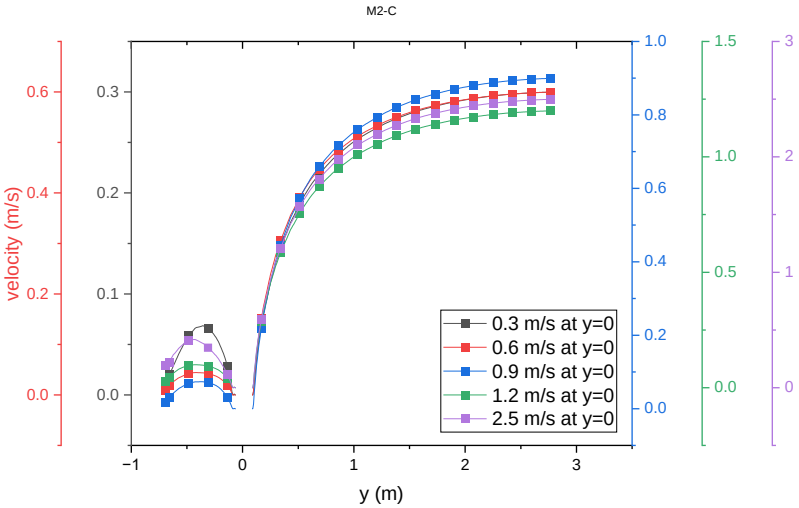

(d)

Figure 48. Velocity magnitude with respect to position for all models.
(a)-validation model, (b)-M2-A, (c)-M2-B, (d)-M2-C

In the case of downwash wind flow, the wind exhibit keeping its inlet velocity of 0.3, 0.6, 0.9, 1.2 and 2.5 m/s with a slight decline in a fraction of integers till a position of 2.5 m above the origin (inlet flow) of all the models in common. In figure 48-a, after a location of 2.5 m high, the velocity visibly becomes decline until a position of 0.5 m and shows a rise by a value of 0.09 m/s on all speed ranges, this is due to the particles have got a free streamline at that position. Declines back constantly where a surface has met at 0.47 m location and constantly flows as it reaches the top surface.

After leaving the origin, since it is leaving the bottom surface of the body besides, it gains a free stream space, its velocity increases again from 0 to 0.1 m/s for 0.9 m/s inlet velocity, 0 to 0.08 m/s for 0.6 m/s inlet velocity, 0 to 0.27 m/s for 2.5 m/s, 0 to 0.17 m/s for 1.2 m/s inlet velocity and 0 to 0.07 m/s for 0.3 m/s inlet velocity. A major difference in magnitude between the models was seen at the outflow. Another important finding was that, a decline in velocity magnitude after a location of 0.5 m below origin was observed caused due to the ground wall boundary condition. This profile applied on all models.

It was detected a similar velocity magnitude decline in the rest of the models as shown in figures 48-b-c-d for inflow region. The difference in magnitude lies at the outflow. Maximum wind speed of 0.47 m/s, 0.53 m/s and 0.48 m/s on M2-A, M2-B and M2-C for 2.5 m/s inlet velocity (wind speed) were respectively, observed. This showed how significant geometrical shape is for aerodynamic study particularly at the outflow region.

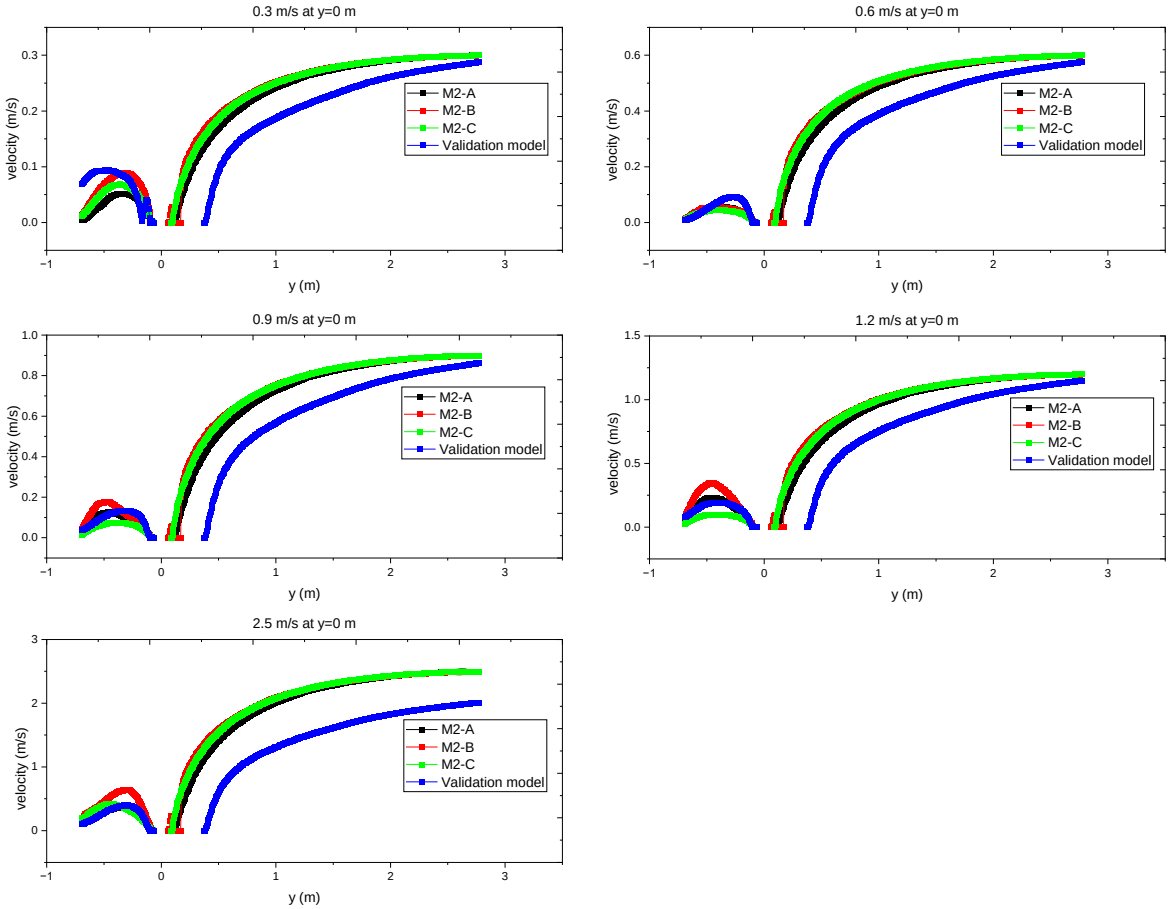

Figure 49. Models compiled plot of velocity magnitude vs position at variable wind speeds.

Compilation of velocity magnitude of variable wind speeds on all models is presented in figure 49. This plot compares magnitude and profile of wind velocity effect on each model. It was observed that, validation model had a 9.94 % deviated variance from the rest of the models within the five wind speed ranges. In general, the plot above showed a common-sense depicting velocity decline at inflow and a rise at a position of 0.5 m during outflow. Which shows that the method is acceptable for further analysis. Apart from this, M2-B showed a large velocity at 0.5 m position during outflow after 0.9 m/s of wind inlet as compared to all other models.

4.1.2. Pressure distribution

The profile of the pressure distribution during downwash over the entire zone for all the models in terms of their position is plotted below.

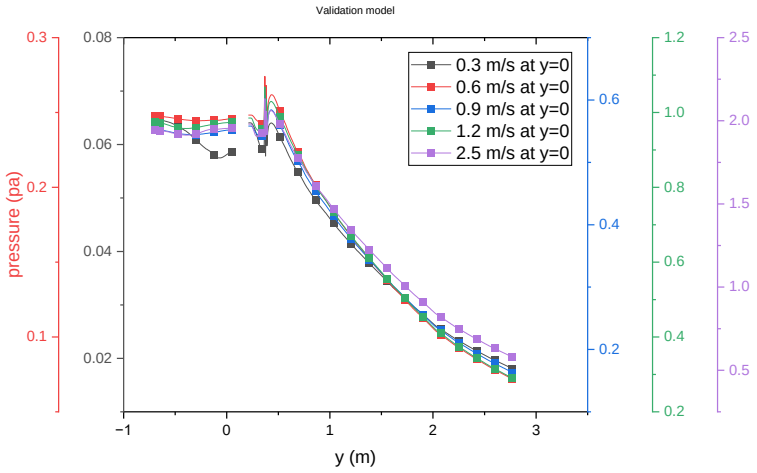

(a)

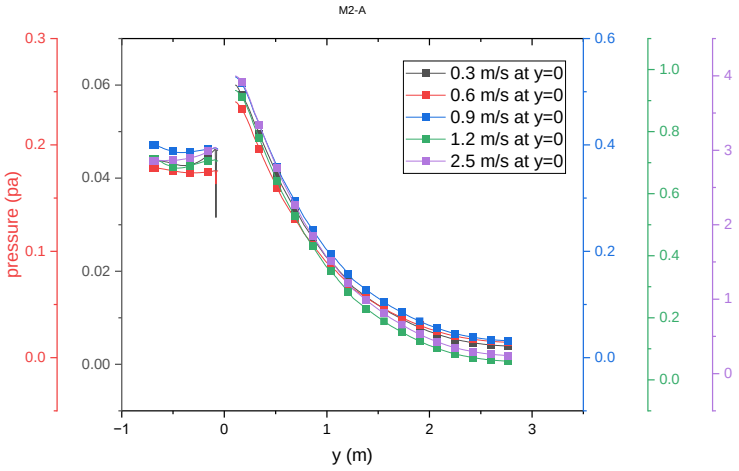

(b)

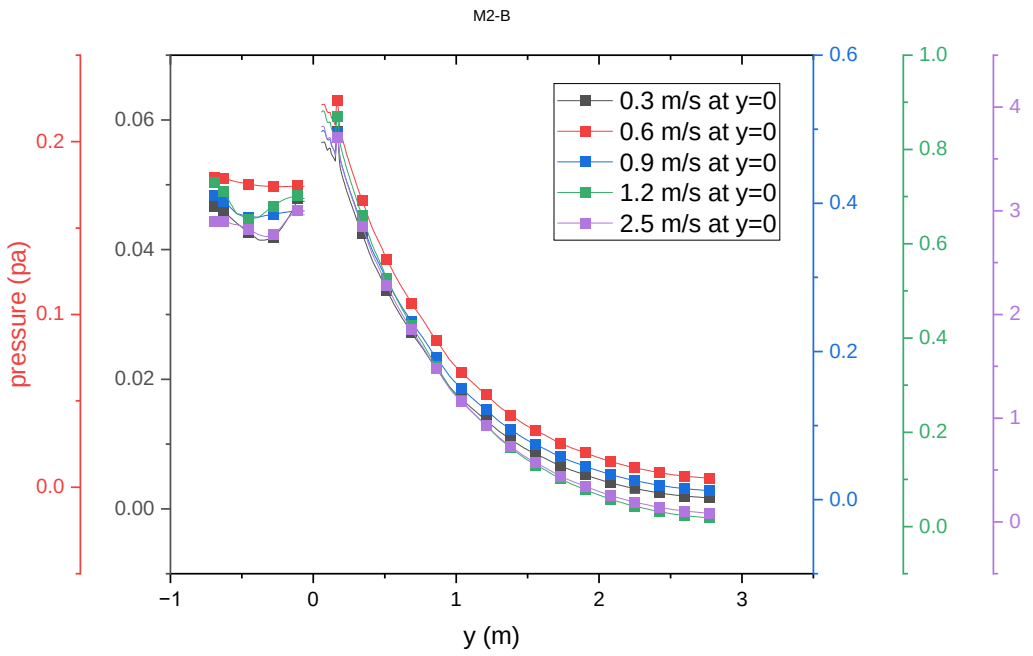

(c)

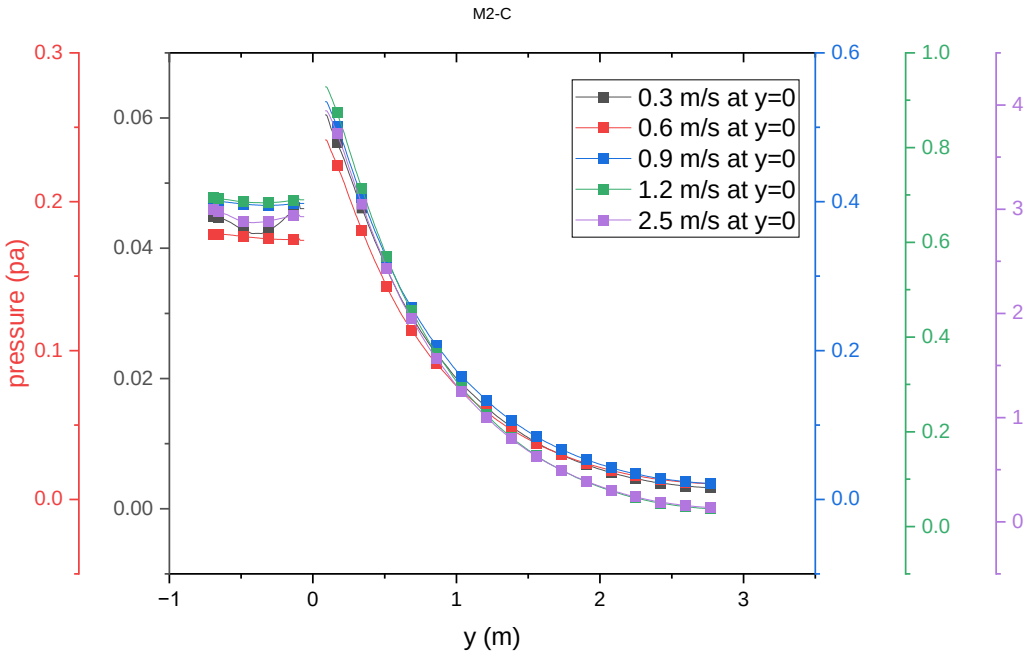

(d)

(a)-validation model, (b)-M2-A, (c)-M2-B, (d)-M2-C

Figure 50. Pressure with respect to position for all models.

Contours of velocity distribution during horizontal flow on all models at all wind speed ranges has been collectively presented under appendix D, figure D-13 and D-15.

From figure 50-a, pressure magnitude of validation model due to the wind effect can be seen. When the inlet velocity was 0.3 m/s, the minimum inlet pressure was 0.019 pa which means almost an atmospheric pressure. Visibly as particle flow approaches the surface of the model, the pressure showed a rise to a maximum value of 0.061 pa which is still a lower value as compared to the remaining wind speeds which reaches to 2 Pa at 2.5 m/s inflow. During outflow, the pressure showed a 2% decline & kept flowing constant. Correspondingly, figures 50-b-c-d reveals findings of pressure magnitude for M2-A, M2-B and M2-C respectively. During inflow, at a position of 2.7 m, a minimum pressure value with the extent of atmosphere was seen in common. Increasing linearly, when in contact with the top surface of the three models where flow separation/boundary layers appear, its pressure rises to a maximum value of 0.059 Pa for 0.3 m/s inflow, 0.242 Pa for 0.6 m/s inflow, 0.52 Pa for 0.9 m/s inflow, 0.91 Pa for 1.2 m/s inflow and 3.91 Pa for 2.5 m/s inflow for M2-A. During outflow, the pressure showed a 14% decline, rise at 0.45 m location below origin & kept flowing constant. The data point records showed approximately a similar pressure value trend on remaining models M2-B & M2-C.

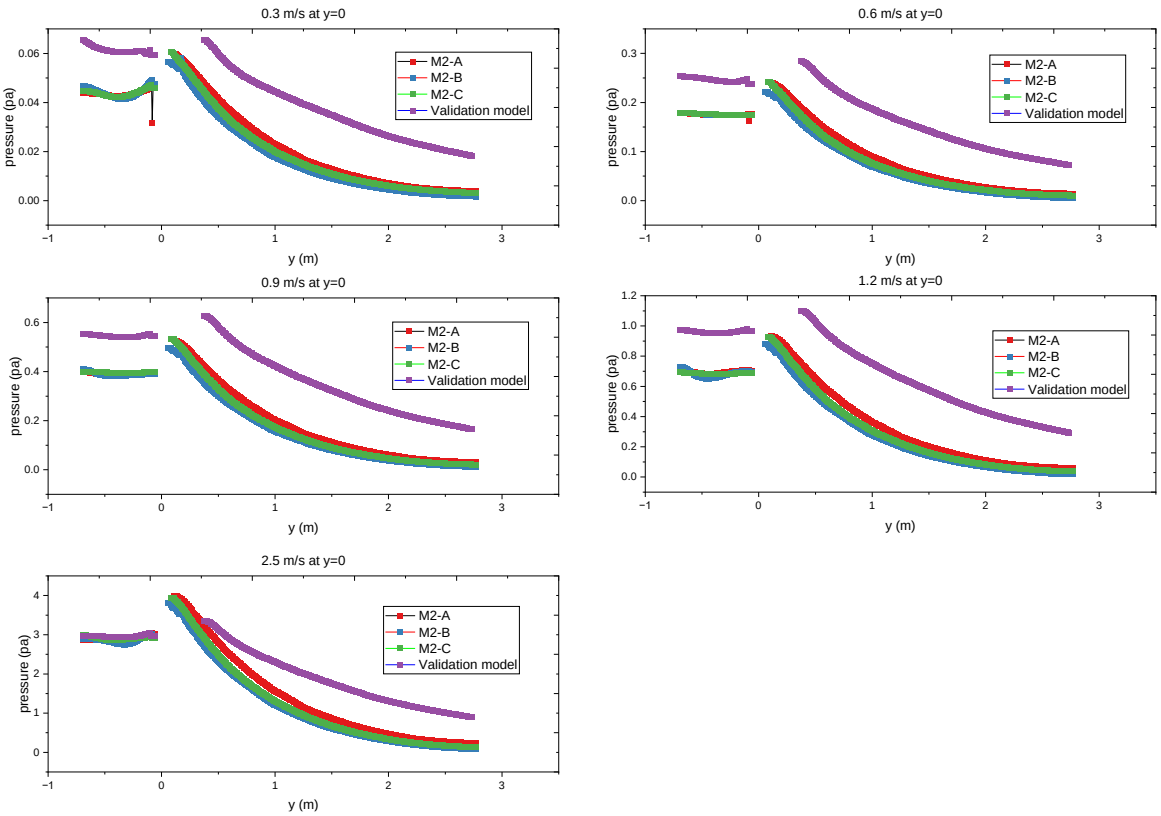

Figure 51. Models compiled plot of pressure vs position at variable wind speeds.

Each plot of pressure distribution versus position for all wind speed as shown in figure 51 has a viewable deviation. In common, the pressure flow at the inlet is low while it becomes increased till position of 0.175 m before reaching the local origin of the body. This is because the velocity decreases as it reaches the frontal face due to impact flow separation occur and pressure develops. Except 3.5 % error deviation of M2-B from M2-A & M2-C on all wind speed ranges, except between the position of 0.5 – 2.5 m during inflow, the profile overlaps & values are close on the remaining locations. Other finding lies in the region of outflow where at initial stage of outflow pressure difference was generated, in the middle at 0.5 m domain location, pressure declines due to free stream high velocity rate after that rises because of the ground surface effect & flows constant.

4.1.3. Drag coefficients and forces

The drag expected to occur on the surface of the rectangular solid, crossed helical, and mobius ring all with elliptical hopper geometry of drag effect simulated relative to the variable wind speed ranges for downwash flow is shown below.

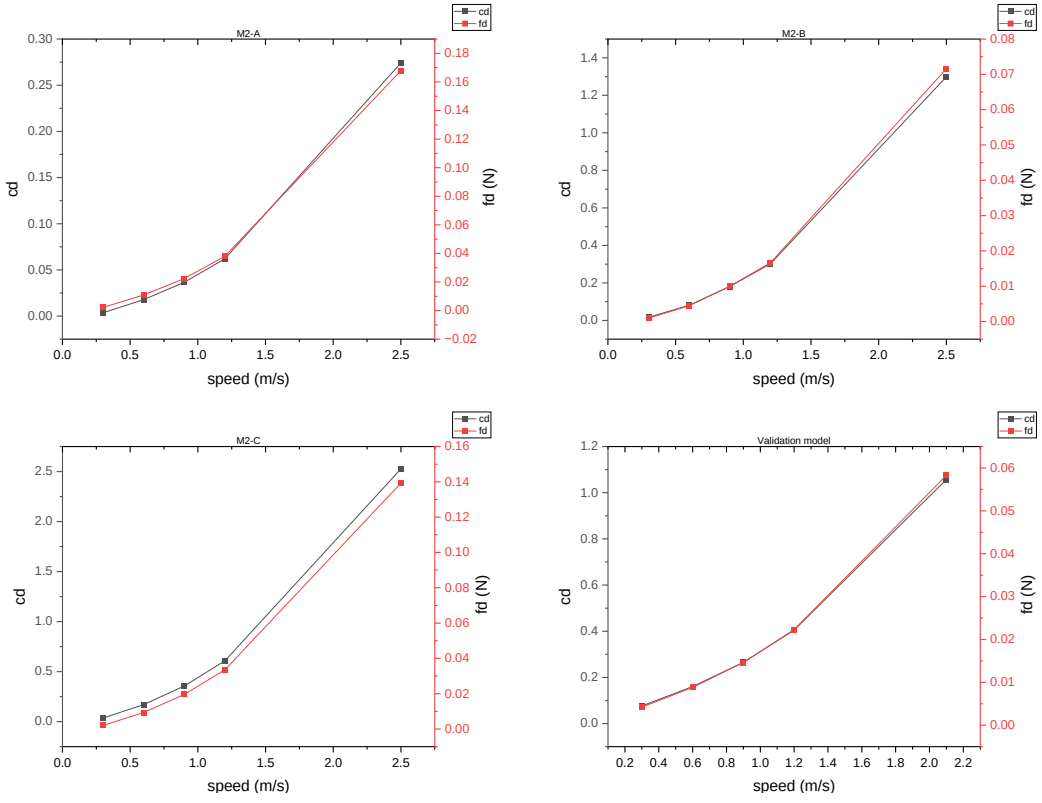

Figure 52. Drag force and coefficients with respect to variable wind speed.

As the air speed increases, the drag force (fd) and drag coefficient (cd) that is anticipated to occur on the surface of all model geometries increases and is projected to the extent of scientific discoveries of (Paz et al., 2020). According to (Prudden et al., 2018), drag also has its own effect on stability so a minimum amount is desirable. In comparison as shown in figure 52, the drag coefficient value of model 2-A tells that at wind speed of 0.3 m/s is 0.00355 but it reaches 0.274 for wind speed of 2.5 m/s where the altitude has increased. While M2-B had minimum cd of 0.0167 at 0.3 m/s wind flow, maximum cd of 1.29, M2-C resulted a minimum cd of 0.0369 at 0.3 m/s wind flow, maximum cd of 2.5 at 2.5 m/s and validation model had revealed a minimum cd of 0.076 at 0.3 m/s wind flow, maximum cd of 1.057 at 2.5 m/s which showed a desired cd value on M2-A.

4.1.4. Pressure contour & stability effect

Figure 53-a, b below shows pressure contour over the entire zone for all the models in terms of their wind speed. From previous section, stability was determined in-terms of moment coefficients that are created during orientation of the models due to wind gust.

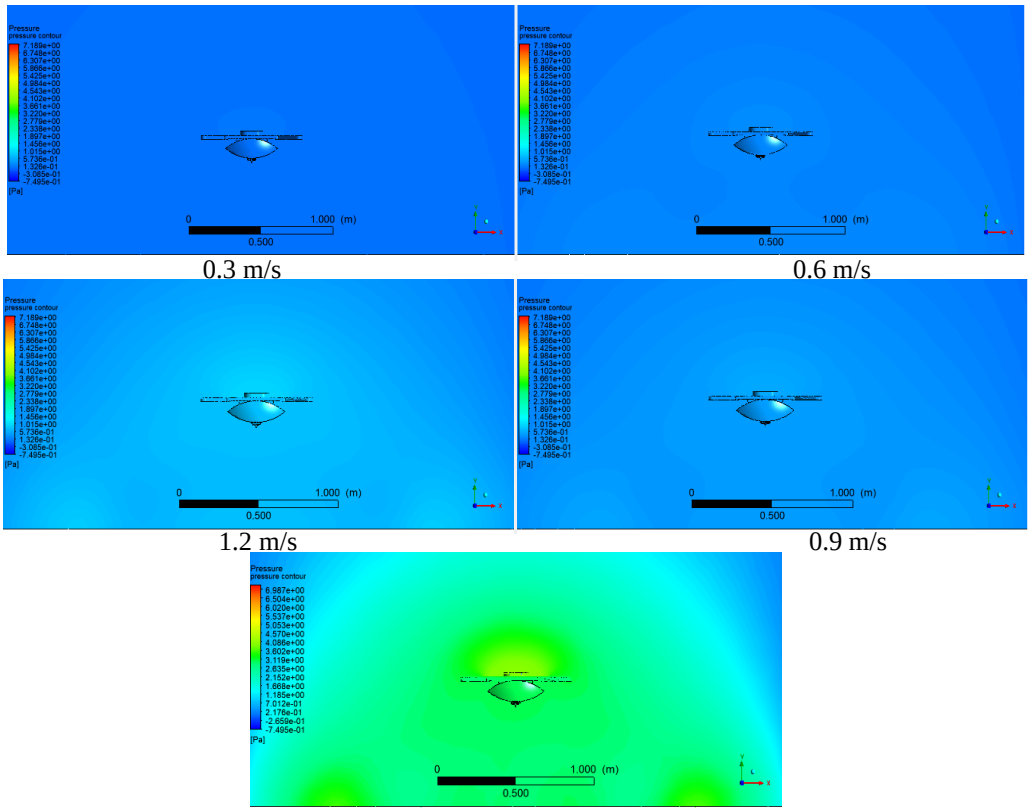

0.3 m/s 0.6 m/s

1.2 m/s 0.9 m/s

2.5 m/s

(a)- pressure contour

Contours of static pressure on the ambient and surface of the models is presented in figure 53-a. referring from the simulation result presented in the figure, variation of pressure contour/magnitude was visibly seen at each wind flow speeds. The maximum pressure on the ambient was 0.137 pa & model was 0.75 pa near and top surface around the deadweight. Then there was a decrease after flow separation where it thinks to develop a negative pressure. Magnitude of pressure contour for the remaining wind speed (0.6, 0.9, 1.2 & 2.5 m/s) depicted the same trend. A maximum pressure of 3.827 Pa has been observed when the wind flows at 2.5 m/s asshown in figure 53-b.

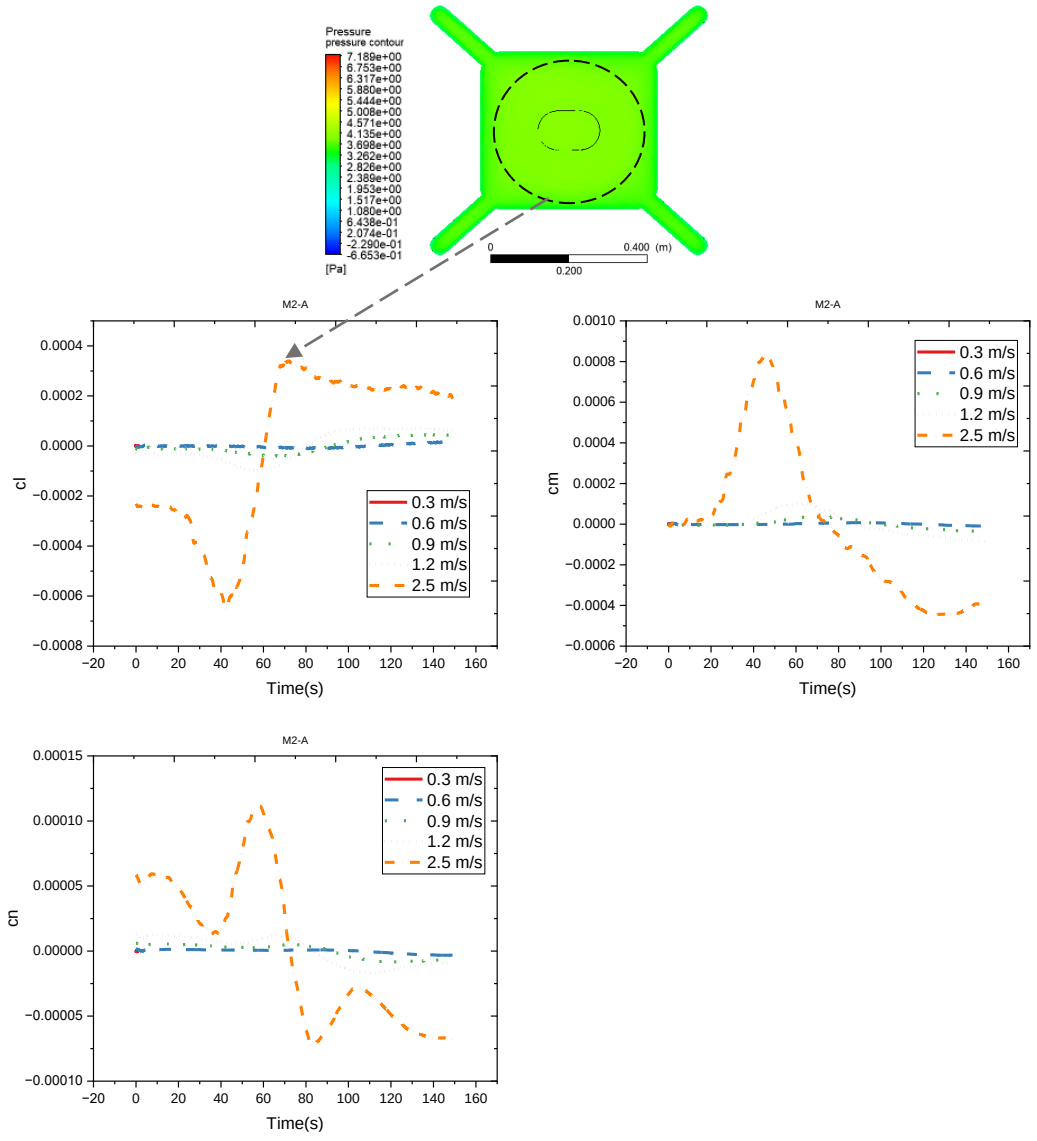

(b)- time response of moment coefficients

Figure 53. Contour plot and impulse response of model 2-A along downwash flow.

Findings of stability in-terms of impulse response, according to the scientific statement of (Paz et al., 2020), the impulse response of all coefficients should converge constantly to almost zero after a certain wind disturbance or have a continuous sine wave. Following these, as shown in figure 53-b, a pressure of 3.827 pa has resulted a disturbance impact for about 110s creating alteration on all moment coefficients. Specifically, cl and cm were imposed by 0.0004 & 0.0008 at 2.5 m/s. after 120s, the result outlines the convergence of cl, cm and cn for all wind speed ranges. The justification for a start of negative amplitude on cl indicated that, the extent of disturbance created was to anti-clockwise direction with a magnitude of 0.00022.

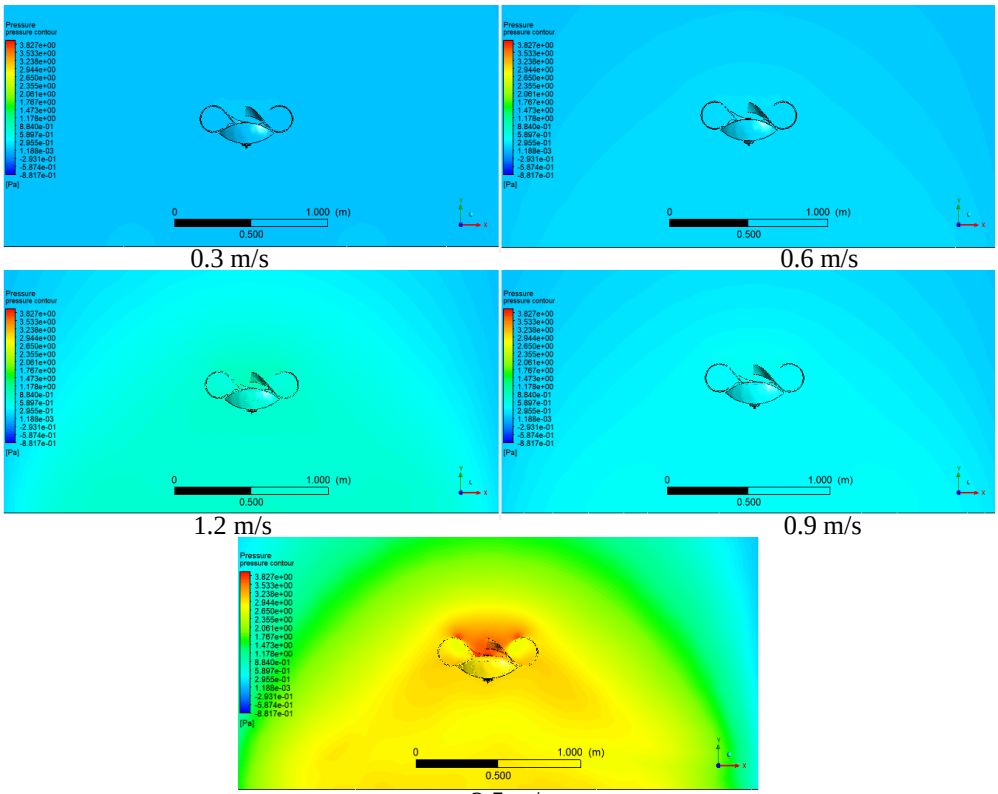

(a)- pressure contour

Pressure on the ambient and surface of the models is presented in figure 54-a. From the simulation result, variation of pressure contour/magnitude was visibly seen at each wind flow speeds. Pressure at inflow wind speed of 0.3 m/s experienced a maximum value at top & inside frame region of 0.295 Pa. The maximum pressure on the ambient was 2.65 Pa & model was 3.827 Pa near top surface around the deadweight & frame surfaces when the wind flows at 2.5 m/s.

Then showed a decrease after flow separation where it thinks to develop a wake propagation. Magnitude of pressure for 0.6, 0.9 and 1.2 m/s wind speeds depicted the same trend except a magnitude of pressure occurrence. Location of surfaces of max. contour was shown in figure 54-b. during all speed ranges, another maximum pressure regions were observed near the ground with a value of 0.78 Pa at 0.6 m/s, 0.88 Pa at 0.9 m/s and 1.1 Pa at 1.2 m/s wind flow.

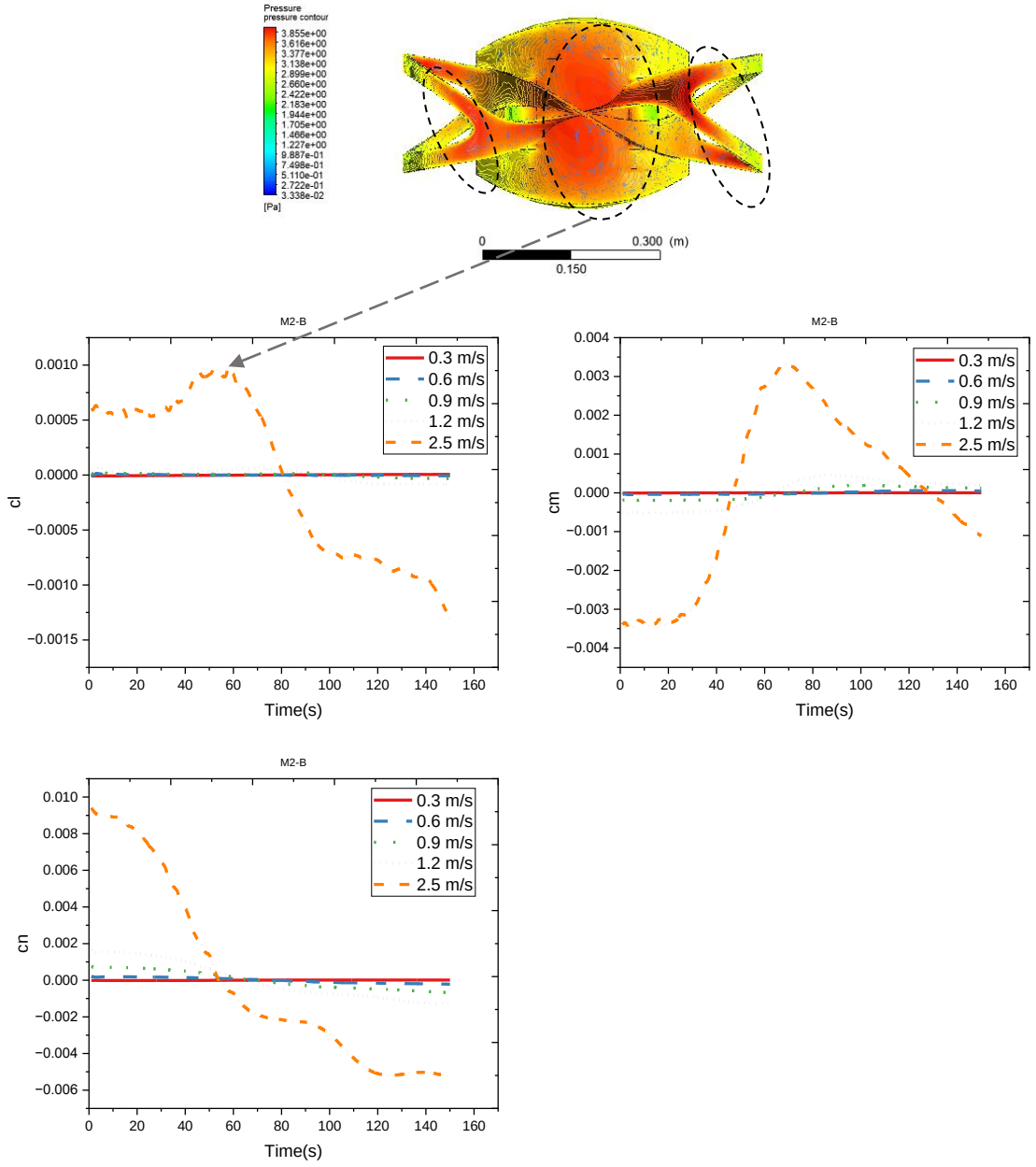

(b)- time response of moment coefficients

Figure 54. Contour plot and impulse response of model 2-B along downwash flow.

As shown in figure 54-b, one factor wind/pressure load due to downwash flow had resulted an alteration in moment coefficients. The impulse response of all coefficients showed a disturbance until 120 s with variable extent of wave peak & valley. This was due to a pressure of 3.855 Pa which has resulted a disturbance impact for about 120s creating alteration on cl, cm & cn for higher band.

No wavelets were imposed at 0.3 m/s inflow in figure 54-b. which shows that stability was constant. Less than 0.0005 peak wave with constant convergence after 100 s at 0.6 m/s flow, < 0.001 peak wave with constant convergence after 100 s at 0.9 m/s flow, and < 0.0019 peak wave with constant convergence after 100 s was seen at 1.2 m/s inflow. which finally shows the amplitude of moment coefficients was less disturbed for 100 seconds varying in peak values at 0.6-1.2 m/s wind speeds. As compared, the disturbance was more on yaw (cn) moment. While a higher wavelet of 0.01 have resulted instability on cl, cm with low rate of constant convergence and higher instability and convergence on cn. The justification for a start of negative amplitude on cm indicated that, the extent of disturbance created was to anti-clockwise direction with a magnitude of 0.0032.

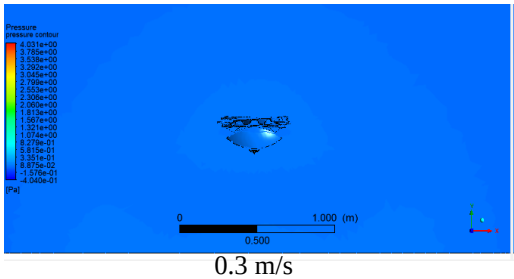

0.3 m/s

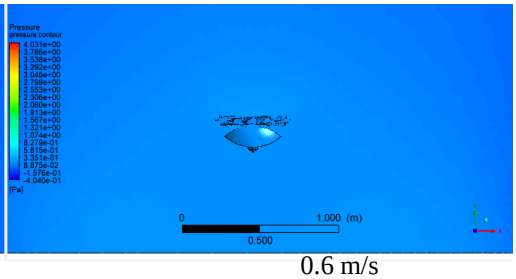

0.6 m/s

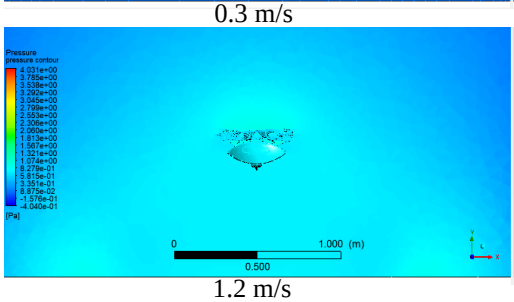

1.2 m/s

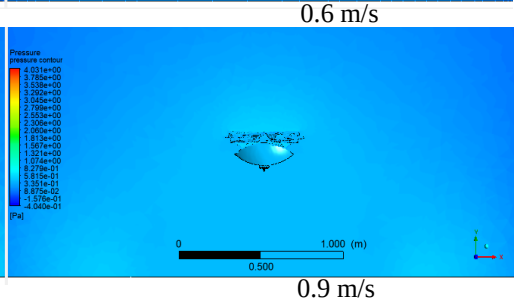

0.9 m/s

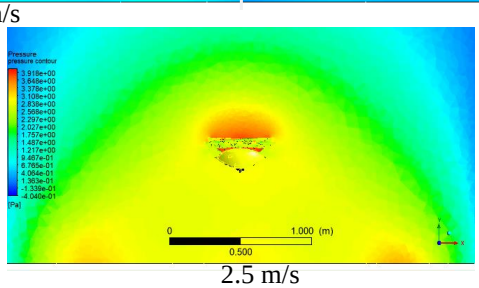

2.5 m/s

(a)- pressure contour

Figure 55-a shows the static pressure contours on the models' surface and surrounding air. Referring to the simulation result shown in figure 55-a, the profile and amount of the pressure varied noticeably at each wind speed. The deadweight & frame surface was surrounded by 3.91 pa of model and maximum ambient pressure. Then, after flow separation, it showed a reduction where it appeared to be developing a negative pressure. The magnitude of pressure showed the same pattern at wind speeds of (0.6, 0.9, 1.2, and 2.5 m/s). A maximum pressure of 3.931 Pa has been recorded at 2.5 m/s wind speed. Besides, region of maximum pressure near the ground was observed due to wall boundary layer and flow separation. Maximum contour was shown in figure 55-b.

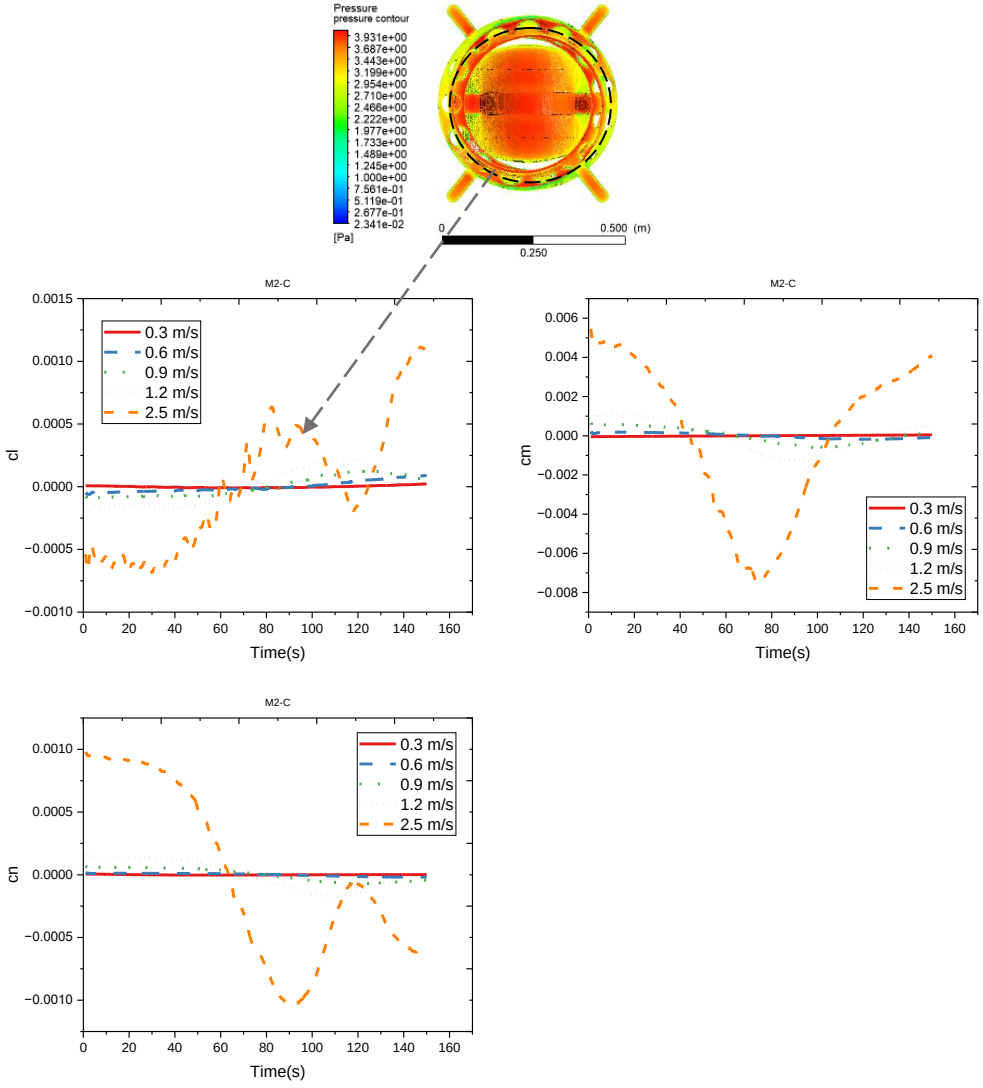

(b)- time response of moment coefficients

Figure 55. Contour plot and impulse response of model 2-C along downwash flow.

The impulse response of cl, cm and cn at 0.3 – 2.5 m/s wind speeds was plotted. As shown in figure 55-b, a pressure of 3.931 pa has resulted an impact for about 120s creating alteration on all moment coefficients for lower band pass and 100s for high band pass. In figure 55-b, no wavelets were applied at 0.3 m/s inflow, demonstrating that stability was constant. At 0.6 m/s flow, a peak wave with constant convergence after 120 seconds was less than 0.0001, at 0.9 m/s flow, a peak wave with constant convergence after 120 seconds was less than 0.00098, and at 1.2 m/s inflow, a peak wave with constant convergence after 120 seconds was less than 0.001. It demonstrated that for 120 seconds, moment coefficient amplitude was less disrupted, with peak values occurring at wind speeds between 0.6 and 1.2 m/s. In contrast, the roll (cl) moment disruption was more pronounced. While a higher wavelet of 0.01 at 2.5 m/s has led to stronger instability and convergence on cm, cl, and cn with low rates of constant convergence. The justification for a start of negative amplitude on cl indicated that, the extent of disturbance created was to anti-clockwise direction with a magnitude of 0.00052.

4.2. Horizontal wind field at 0.5 m hovering height with alteration of altitude

Similarly, besides findings of objective parameters at 0.5 m height and constant altitude from the ground, results of parameters at 0.5 m height but when the altitude increases (wind speed increase) have also been presented.

4.2.1. Velocity magnitude

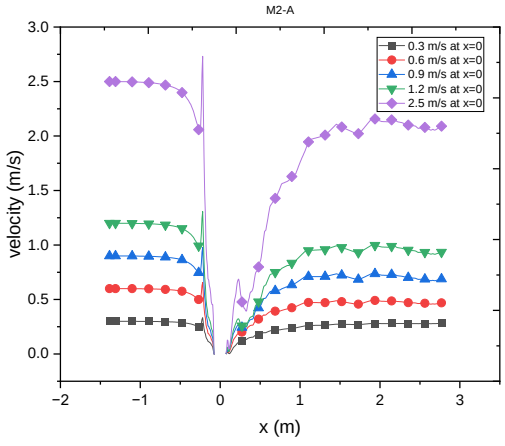

(a)

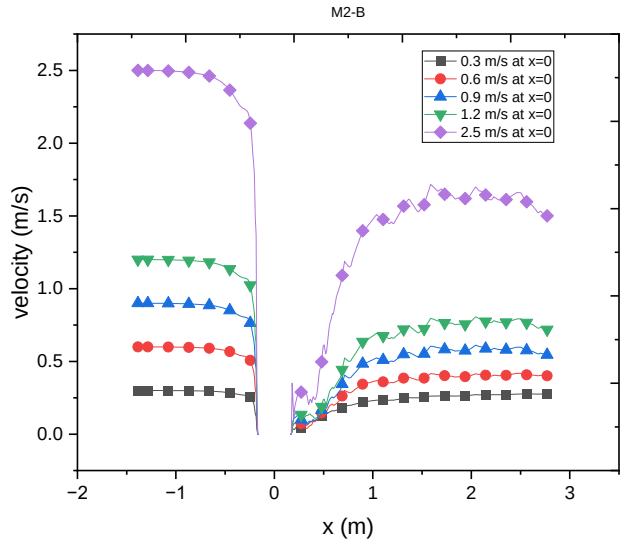

(b)

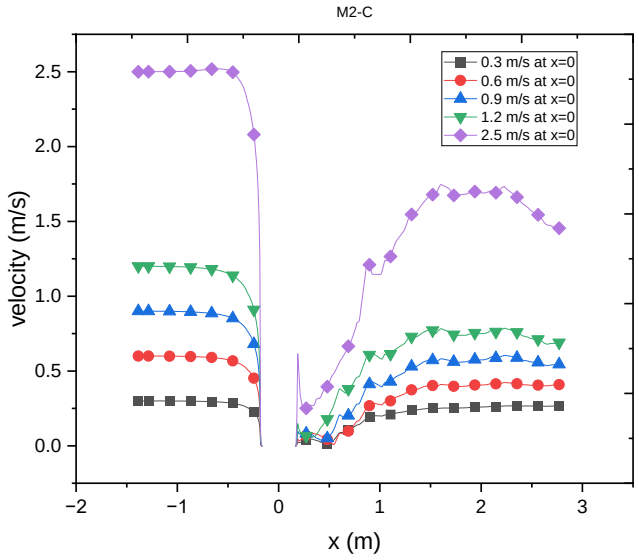

(c)

Figure 56. Plots of velocity magnitude for three models along horizontal wind flow.

Velocity magnitude of wind flow coming along sideways horizontally has an inlet and outlet profiles. Variable wind speeds from 0.3 – 2.5 m/s have shown a common profile that there exists a constant wind flow before reaching the frontal surface of the UAV models at average location of 0.078 m from both sides in figure 56 a-b-c.

After 0.078 m location from left side/inflow or as wind particles starts contacting the surface of the models these velocity vs position plots have visibly showed a decline on all 0.3-0.6-0.9-1.2-2.5 m/s speed ranges. This is because, particles energy due to motion due to contact & collision of particles with the surface of models converted in to the energy due to pressure. In between the region of 0.078 m from both sides since they are rigid bodies wind particles cannot pass through the walls as this plot was generated horizontally along the center of the bodies.

4.2.2. Pressure distribution

Pressure contour plot of a wind field coming horizontally along x on all models was obtained in figure below. Figure 57-a showed a common contour profile at the inlet where the pressure is around 0.08 Pa to a location of 0.65 m from each side. As the wind approaches the frontal surface its pressure magnitude starts to increase 0.15 Pa for 0.3 m/s, 0.42 Pa for 0.6 m/s, 0.51 Pa for 0.9 m/s, 0.75 Pa for 1.2 m/s and 3.82 Pa for 2.5 m/s for M2-A.

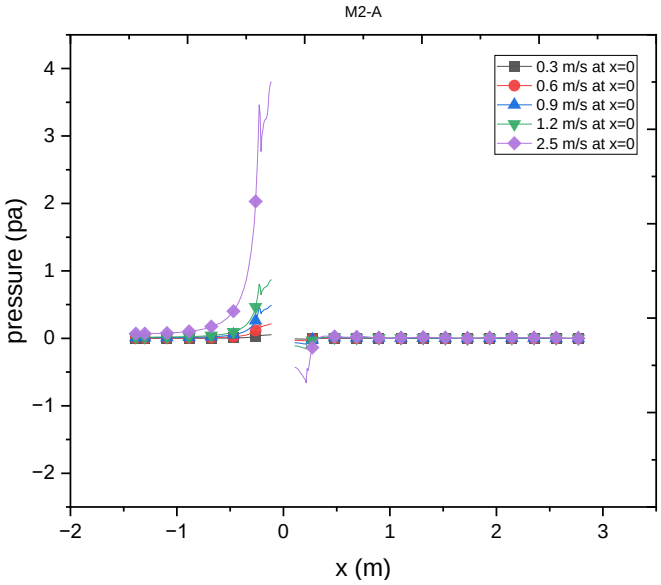

(a)

As the wind approaches the frontal surface, its pressure magnitude starts to increase 0.09 Pa for 0.3 m/s, 0.2 Pa for 0.6 m/s, 0.48 Pa for 0.9 m/s, 0.65 Pa for 1.2 m/s and 3.2 Pa for 2.5 m/s for M2-B shown in figure 57-b.

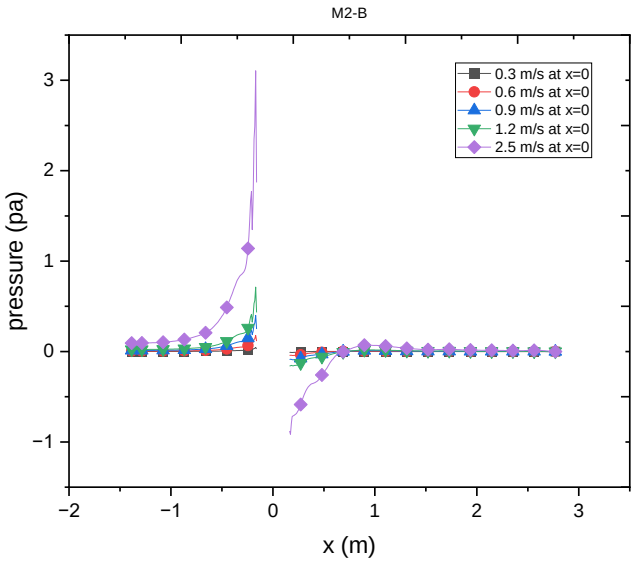

(b)

As the wind approaches the frontal surface its pressure magnitude starts to increase 0.056 Pa for 0.3 m/s, 0.22 Pa for 0.6 m/s, 0.488 Pa for 0.9 m/s, 0.875 Pa for 1.2 m/s and 4.076 Pa for 2.5 m/s inflow for M2-C shown in figure 57-c.

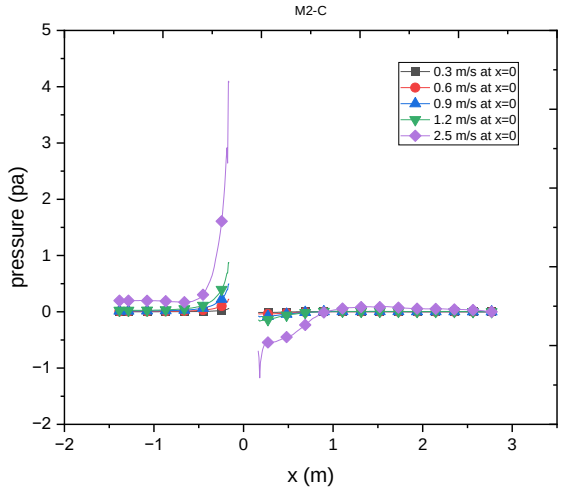

(c)

Figure 57. Plots of pressure magnitude for three models along horizontal wind flow.

To a great extent, the maximum pressure induced surface is expected to be subjected to pressure force for positive pressure, and a negative induced at flow separation (Qi et al., 2022). Pressure has showed inverse relationship with velocity.

4.2.3. Drag coefficients and forces

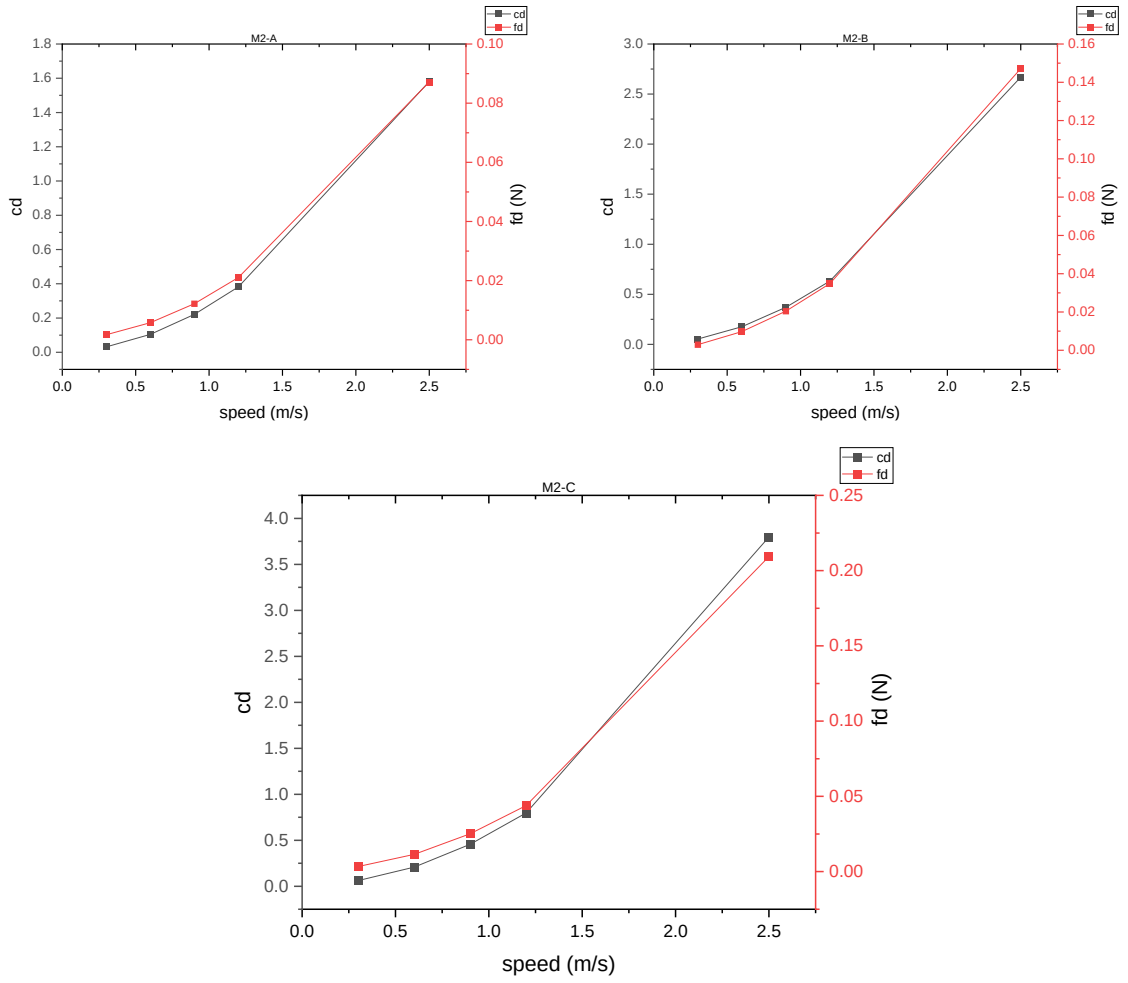

Figure 58. Drag force and coefficient relative to wind speed variation during horizontal flow.

Findings of drag effect during horizontal wind flow in figure 58 also corresponds with scientific reasons as outlined in downwash section under drag plot. As drag is linearly proportional with wind speed, figure 58 showed a minimum cd of 0.0314, maximum cd – 1.5 on M2-A, a minimum cd of 0.053, maximum cd – 2.6 on M2-B and a minimum cd of 0.0617, maximum cd – 3.7 on M2-C. following these, it was observed that M2-A a desired maximum drag as compared with the other models. The major factor that created this difference is shape effect. The front surface with thickness of 100 mm has a flat profile where maximum pressure was observed. The geometrical size of that profile is less as compared to the size of maximum pressure occurrence on the other models.

4.2.4. Pressure contour & stability effect

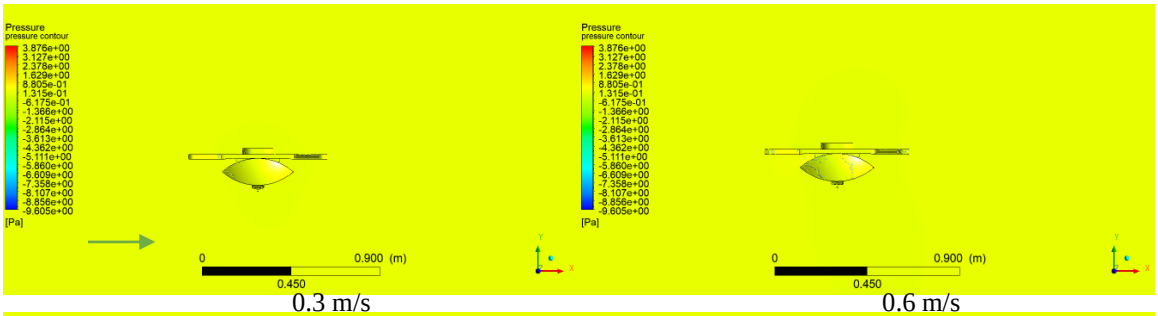

0.3 m/s 0.6 m/s

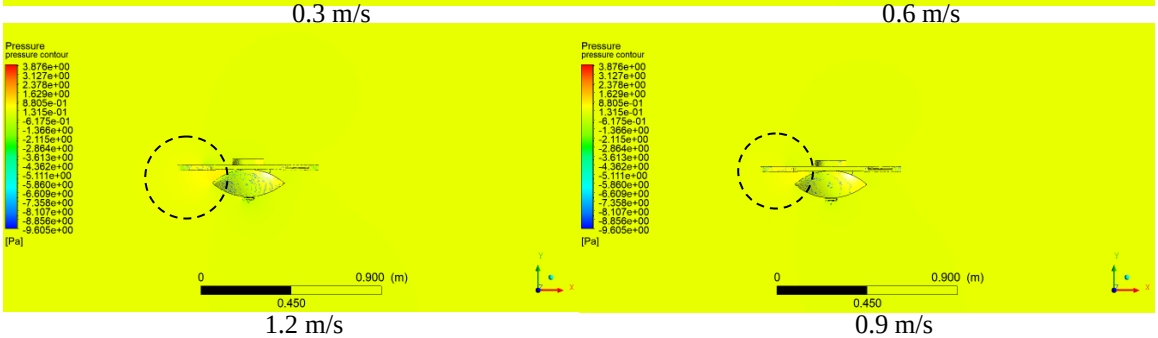

1.2 m/s 0.9 m/s

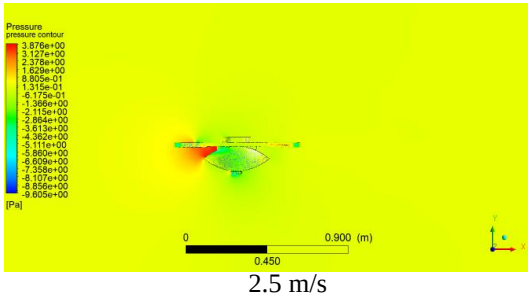

2.5 m/s

(a) pressure contour

During horizontal wind flow over the surface of the models, particles of wind first tend to contact the frontal face where the velocity of particles declined as energy was converted and high pressure developed as shown in figure 59-a. A maximum pressure developed from 0.135 Pa at 0.9 m/s wind speed to 3.87 Pa at 2.5 m/s wind speed. The other scientific finding was at flow separation/boundary layer, it showed how a pressure difference developed (Paz et al., 2020).

Turbulence is a chaotic effect which is unpredictable and cannot be determined linearly. Therefore, noise generated due to wind gust at pass filter to determine the alteration of moments in terms of amplitude of turbulence was plotted.

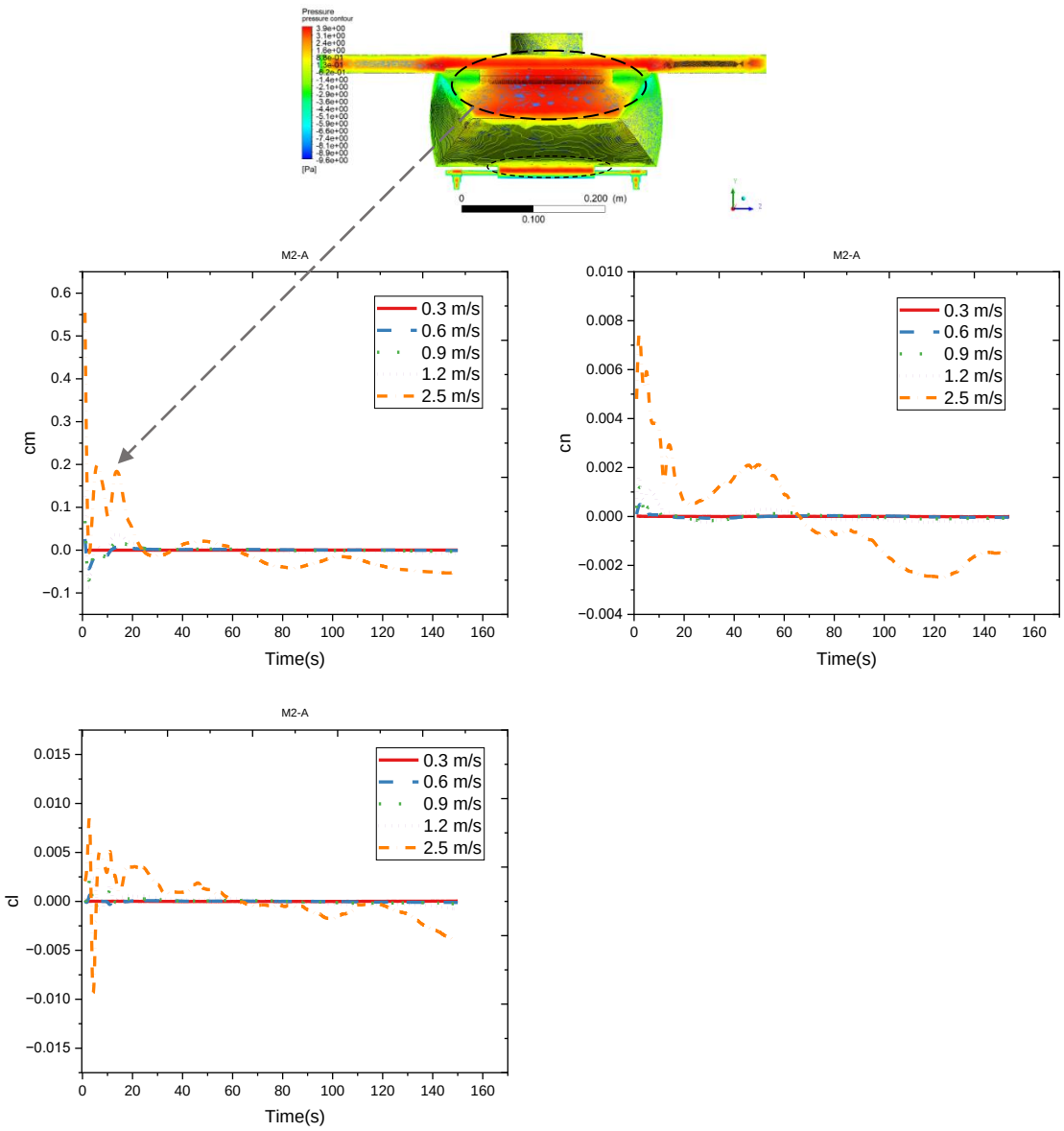

(b) time response of moment coefficients

Figure 59. Contour plot and impulse response of model 2-A along horizontal flow.

Figure 59-b shows the impulse response of cl, cm, and cn for wind speeds between 0.3 and 2.5 m/s. The figure illustrates how a pressure of 3.9 pa coming horizontally had an impact for around 80 seconds on cm for wind speeds < 2.5 m/s, 120s for 2.5 m/s inflow. Although the peak amplitude was high 0.55 at 2.5 m/s on cm, it showed a convergence after 120s. Peak waves with steady convergence after 120 seconds were less than 0.05 at 1.2 m/s flow on cm, less than 0.002 at 1.2 m/s flow on cn, and less than 0.005 at 1.2 m/s inflow on cl.

Moment coefficient amplitude was shown to be less disturbed over 120 seconds, with peak values occurring at wind speeds between 1.2 and 2.5 m/s. In common except 1.2 & 2.5 m/s inflows, other wind speeds showed good stability on cm, cn and cl. The roll (cl) & yaw (cn) moment disruptions, however, was more pronounced. The convergence on cl was less with a higher wavelet of 0.008 at 2.5 m/s. To a great extent, considering magnitude, cm was initially highly disrupted.

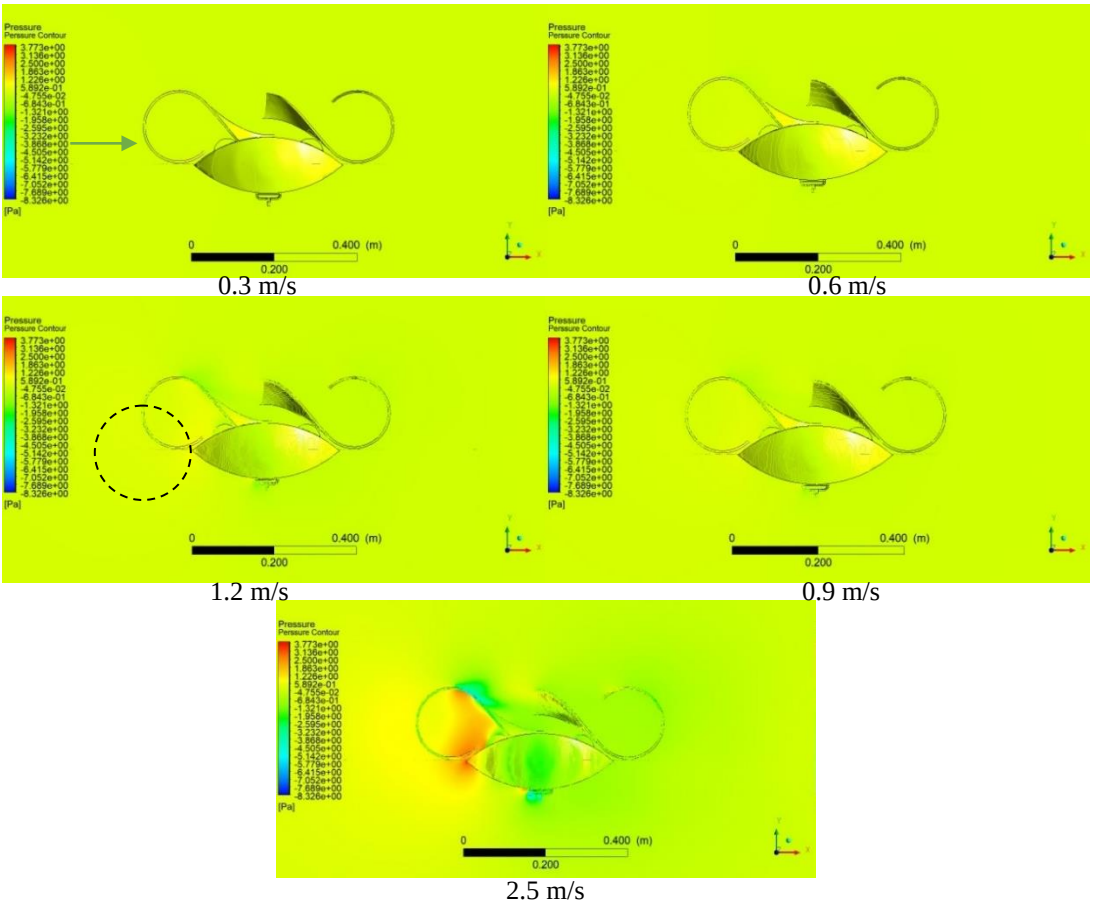

0.3 m/s 0.6 m/s

1.2 m/s 0.9 m/s

2.5 m/s

(a) pressure contour

The principle of aerodynamics in reality presented in scientific papers also worked for simulation result of horizontal wind field on model 2-B at variable wind speeds in figure 60-a. With a constant incoming pressure after a close location to the surface in relation with wind speeds starts to rise from 0.521 Pa at 0.3 m/s inflow to 3.773 Pa at 2.5 m/s inflow.

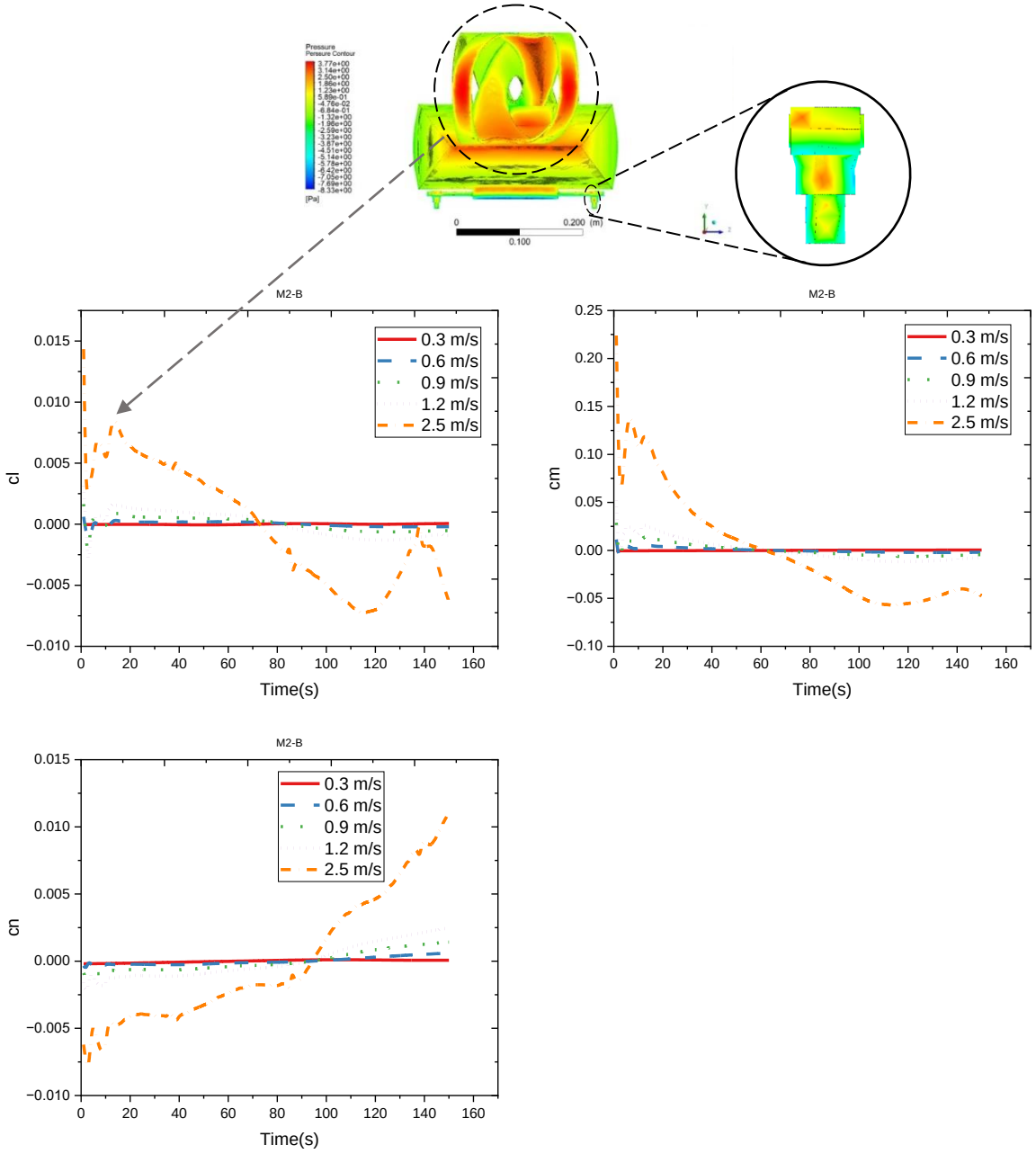

(b) time response of moment coefficients

Figure 60. Contour plot and impulse response of model 2-B along horizontal flow.

A horizontal wind field coming at 0.6 m/s on cl, cm & cn had a peak wavelet of near 0, which aligns with good stability constant curve at 0.3 m/s as shown in figure 60-b. In common, when wind speed increases from 0.9 – 2.5 m/s, peak wavelets have also increased from 0.0009 to 0.25 respectively up to 120 s, where maximum was observed on cm. cl and cm showed less disturbance until 110 s and started to constantly converge for

wind speeds below 2.5 m/s. Though, impulse response of cl at 2.5 m/s also showed low rate of convergence. cn (yaw moment) however showed a more noticeable disruption. To a great extent, considering magnitude, cm was initially highly disrupted. The justification for a start of negative amplitude on cn indicated that, the extent of disturbance created was to anti-clockwise direction with a magnitude of 0.0052.

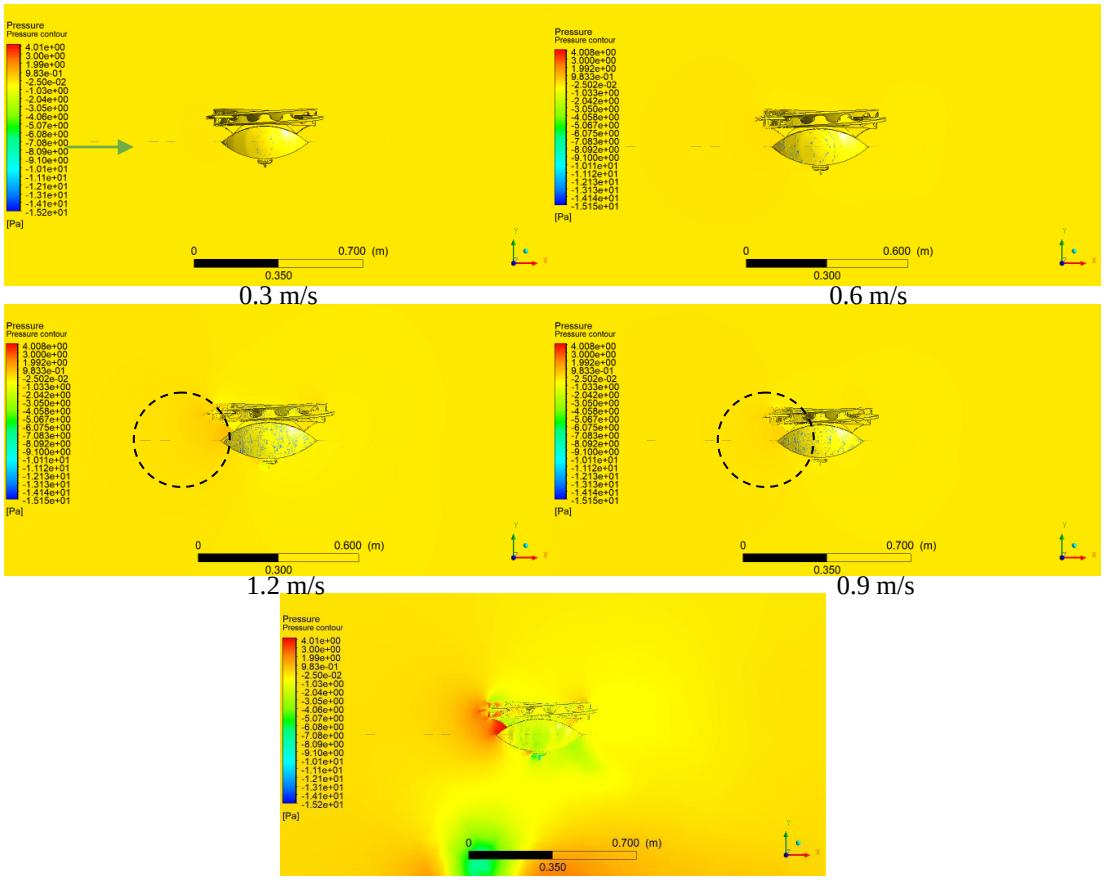

(a) pressure contour

Figure 61-a shows contour of pressure effect on ambient and model 2-C for a horizontal wind flow. A similar trend was observed as like as contour distribution on models 2-A&B except in magnitude. The pressure was 0.15 Pa at 0.3 m/s inflow, 0.52 Pa at 0.6 m/s inflow, 0.87 Pa at 0.9 m/s, 0.92 Pa at 1.2 m/s inflow & 4.01 Pa at 2.5 m/s inflow all when particles contact with surface. Attributable to shape of M2-C, a different profile was observed beneath the bottom of the nozzles. Reminding its scientific truth, the negative pressure vector after boundary layer separation flows down to the ground which was visible at 2.5 m/s inflow.

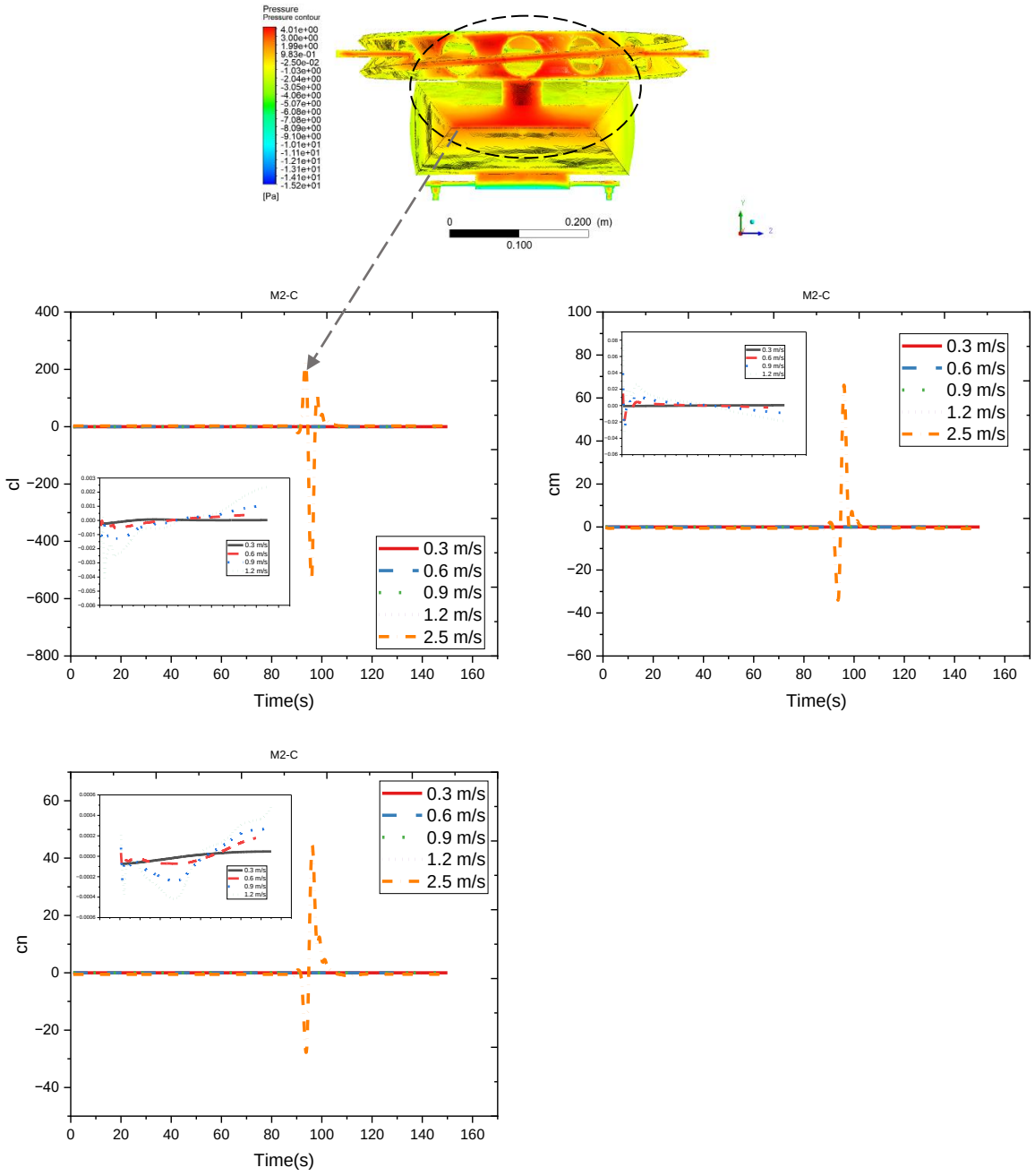

(b) time response of moment coefficients

Figure 61. Contour plot and impulse response of model 2-C along Horizontal flow.

The impulse response of cl, cm, and cn for winds between 0.3 and 2.5 m/s is depicted in Figure 61-b. The graph shows how a pressure of 4.01 Pa arriving horizontally affected cm at 90s seconds when the wind speed was 2.5 m/s.

This was a sudden impact occurred. As shown in figure 61-b, all cl, cm, & cn moment coefficients were stable up to 90s for 2.5 m/s inflow. Despite having a high peak amplitude of 40 on cn, 70 on cm, 500 on cl at 2.5 m/s, the time domain curve described a stability on all coefficients, it had stabilized for 89 s and began to condense after 110 seconds after a short time disturbance. A zoomed-in data capture on cl in figure 61-b revealed another hidden finding. It was that impulse response of wind speed ranges of 0.3 – 1.2 m/s was swallowed by the 2.5 m/s. The zoomed in figure describes the existence of disturbance till 120 s for speed ranges less than 2.5 m/s as well. The scientific concept depicted similar trend with previous discussion. To a great extent, considering magnitude, cl was initially highly disrupted. To give final outline of the results obtained from the objective parameters drag force & coefficients, pressure distribution and moment coefficient, model variant 2-A (rectangular solid geometry with elliptical hopper) had shown a lower drag force and coefficients and good stability in terms of moment coefficients than the other two models.

CHAPTER FIVE

CONCLUSION AND RECOMMENDATIONS

5.1. Conclusion

To a great extent, this research was directed in analyzing aerodynamic parameters and stability of three quadcopter UAV model variants due to wind gust using numerical CFD simulation at a constant hovering height of 0.5 m intended for the purpose of keeping precise agricultural seeding and their comparison. This instability case was observed by effects in pressure contour, drag force, drag coefficients and moment coefficients. To make the research feasible, wind speeds of 0.3, 0.6 & 0.9 m/s were used at low or ground level altitude and wind speeds of 1.2 & 2.5 m/s were considered for cases of an increase in altitude above 0.5 m still keeping the constant hovering height of 0.5 m.

- Keeping its velocity from inlet, it has been seen that, as the wind flow reaches the surface of the UAV models, its pressure contour increases for all the models except the extent of pressure magnitude for both down wash and horizontal wind flow. Horizontal wind flow showed maximum pressure magnitude of 3.87 pa on M2-A, 3.773 pa on M2-B, 4.01 pa on M2-C and for the downwash flow, a maximum pressure of 4.608 pa, 3.827 pa, 3.918 pa at M2-A, M2-B and M2-C bodies had been observed respectively.
- Variation of wind speed ranges has also revealed the effect it has on pressure profile and drag. As wind speed increased from 0.3 m/s to 2.5 m/s the pressure showed an increase so does drag for all models M2-A, M2-B & M2-C respectively.
- Wind speed had a positive effect on amplitude/impulse response of moment coefficients stability. As wind speed increased, the disturbance amplitude also increased.
- Stability in terms of wave amplitude response of M2-A showed a desirable stability response as compared to M2-B & M2-C during both horizontal and downwash flow. While a sudden instability was observed at 2.5 m/s wind speed acting up on model 2-C on all of its moment coefficients.

- During downwash wind field, cl & cm on M2-A, cn on M2-B and cl & cm on M2-C were more pronounced. When wind flow horizontally, cm on M2-A & M2-B and all on M2-C were more pronounced. This phenomenon revealed how shape significantly affected aerodynamic parameters and stability. High impact on M2-C was lightweight due to concentrated mass around edges of holes.
- It has been detected that 2.5 m/s had resulted a visible disturbance but with less magnitudes of moment coefficients, the remaining wind speeds doesn't bring a higher wind/pressure load except low and short period impulse.
- M2-A has shown low drag effect & impulse response hence, optimum aerodynamic profile/shape was interpreted on M2-A based on numerical result.

5.2. Recommendations

To get the best stable model from the aerodynamic CFD analysis, considering the following suggestions is vital.

- This study considered full model scale, in order to reduce computing time/solution convergence, quarter model along with flow domain can be used.
- As compared to the other two models, since M2-A had less stability disturbance due to less drag, pressure effect, and impulse response, it is recommended to further develop M2-A.

5.3. Future work

After all the results obtained, few extended works recommended as a future work includes,

- Additional 4 to 5 wind speed ranges in relation with altitude are imperative to consider.
- Sideway horizontal fluid flow simulation along z can also be studied.
- Integrate particle deposition drift simulation using discrete element method.
- This model can be 3D printed and an experimental wind tunnel CFD analysis should be led as a second phase research.

REFERENCES

Ababa, A., Science, V., Dereje, G., Balemi, T., & Ashagre, H. (2018). *Effect of Weed Interference and Plant Density on Maize Grain Yield*. *6*(1).

Abbas, M. A. (2018). Comparison of convergence rate of higher order tetrahedral and hexahedral elements for Linear Static Structural FEA. *International Journal of Pure and Applied Mathematics*, *119*(10), 1927–1933. http://www.ijpam.eu

Abichandani, P., Lobo, D., Ford, G., Bucci, D., & Kam, M. (2020). Wind Measurement and Simulation Techniques in Multi-Rotor Small Unmanned Aerial Vehicles. *IEEE Access*, *8*, 54910–54927. https://doi.org/10.1109/ACCESS.2020.2977693

Abu-Zidan, Y., Mendis, P., & Gunawardena, T. (2021). Optimising the computational domain size in CFD simulations of tall buildings. *Heliyon*, *7*(4), e06723. https://doi.org/10.1016/j.heliyon.2021.e06723

Ahmed, F., Mohanta, J. C., Keshari, A., & Yadav, P. S. (2022). Recent Advances in Unmanned Aerial Vehicles: A Review. *Arabian Journal for Science and Engineering*, *47*(7), 7963–7984. https://doi.org/10.1007/s13369-022-06738-0

Anand, K., & R., G. (2019). An Autonomous UAV for Pesticide Spraying. *International Journal of Trend in Scientific Research and Development*, *Volume-3*(Issue-3), 986–990. https://doi.org/10.31142/ijtsrd23161

Ariante, G., Ponte, S., Papa, U., & Del Core, G. (2021). Estimation of airspeed, angle of attack, and sideslip for small unmanned aerial vehicles (Uavs) using a micro-pitot tube. *Electronics (Switzerland)*, *10*(19), 1–20. https://doi.org/10.3390/electronics10192325

Atiqah BADALUDDIN, N., Iskandar KHALIT, S., Afiza BADALUDDIN, N., Saibani, N., & Haqeem MOHAMED RAMELI, R. (2020). Introduction to Drone Technology for Agriculture Purposes: A Brief Review Author's Details. *International Journal of Agriculture and Biological Sciences-ISSN*, *4*(August), 2522–6584. https://doi.org/10.5281/zenodo.4040897

Atmaca, M., Çetin, B., & Yılmaz, E. (2019). CFD analysis of unmanned aerial vehicles (UAV) moving in flocks. *Acta Physica Polonica A*, *135*(4), 694–696. https://doi.org/10.12693/APhysPolA.135.694

Belete, A. S. (2020). Analysis of technical efficiency in maize production in Guji Zone: stochastic frontier model. *Agriculture and Food Security*, *9*(1), 1–15. https://doi.org/10.1186/s40066-020-00270-w

Berner, B. (2020). Fertilization and Sowing From Unmanned Aerial Vehicles. *Polish Technical Review*, *2*, 18–22. https://doi.org/10.15199/180.2020.2.2

Biglia, A., Grella, M., Bloise, N., Comba, L., Mozzanini, E., Sopegno, A., Pittarello, M., Dicembrini, E., Alcatrão, L. E., Guglieri, G., Balsari, P., Aimonino, D. R., & Gay, P. (2022). UAV-spray application in vineyards: Flight modes and spray system adjustment effects on canopy deposit, coverage, and off-target losses. *Science of The*

Total Environment, *845*(April), 157292. https://doi.org/10.1016/j.scitotenv.2022.157292

Brar, I. S., Dixit, A. K., Khurana, R., & Gautam, A. (2017). Studies on Physical Properties of Maize (Zea mays L.) Seeds. *International Journal of Current Microbiology and Applied Sciences*, *6*(10), 963–970. https://doi.org/10.20546/ijcmas.2017.610.116

Chamola, V., Kotesh, P., Agarwal, A., Naren, Gupta, N., & Guizani, M. (2021). A Comprehensive Review of Unmanned Aerial Vehicle Attacks and Neutralization Techniques. *Ad Hoc Networks*, *111*(12), 102324. https://doi.org/10.1016/j.adhoc.2020.102324

Chen, S. De, Lan, Y. Bin, Li, J. Y., Zhou, Z. Y., Liu, A. M., & Mao, Y. D. (2017). Effect of wind field below unmanned helicopter on droplet deposition distribution of aerial spraying. *International Journal of Agricultural and Biological Engineering*, *10*(3), 67–77. https://doi.org/10.3965/j.ijabe.20171003.3078

Cummings, R. M., Liersch, C. M., Schütte, A., & Huber, K. C. (2018). Aerodynamics and Conceptual Design Studies on an Unmanned Combat Aerial Vehicle Configuration. *Journal of Aircraft*, *55*(2), 454–474. https://doi.org/10.2514/1.C033808

Delavarpour, N., Koparan, C., Nowatzki, J., Bajwa, S., & Sun, X. (2021). A Technical Study on UAV Characteristics for Precision Agriculture Applications and Associated Practical Challenges. *Remote Sensing*, *13*(6), 1204. https://doi.org/10.3390/rs13061204

Deployable, B., Uav, M., Henderson, L., Glaser, T., & Kuester, F. (2017). Towards Bio-Inspired Structural Design of a 3D. *2017 IEEE Aerospace Conference*, 1–7.

Diaz, P. V., & Yoon, S. (2018). *High-Fidelity Computational Aerodynamics of Multi-Rotor Unmanned Aerial Vehicles*. 1–22.

Diwate, S., Nitnaware, V., … K. A.-R. J. of, & 2018, U. (2018). Design and development of application specific drone machine for seed sowing. *International Research Journal of Engineering and Technology*, *5*(5), 4003–4007. https://www.academia.edu/download/58282768/IRJET-V5I5853.pdf

Edosa, T. T., Kebede, T., & Shumeta, Z. (2019). Analysis of Price Efficiency of Smallholder Farmers in Maize Production in Gudeya Bila District, Oromia National Regional State, Ethiopia: Stochastic, Dual Cost approach. *International Journal of Contemporary Research and Review*, *10*(04), 21480–21487. https://doi.org/10.15520/ijcrr.v10i04.690

EIAR. (2003). *The Ethiopian Institute of Agricultural Research* (Issue August).

Engels, T., Kolomenskiy, D., Schneider, K., Farge, M., Lehmann, F. O., & Sesterhenn, J. (2019). Impact of turbulence on flying insects in tethered and free flight: High-resolution numerical experiments. *Physical Review Fluids*, *4*(1), 1–21. https://doi.org/10.1103/PhysRevFluids.4.013103

Felismina, R., Silva, M., Mateus, A., & Malça, C. (2017a). Development of a Universal Seeder System to Be Applied in Drones. *Journal of Advanced Agricultural Technologies*, *4*(2), 123–127. https://doi.org/10.18178/joaat.4.2.123-127

Felismina, R., Silva, M., Mateus, A., & Malça, C. (2017b). Study on the aerodynamic behavior of a UAV with an applied seeder for agricultural practices. *AIP Conference Proceedings*, *1836*(June 2017), 020049. https://doi.org/10.1063/1.4981989

Gezahegn, A. M. (2019). *Review on Effect of Plant Density and Planting Arrangement on Faba Bean Production Planting Arrangement on Faba Bean Production*. *January*. https://doi.org/10.5829/idosi.wjas.2019.261.268

Gianfelice, M., Aboshosha, H., & Ghazal, T. (2022). Real-time Wind Predictions for Safe Drone Flights in Toronto. *Results in Engineering*, *15*(April), 100534. https://doi.org/10.1016/j.rineng.2022.100534

Gugan, G., & Haque, A. (2023). *Path Planning for Autonomous Drones : Challenges and Future Directions*.

Hafeez, A., Husain, M. A., Singh, S. P., Chauhan, A., Khan, M. T., Kumar, N., Chauhan, A., & Soni, S. K. (2023). Implementation of drone technology for farm monitoring & pesticide spraying: A review. *Information Processing in Agriculture*, *10*(2), 192–203. https://doi.org/10.1016/j.inpa.2022.02.002

Hassan, S., Molla, M. M., Nag, P., Akhter, N., & Khan, A. (2022). Unsteady RANS simulation of wind flow around a building shape obstacle. *Building Simulation*, *15*(2), 291–312. https://doi.org/10.1007/s12273-021-0785-8

Huang, X., Zhang, S., Luo, C., Li, W., & Liao, Y. (2020). Design and experimentation of an aerial seeding system for rapeseed based on an air-assisted centralized metering device and a multi-rotor crop protection UAV. *Applied Sciences (Switzerland)*, *10*(24), 1–14. https://doi.org/10.3390/app10248854

Jayakrishnan, H. J. (2016). Position and attitude control of a quadrotor UAV using super twisting sliding mode. *IFAC-PapersOnLine*, *49*(1), 284–289. https://doi.org/10.1016/j.ifacol.2016.03.067

Kim, J., Kim, S., Ju, C., & Son, H. Il. (2019). Unmanned Aerial Vehicles in Agriculture: A Review of Perspective of Platform, Control, and Applications. *IEEE Access*, *7*, 105100–105115. https://doi.org/10.1109/ACCESS.2019.2932119

Kumar, R., Rohit, Kumar, G., Zunaid, M., & Ansari, N. A. (2021). Numerical analysis of quadcopter in different weather conditions of regions in India. *Materials Today: Proceedings*, *43*, 378–382. https://doi.org/10.1016/j.matpr.2020.11.681

Lee, C., Kim, S., & Chu, B. (2021). A Survey : Flight Mechanism and Mechanical Structure of the UAV. *International Journal of Precision Engineering and Manufacturing*, *22*(4), 719–743. https://doi.org/10.1007/s12541-021-00489-y

Lei, Y., & Lin, R. (2019). Effect of wind disturbance on the aerodynamic performance of coaxial rotors during hovering. *Measurement and Control (United Kingdom)*, *52*(5–6), 665–674. https://doi.org/10.1177/0020294019834961

Lei, Y., & Wang, H. (2020). Aerodynamic Performance of a Quadrotor MAV Considering the Horizontal Wind. *IEEE Access*, *8*, 109421–109428. https://doi.org/10.1109/ACCESS.2020.3002706

Leitch, K. J., Ponce, F. V., Dickson, W. B., Van Breugel, F., & Dickinson, M. H. (2021). The long-distance flight behavior of Drosophila supports an agent-based model for wind-assisted dispersal in insects. *Proceedings of the National Academy of Sciences of the United States of America*, *118*(17). https://doi.org/10.1073/pnas.2013342118

Li, H., Zhu, H., Jiang, Z., & Lan, Y. (2022). Performance characterization on downwash flow and spray drift of multirotor unmanned agricultural aircraft system based on CFD. *International Journal of Agricultural and Biological Engineering*, *15*(3), 1–8. https://doi.org/10.25165/j.ijabe.20221503.7315

Ling, W., Du, C., Mengchao, Z., Yu, W., Ze, Y., & Shumao, W. (2018). CFD Simulation of Low-attitude Droplets Deposition Characteristics for UAV based on Multi-feature Fusion. *IFAC-PapersOnLine*, *51*(17), 648–653. https://doi.org/10.1016/j.ifacol.2018.08.123

Liu, W., Zou, S., Xu, X., Gu, Q., He, W., Huang, J., Huang, J., Lyu, Z., Lin, J., Zhou, Z., Jiang, R., & Luo, X. (2022). Development of UAV-based shot seeding device for rice planting. *International Journal of Agricultural and Biological Engineering*, *15*(6), 1–7. https://doi.org/10.25165/j.ijabe.20221506.7301

Liu, X., & Li, X. (2023). The Influence of Agricultural Production Mechanization on Grain Production Capacity and Efficiency. *Processes*, *11*(2), 487. https://doi.org/10.3390/pr11020487

Lysych, M., Bukhtoyarov, L., & Druchinin, D. (2021). Design and research sowing devices for aerial sowing of forest seeds with uavs. *Inventions*, *6*(4). https://doi.org/10.3390/inventions6040083

Meier, K., Hann, R., Skaloud, J., & Garreau, A. (2022). Wind Estimation with Multirotor UAVs. *Atmosphere*, *13*(4), 1–23. https://doi.org/10.3390/atmos13040551

Mohamedzain, A. O., Chua, H., Yap, K., Uthayasurian, P., & Jiehan, T. (2022). Novel Drone Design Using an Optimization Software with 3D Model, Simulation, and Fabrication in Drone Systems Research. *Drones*, *6*(4). https://doi.org/10.3390/drones6040097

Mohan, M., Richardson, G., Gopan, G., Aghai, M. M., Bajaj, S., Galgamuwa, G. A. P., Vastaranta, M., Arachchige, P. S. P., Amorós, L., Corte, A. P. D., De-Miguel, S., Leite, R. V., Kganyago, M., Broadbent, E. N., Doaemo, W., Shorab, M. A. Bin, & Cardil, A. (2021). UAV-Supported Forest Regeneration: Current Trends, Challenges and Implications. *Remote Sensing*, *13*(13), 2596. https://doi.org/10.3390/rs13132596

Mondejar, M. E., Avtar, R., Diaz, H. L. B., Dubey, R. K., Esteban, J., Gómez-Morales, A., Hallam, B., Mbungu, N. T., Okolo, C. C., Prasad, K. A., She, Q., & Garcia-Segura, S. (2021). Digitalization to achieve sustainable development goals: Steps towards a Smart Green Planet. *Science of the Total Environment*, *794*(June). https://doi.org/10.1016/j.scitotenv.2021.148539

Nowak, B. (2021). Precision Agriculture : Where do We Stand ? A Review of the Adoption of Precision Agriculture Technologies on Field Crops Farms in Developed Countries. *Agricultural Research*. https://doi.org/10.1007/s40003-021-00539-x

Olejnik, D. A., Muijres, F. T., Karásek, M., Honfi Camilo, L., De Wagter, C., & de Croon, G. C. H. E. (2022). Flying Into the Wind: Insects and Bio-Inspired Micro-Air-Vehicles With a Wing-Stroke Dihedral Steer Passively Into Wind-Gusts. *Frontiers in Robotics and AI*, *9*(February), 1–17. https://doi.org/10.3389/frobt.2022.820363

Paz, C., Su, E., Gil, C., & Baker, C. (2020). *Journal of Wind Engineering & Industrial Aerodynamics CFD analysis of the aerodynamic effects on the stability of the fl ight of a quadcopter UAV in the proximity of walls and ground*. *206*(September). https://doi.org/10.1016/j.jweia.2020.104378

Polivanov, P. A., & Sidorenko, A. A. (2021). Aerodynamic characteristics of a quadcopter with propellers. *AIP Conference Proceedings*, *2351*(May), 040053. https://doi.org/10.1063/5.0051951

Prudden, S., Fisher, A., Marino, M., Mohamed, A., Watkins, S., & Wild, G. (2018). Measuring wind with Small Unmanned Aircraft Systems. *Journal of Wind Engineering and Industrial Aerodynamics*, *176*(December 2017), 197–210. https://doi.org/10.1016/j.jweia.2018.03.029

Qi, P., Wang, Z., Wang, C., Xu, L., Jia, X., Zhang, Y., Wang, S., Han, L., Li, T., Chen, B., Li, C., Mei, C., Pan, Y., Zhang, W., Müller, J., Liu, Y., & He, X. (2022). Development of multifunctional unmanned aerial vehicles versus ground seeding and outplanting: What is more effective for improving the growth and quality of rice culture? *Frontiers in Plant Science*, *13*(July), 1–19. https://doi.org/10.3389/fpls.2022.953753

Radoglou-grammatikis, P., Sarigiannidis, P., & Lagkas, T. (2020). A compilation of UAV applications for precision agriculture. *Computer Networks*, *172*(February), 107148. https://doi.org/10.1016/j.comnet.2020.107148

Rejeb, A., Abdollahi, A., Rejeb, K., & Treiblmaier, H. (2022). Drones in agriculture: A review and bibliometric analysis. *Computers and Electronics in Agriculture*, *198*(May), 107017. https://doi.org/10.1016/j.compag.2022.107017

Results of Agricultural Machinery and Post-harvest Engineering Research 2018. (2018).

Shukla, D., & Komerath, N. (2018). Multirotor Drone Aerodynamic Interaction Investigation. *Drones*, *2*(4), 43. https://doi.org/10.3390/drones2040043

Sugandi, T. S., Nathan, Subrata, S. K., Arifianto, O., & Moelyadi, M. A. (2018). Prediction of static stability in tandem wing unmanned aerial vehicle. *Journal of Physics: Conference Series*, *1130*(1), 012028. https://doi.org/10.1088/1742-6596/1130/1/012028

Teklewold, A., Alemu, D., Kiyoshi, S., & Kirub, A. (2012). *Seed Demand Assessment: practices, challenges and Options* (Issue 5).

Tesfaye, B., Mesfin, K., Tolera, A., Gebresilasie, H., Gebreyes, G., & Fite, G. (2019). Some maize agronomic practices in Ethiopia: A review of research experiences and lessons from agronomic panel survey in Oromia and Amhara regions. *African Journal of Agricultural Research*, *14*(33), 1749–1763. https://doi.org/10.5897/ajar2019.14338

Tewari, N. (2023). Drone Technology in Smart Agriculture and Precision Farming. *Just Agriculture*, *3*(5), 119–124. https://www.researchgate.net/publication/368460460

Wang, B. H., Wang, D. B., Ali, Z. A., Ting Ting, B., & Wang, H. (2019). An overview of various kinds of wind effects on unmanned aerial vehicle. *Measurement and Control*, *52*(7–8), 731–739. https://doi.org/10.1177/0020294019847688

Wen, S., Zhang, Q., Deng, J., Lan, Y., Yin, X., & Shan, J. (2018). Design and Experiment of a Variable Spray System for Unmanned Aerial Vehicles Based on PID and PWM Control. *Applied Sciences*, *8*(12), 2482. https://doi.org/10.3390/app8122482

Yael, F. L., & Arias-montano, A. (2020). *Aerodynamic Analysis for the Mathematical Model of a Dual-System UAV*.

Yang, F. B., Xue, X. Y., Zhang, L., & Sun, Z. (2017). Numerical simulation and experimental verification on downwash air flow of six-rotor agricultural unmanned aerial vehicle in hover. *International Journal of Agricultural and Biological Engineering*, *10*(4), 41–53. https://doi.org/10.25165/j.ijabe.20171004.3077

Yatribi, T. (2020). Factors Affecting Precision Agriculture Adoption: A Systematic Litterature Review. *Economics*, *8*(2), 103–121. https://doi.org/10.2478/eoik-2020-0013

Yenge, G. B., Kad, V. P., & Nalawade, S. M. (2018). Physical Properties of Maize (Zea mays L.) Grain . *Journal of Krishi Vigyan*, *7*(special), 125. https://doi.org/10.5958/2349-4433.2018.00173.3

Yinka-Banjo, C., & Ajayi, O. (2020). Sky-Farmers: Applications of Unmanned Aerial Vehicles (UAV) in Agriculture. In *Autonomous Vehicles*. IntechOpen. https://doi.org/10.5772/intechopen.89488

Zdancevic, E. (2015). *Maize grain shape approaches for DEM modelling*. *118*, 247–258. https://doi.org/10.1016/j.compag.2015.09.004

Zhang, C., & Kovacs, J. M. (2012). The application of small unmanned aerial systems for precision agriculture: a review. *Precision Agriculture*, *13*(6), 693–712. https://doi.org/10.1007/s11119-012-9274-5

Zheng, J., Tao, Q., & Li, L. (2020). Wind pressure coefficient on a multi-storey building with external shading louvers. *Applied Sciences (Switzerland)*, *10*(3). https://doi.org/10.3390/app10031128

Zhou, L., Yu, J., Wang, Y., Yan, D., & Yu, Y. (2020). A study on the modelling method of maize-seed particles based on the discrete element method. *Powder Technology*, *374*, 353–376. https://doi.org/10.1016/j.powtec.2020.07.051

Zhu, H., Li, H., Zhang, C., Li, J., & Zhang, H. (2019). Performance Characterization of the UAV Chemical Application Based on CFD Simulation. *Agronomy*, *9*(6), 308. https://doi.org/10.3390/agronomy9060308

APPENDICES

Appendix A. Plane of symmetry

The picture below is to show the symmetries of the geometries using a plane. It can be seen that analyzing the quarter half was also sufficient to represent the whole assembly.

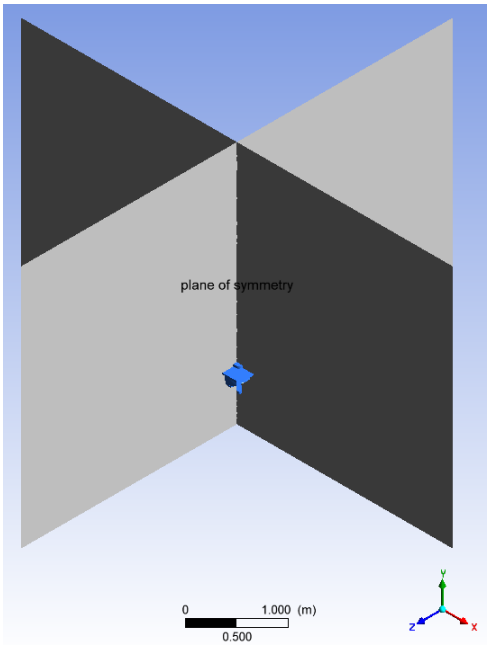

Figure A 62. Representation of symmetries of the models in terms of planes.

Appendix B. Model for validation

The image underneath is to express the model modeled using a software as per the dimensions given in the article, numerically simulate and to qualify our results methodologically.

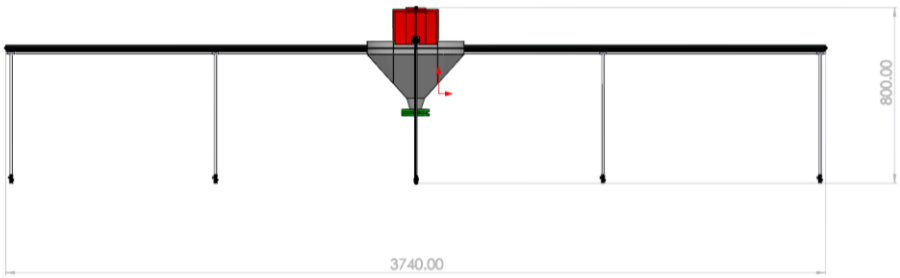

Figure B 63. Schematic representation of external model.

Appendix C. Mesh independence

As per the references cited in the main section, two of the ways to check the grid independence is by plot the constant convergence graph of a certain parameter vs number of elements and by obtaining a maximum skewness value less than 0.98 in the mesh metrics. Following this, this paper has attested both and presented the plot in the main text while the skewness chart in the appendix as shown below for all the models including the validation.

M2-A

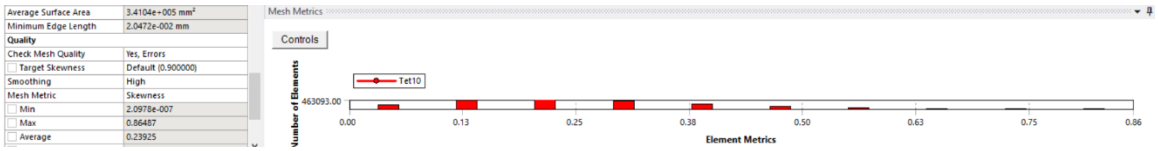

M2-B

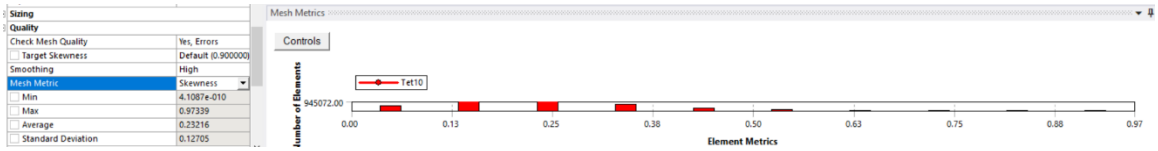

M2-C

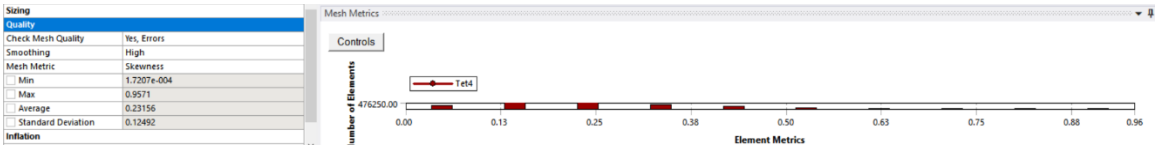

Validation model

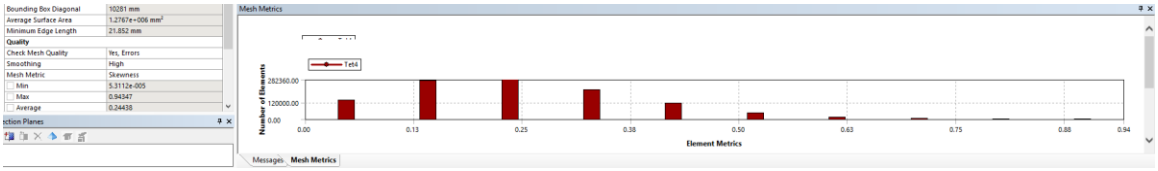

Figure C 64. Captured images of skewness metrics of all models.

Appendix D. Graphics reports

Table D-10. Plot of velocity contour for M2-A & M2-B along downwash wind flow.

<table>
<tr><td colspan="4">Downwash wind flow velocity contour</td></tr>
<tr><td colspan="2">M2-A</td><td colspan="2">M2-B</td></tr>
<tr><td colspan="2"> 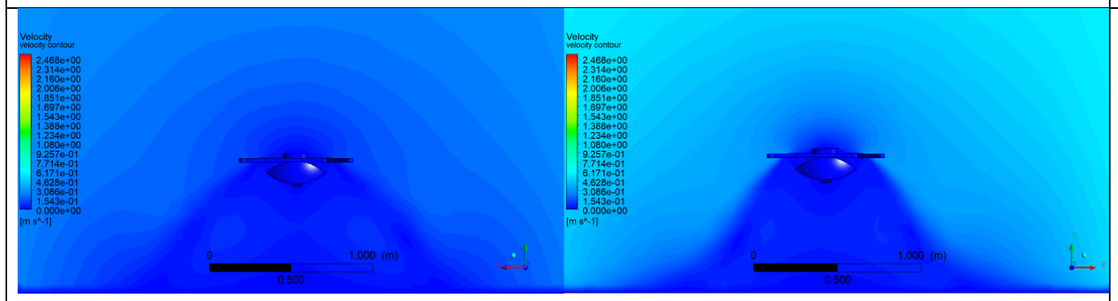
</td><td colspan="2"> 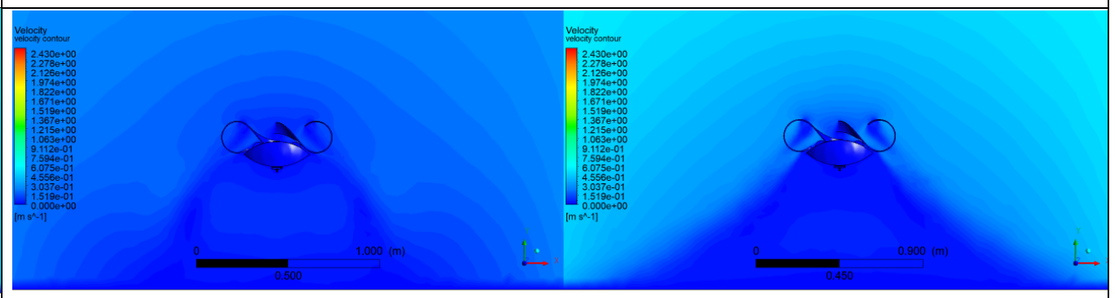
</td></tr>
<tr><td>0.3 m/s</td><td>0.6 m/s</td><td>0.3 m/s</td><td>0.6 m/s</td></tr>
<tr><td colspan="2"> 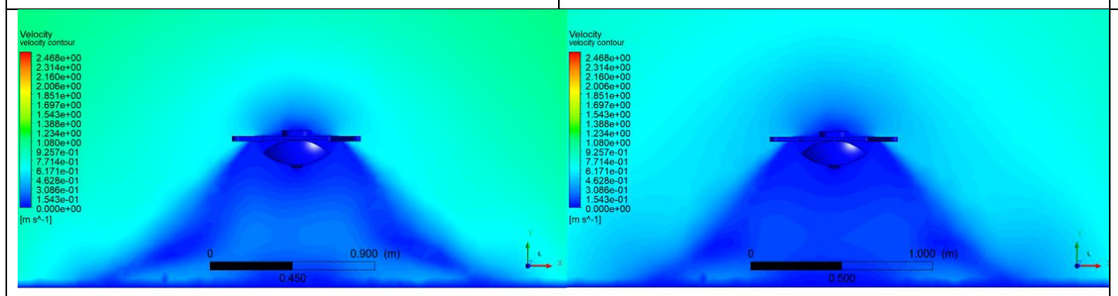
</td><td colspan="2"> 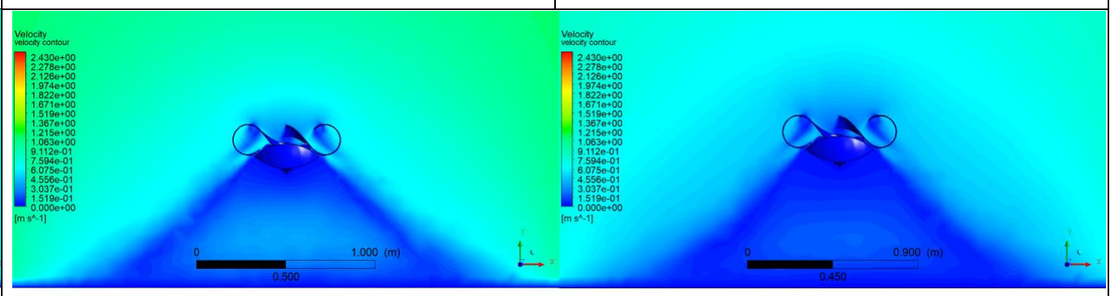
</td></tr>
<tr><td>1.2 m/s</td><td>0.9 m/s</td><td>1.2 m/s</td><td>0.9 m/s</td></tr>
<tr><td colspan="4">At 0.5 m hovering height</td></tr>
<tr><td colspan="2"> 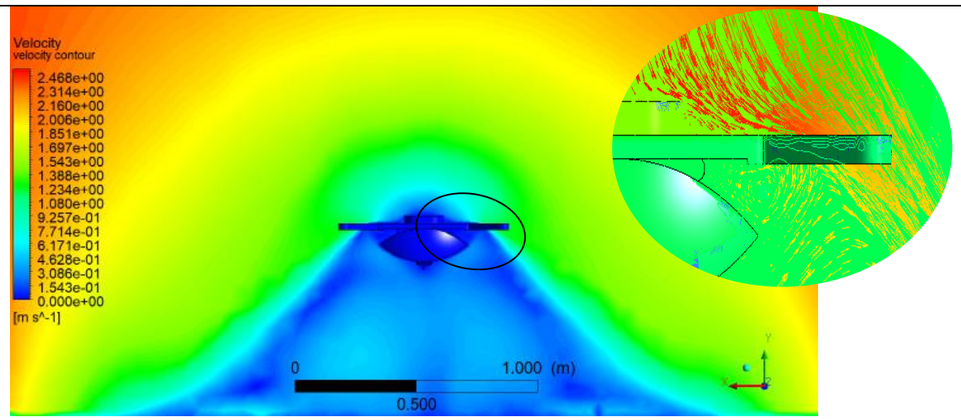
</td><td colspan="2"> 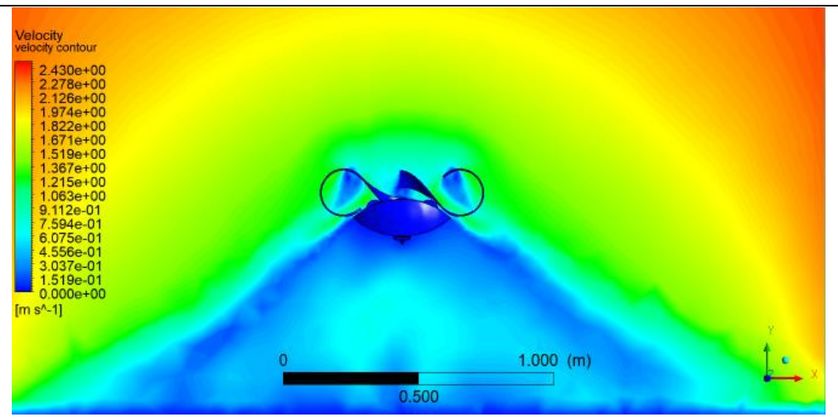
</td></tr>
<tr><td colspan="2">2.5 m/s</td><td colspan="2">2.5 m/s</td></tr>
<tr><td colspan="4">At elevated hovering height</td></tr>
</table>

Table D-11. Plot of velocity contour for M2-C along downwash flow

Downwash wind flow velocity contour	
M2-C	
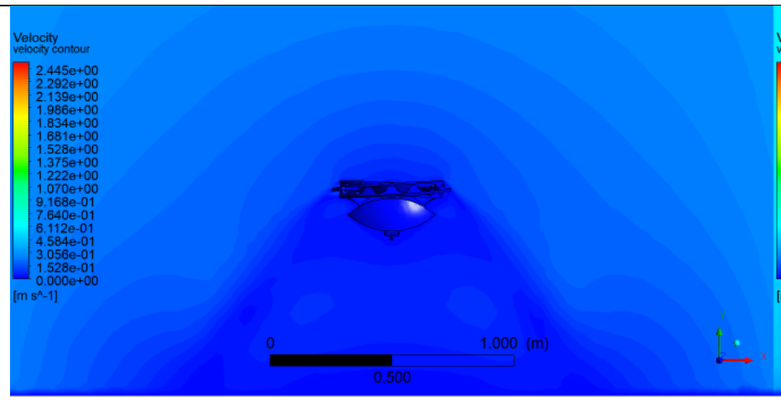	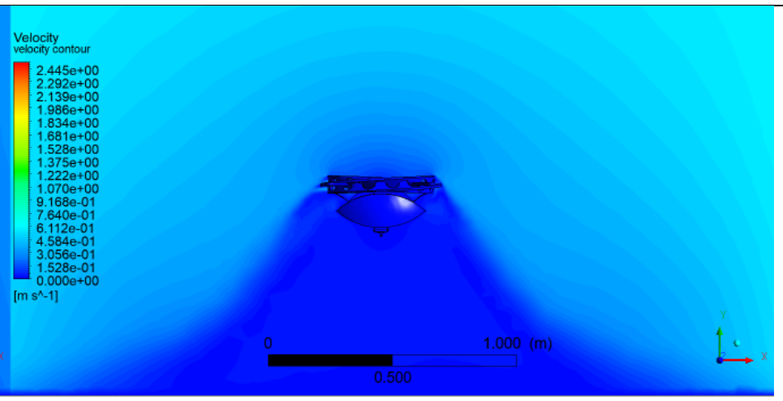
0.3 m/s	0.6 m/s
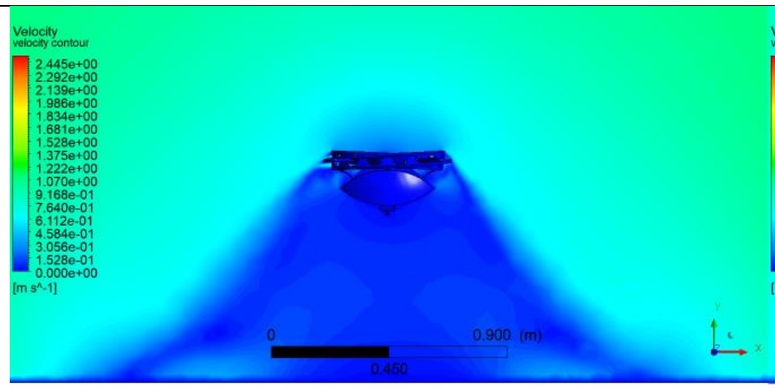	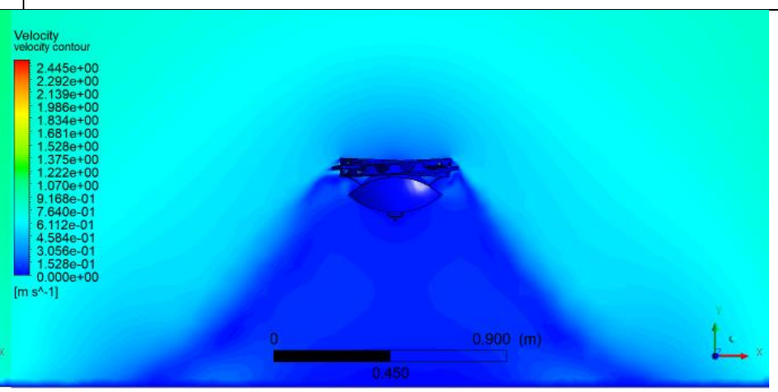
1.2 m/s	0.9 m/s
At 0.5 m hovering height	
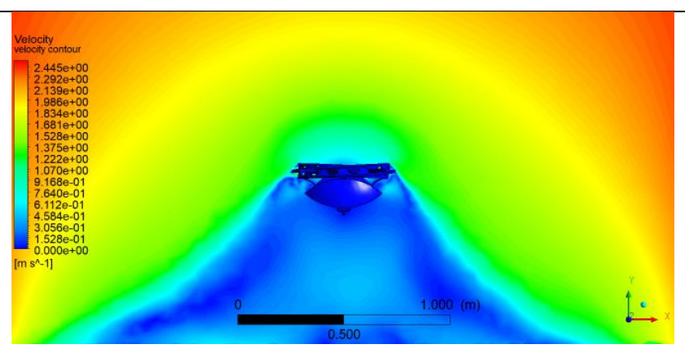	
2.5 m/s	
At elevated hovering height	

Table D-12. Plot of velocity contour for M2-A & M2-B along horizontal wind flow.

<table>
<tr><td colspan="4">Horizontal wind flow velocity contour</td></tr>
<tr><td colspan="2">M2-A</td><td colspan="2">M2-B</td></tr>
<tr><td colspan="2"> 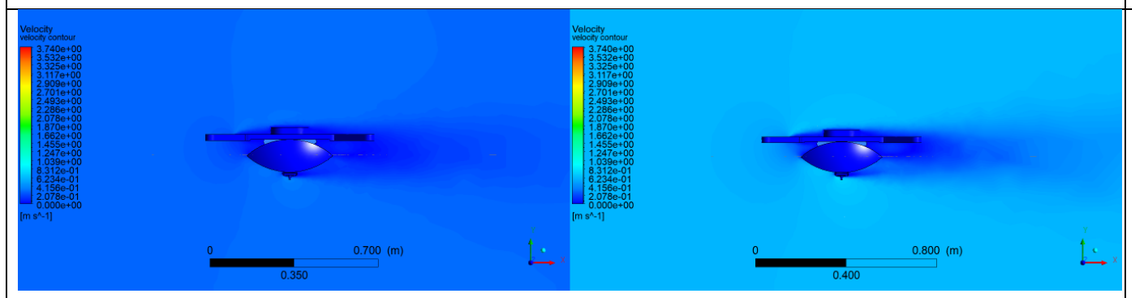 </td><td colspan="2"> 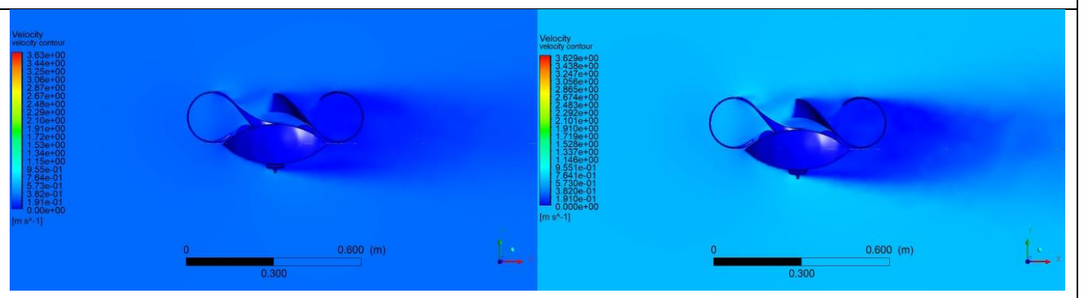 </td></tr>
<tr><td>0.3 m/s</td><td>0.6 m/s</td><td>0.3 m/s</td><td>0.6 m/s</td></tr>
<tr><td colspan="2"> 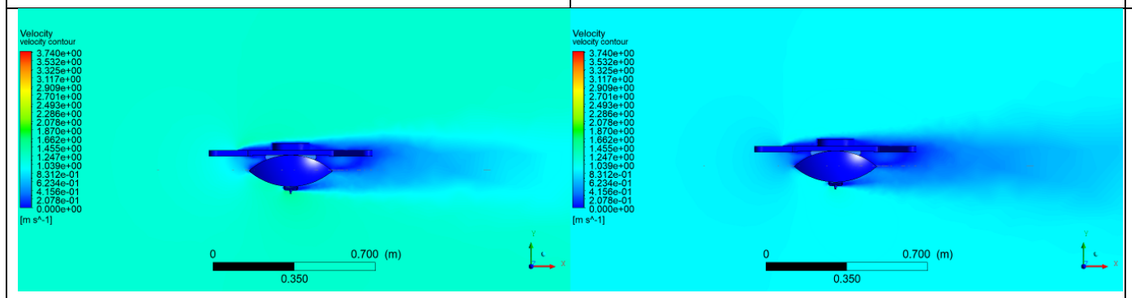 </td><td colspan="2"> 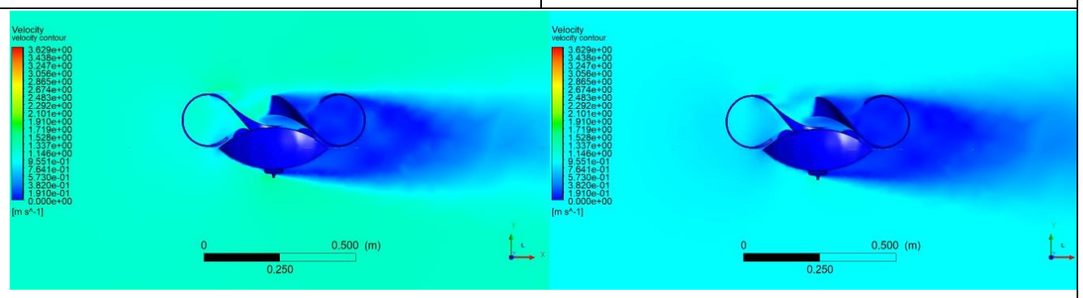 </td></tr>
<tr><td>1.2 m/s</td><td>0.9 m/s</td><td>1.2 m/s</td><td>0.9 m/s</td></tr>
<tr><td colspan="4">At 0.5 m hovering height</td></tr>
<tr><td colspan="2"> 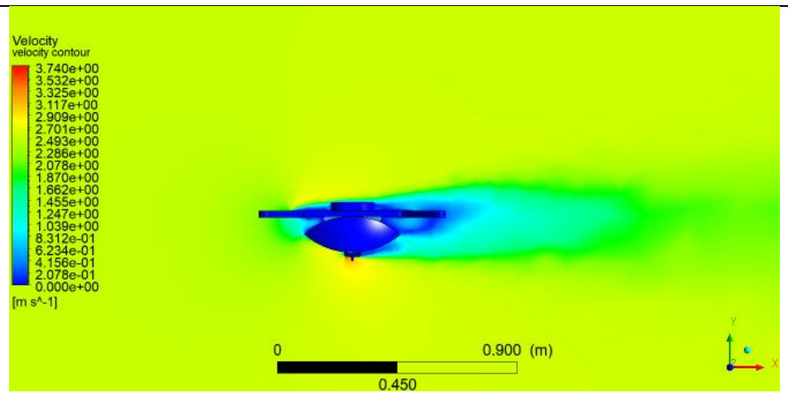 </td><td colspan="2"> 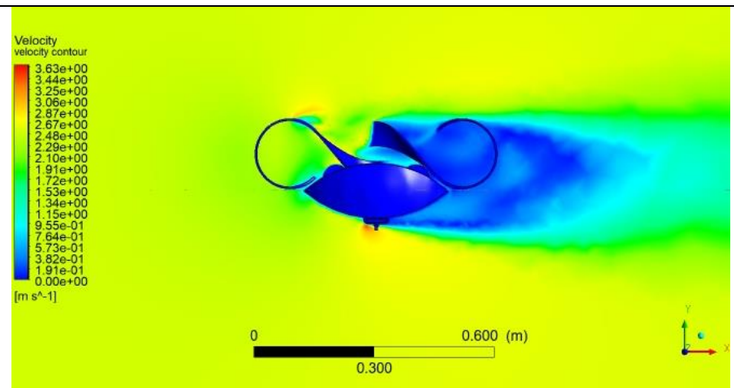 </td></tr>
<tr><td colspan="2">2.5 m/s</td><td colspan="2">2.5 m/s</td></tr>
<tr><td colspan="4">At elevated hovering height</td></tr>
</table>

Table D-13. Plot of velocity contour for M2-C along horizontal wind flow

Horizontal wind flow velocity contour	
M2-C	
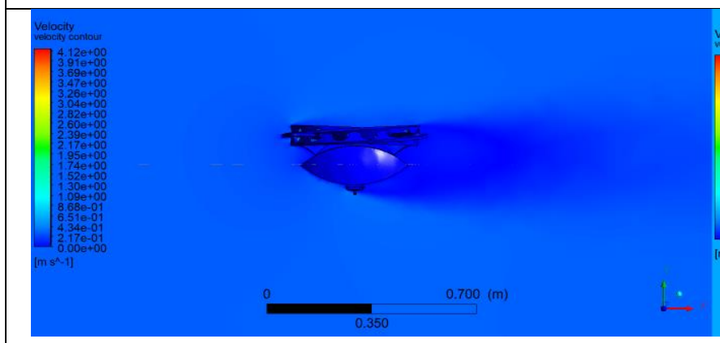	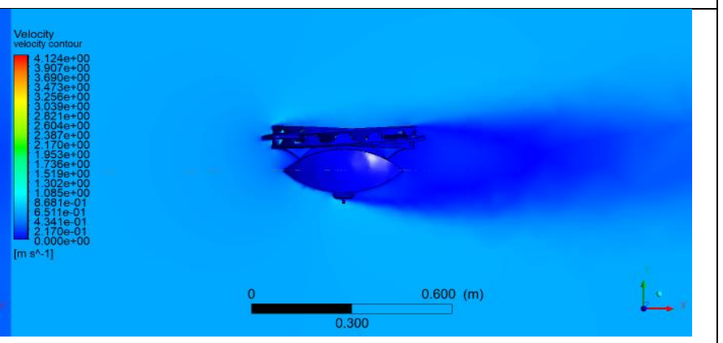
0.3 m/s	0.6 m/s
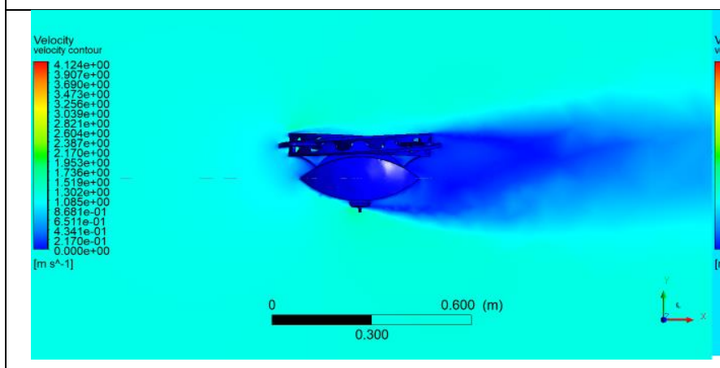	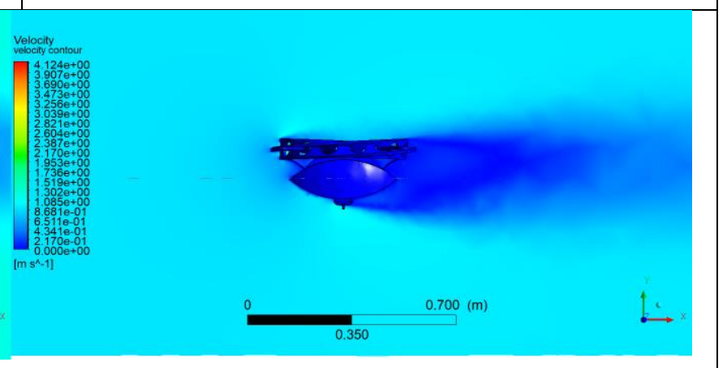
1.2 m/s	0.9 m/s
At 0.5 m hovering height	
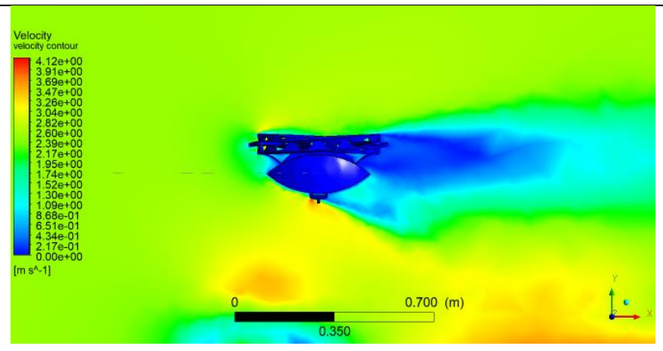	
2.5 m/s	
At elevated hovering height	

Appendix E. Velocity data points

The data points are values obtained directly from the simulation software. Below is datapoint value of velocity magnitude for model 2-A when the flow is downwash.

Table E-14. Data point of velocity vs position along with wind speeds.

y	velocity y	y	0.6 m/s at y=0	y		y		y	
m	m/s	m		m		m		m	
	0.3 at y=0	x	M2-A	x	0.9 m/s at y=0	x	1.2 m/s at y=0	x	2.5 m/s at y=0
2.77	0.299851	2.77	0.599693	2.77	0.89953	2.77	1.199384	2.77	2.498683
2.763061	0.299831	2.763061	0.599651	2.763061	0.899467	2.763061	1.1993	2.763061	2.498507
2.756122	0.299811	2.756122	0.59961	2.756122	0.899404	2.756122	1.199216	2.756122	2.49833
2.749183	0.299791	2.749183	0.599569	2.749183	0.899341	2.749183	1.199132	2.749183	2.498153
2.742244	0.29977	2.742244	0.599527	2.742244	0.899278	2.742244	1.199047	2.742244	2.497974
2.735305	0.299748	2.735305	0.599483	2.735305	0.89921	2.735305	1.198957	2.735305	2.497785
2.728366	0.299727	2.728366	0.599439	2.728366	0.899143	2.728366	1.198867	2.728366	2.497595
2.721427	0.299705	2.721427	0.599395	2.721427	0.899076	2.721427	1.198778	2.721427	2.497406
2.714489	0.299681	2.714489	0.599347	2.714489	0.899003	2.714489	1.198681	2.714489	2.497201
2.70755	0.299656	2.70755	0.599295	2.70755	0.898924	2.70755	1.198576	2.70755	2.496979
2.700611	0.299631	2.700611	0.599245	2.700611	0.898848	2.700611	1.198473	2.700611	2.496764
2.693672	0.299606	2.693672	0.599195	2.693672	0.898771	2.693672	1.19837	2.693672	2.496549
2.686733	0.299581	2.686733	0.599145	2.686733	0.898694	2.686733	1.198267	2.686733	2.496334
2.679794	0.299556	2.679794	0.599094	2.679794	0.898618	2.679794	1.198165	2.679794	2.496119
2.672855	0.299531	2.672855	0.599044	2.672855	0.898541	2.672855	1.198062	2.672855	2.495903
2.665916	0.299506	2.665916	0.598994	2.665916	0.898465	2.665916	1.197959	2.665916	2.495689
2.658977	0.299481	2.658977	0.598944	2.658977	0.898388	2.658977	1.197856	2.658977	2.495474
2.652038	0.299456	2.652038	0.598893	2.652038	0.898311	2.652038	1.197753	2.652038	2.495259
2.645099	0.299431	2.645099	0.598843	2.645099	0.898235	2.645099	1.19765	2.645099	2.495044
2.63816	0.2994	2.63816	0.59878	2.63816	0.898138	2.63816	1.197521	2.63816	2.494772
2.631221	0.299367	2.631221	0.598715	2.631221	0.898039	2.631221	1.197389	2.631221	2.494493
2.624282	0.299331	2.624282	0.598642	2.624282	0.897928	2.624282	1.19724	2.624282	2.494181
2.617343	0.299294	2.617343	0.598568	2.617343	0.897816	2.617343	1.197089	2.617343	2.493863
2.610404	0.299257	2.610404	0.598494	2.610404	0.897702	2.610404	1.196937	2.610404	2.493543
2.603466	0.299215	2.603466	0.59841	2.603466	0.897573	2.603466	1.196764	2.603466	2.493181
2.596527	0.299173	2.596527	0.598325	2.596527	0.897444	2.596527	1.196591	2.596527	2.492818
2.589588	0.299131	2.589588	0.598241	2.589588	0.897315	2.589588	1.196417	2.589588	2.492456
2.582649	0.299088	2.582649	0.598156	2.582649	0.897185	2.582649	1.196244	2.582649	2.492091
2.57571	0.299046	2.57571	0.59807	2.57571	0.897053	2.57571	1.196068	2.57571	2.491721
2.568771	0.299003	2.568771	0.597985	2.568771	0.896922	2.568771	1.195892	2.568771	2.491351
2.561832	0.29896	2.561832	0.597899	2.561832	0.896791	2.561832	1.195716	2.561832	2.49098
2.554893	0.298917	2.554893	0.597813	2.554893	0.896659	2.554893	1.195539	2.554893	2.49061
2.547954	0.298874	2.547954	0.597728	2.547954	0.896528	2.547954	1.195364	2.547954	2.490239
2.541015	0.29883	2.541015	0.597639	2.541015	0.896393	2.541015	1.195182	2.541015	2.489859
2.534076	0.298785	2.534076	0.59755	2.534076	0.896255	2.534076	1.194998	2.534076	2.489473
2.527137	0.298734	2.527137	0.597448	2.527137	0.896098	2.527137	1.194788	2.527137	2.489032
2.520198	0.298676	2.520198	0.597331	2.520198	0.895921	2.520198	1.19455	2.520198	2.48853
2.513259	0.298618	2.513259	0.597215	2.513259	0.895742	2.513259	1.19431	2.513259	2.488026
2.50632	0.298559	2.50632	0.597098	2.50632	0.895563	2.50632	1.19407	2.50632	2.487521
2.499382	0.298501	2.499382	0.596981	2.499382	0.895384	2.499382	1.19383	2.499382	2.487017
2.492443	0.298442	2.492443	0.596865	2.492443	0.895205	2.492443	1.19359	2.492443	2.486513
2.485504	0.298384	2.485504	0.596748	2.485504	0.895026	2.485504	1.19335	2.485504	2.486008
2.478565	0.298325	2.478565	0.596632	2.478565	0.894848	2.478565	1.19311	2.478565	2.485504
2.471626	0.298267	2.471626	0.596515	2.471626	0.894669	2.471626	1.192871	2.471626	2.485
2.464687	0.298208	2.464687	0.596398	2.464687	0.89449	2.464687	1.192631	2.464687	2.484495
2.457748	0.29815	2.457748	0.596281	2.457748	0.894311	2.457748	1.192391	2.457748	2.483991
2.450809	0.298092	2.450809	0.596165	2.450809	0.894132	2.450809	1.192151	2.450809	2.483486
2.44387	0.298018	2.44387	0.596018	2.44387	0.893908	2.44387	1.19185	2.44387	2.482853
2.436931	0.297943	2.436931	0.595869	2.436931	0.893679	2.436931	1.191543	2.436931	2.482207
2.429992	0.297868	2.429992	0.59572	2.429992	0.89345	2.429992	1.191236	2.429992	2.48156
2.423053	0.297794	2.423053	0.595571	2.423053	0.893221	2.423053	1.190929	2.423053	2.480914
2.416114	0.297719	2.416114	0.595421	2.416114	0.892992	2.416114	1.190622	2.416114	2.480268
2.409175	0.297644	2.409175	0.595272	2.409175	0.892763	2.409175	1.190315	2.409175	2.479621
2.402236	0.297571	2.402236	0.595126	2.402236	0.892538	2.402236	1.190014	2.402236	2.478988
2.395298	0.297501	2.395298	0.594987	2.395298	0.892325	2.395298	1.189729	2.395298	2.478386

2.388359	0.297431	2.388359	0.594848	2.388359	0.892112	2.388359	1.189443	2.388359	2.477784	2.159374	0.294261	2.159374	0.588563	2.159374	0.882462	2.159374	1.176448	2.159374	2.45063
2.38142	0.297361	2.38142	0.594707	2.38142	0.891897	2.38142	1.189155	2.38142	2.477178	2.152435	0.294128	2.152435	0.5883	2.152435	0.882057	2.152435	1.175902	2.152435	2.449489
2.374481	0.297289	2.374481	0.594565	2.374481	0.891679	2.374481	1.188862	2.374481	2.476565	2.145496	0.293995	2.145496	0.588036	2.145496	0.881653	2.145496	1.175357	2.145496	2.448348
2.367542	0.297218	2.367542	0.594423	2.367542	0.891461	2.367542	1.18857	2.367542	2.475951	2.138557	0.293861	2.138557	0.587773	2.138557	0.881248	2.138557	1.174811	2.138557	2.447208
2.360603	0.297147	2.360603	0.594281	2.360603	0.891243	2.360603	1.188277	2.360603	2.475338	2.131618	0.293728	2.131618	0.58751	2.131618	0.880844	2.131618	1.174265	2.131618	2.446067
2.353664	0.297076	2.353664	0.594139	2.353664	0.891026	2.353664	1.187985	2.353664	2.474725	2.124679	0.293594	2.124679	0.587246	2.124679	0.88044	2.124679	1.17372	2.124679	2.444927
2.346725	0.297004	2.346725	0.593997	2.346725	0.890808	2.346725	1.187693	2.346725	2.474112	2.11774	0.293461	2.11774	0.586983	2.11774	0.880035	2.11774	1.173174	2.11774	2.443786
2.339786	0.296933	2.339786	0.593855	2.339786	0.89059	2.339786	1.187401	2.339786	2.473499	2.110801	0.293327	2.110801	0.586719	2.110801	0.879631	2.110801	1.172628	2.110801	2.442646
2.332847	0.296858	2.332847	0.593706	2.332847	0.890361	2.332847	1.187092	2.332847	2.472854	2.103862	0.293194	2.103862	0.586456	2.103862	0.879226	2.103862	1.172083	2.103862	2.441505
2.325908	0.29677	2.325908	0.593532	2.325908	0.890093	2.325908	1.186732	2.325908	2.472102	2.096923	0.293058	2.096923	0.586188	2.096923	0.878815	2.096923	1.171528	2.096923	2.440345
2.318969	0.296682	2.318969	0.593357	2.318969	0.889826	2.318969	1.186372	2.318969	2.47135	2.089984	0.292907	2.089984	0.585891	2.089984	0.878357	2.089984	1.170911	2.089984	2.439054
2.31203	0.296595	2.31203	0.593183	2.31203	0.889558	2.31203	1.186012	2.31203	2.470599	2.083045	0.292755	2.083045	0.585593	2.083045	0.877899	2.083045	1.170294	2.083045	2.437764
2.305091	0.296507	2.305091	0.593009	2.305091	0.88929	2.305091	1.185651	2.305091	2.469847	2.076107	0.292604	2.076107	0.585295	2.076107	0.877441	2.076107	1.169677	2.076107	2.436473
2.298152	0.296419	2.298152	0.592835	2.298152	0.889023	2.298152	1.185291	2.298152	2.469096	2.069168	0.292453	2.069168	0.584998	2.069168	0.876983	2.069168	1.169061	2.069168	2.435183
2.291214	0.296331	2.291214	0.59266	2.291214	0.888755	2.291214	1.184931	2.291214	2.468344	2.062229	0.292301	2.062229	0.584701	2.062229	0.876525	2.062229	1.168444	2.062229	2.433893
2.284275	0.296243	2.284275	0.592486	2.284275	0.888488	2.284275	1.184571	2.284275	2.467592	2.05529	0.292158	2.05529	0.584419	2.05529	0.876091	2.05529	1.16786	2.05529	2.432671
2.277336	0.296164	2.277336	0.592328	2.277336	0.888245	2.277336	1.184244	2.277336	2.46691	2.048351	0.292017	2.048351	0.584141	2.048351	0.875664	2.048351	1.167284	2.048351	2.431465
2.270397	0.296088	2.270397	0.592177	2.270397	0.888013	2.270397	1.183931	2.270397	2.466258	2.041412	0.291876	2.041412	0.583863	2.041412	0.875236	2.041412	1.166707	2.041412	2.43026
2.263458	0.296012	2.263458	0.592026	2.263458	0.887781	2.263458	1.183619	2.263458	2.465606	2.034473	0.291735	2.034473	0.583586	2.034473	0.874808	2.034473	1.166131	2.034473	2.429054
2.256519	0.295936	2.256519	0.591875	2.256519	0.887549	2.256519	1.183307	2.256519	2.464953	2.027534	0.291593	2.027534	0.583308	2.027534	0.87438	2.027534	1.165554	2.027534	2.427848
2.24958	0.29586	2.24958	0.591724	2.24958	0.887317	2.24958	1.182995	2.24958	2.464301	2.020595	0.291452	2.020595	0.58303	2.020595	0.873952	2.020595	1.164978	2.020595	2.426642
2.242641	0.295742	2.242641	0.59149	2.242641	0.886957	2.242641	1.18251	2.242641	2.463289	2.013656	0.291311	2.013656	0.582752	2.013656	0.873524	2.013656	1.164402	2.013656	2.425437
2.235702	0.295618	2.235702	0.591247	2.235702	0.886583	2.235702	1.182006	2.235702	2.462237	2.006717	0.29117	2.006717	0.582474	2.006717	0.873096	2.006717	1.163825	2.006717	2.424231
2.228763	0.295495	2.228763	0.591003	2.228763	0.886209	2.228763	1.181502	2.228763	2.461185	1.999778	0.291029	1.999778	0.582197	1.999778	0.872668	1.999778	1.163249	1.999778	2.423025
2.221824	0.295372	2.221824	0.59076	2.221824	0.885835	2.221824	1.180997	2.221824	2.460132	1.992839	0.290887	1.992839	0.581919	1.992839	0.872241	1.992839	1.162672	1.992839	2.421819
2.214885	0.295249	2.214885	0.590516	2.214885	0.885461	2.214885	1.180493	2.214885	2.45908	1.9859	0.290723	1.9859	0.581597	1.9859	0.871745	1.9859	1.162005	1.9859	2.420423
2.207946	0.295126	2.207946	0.590273	2.207946	0.885087	2.207946	1.179989	2.207946	2.458028	1.978961	0.290551	1.978961	0.581259	1.978961	0.871223	1.978961	1.161304	1.978961	2.418956
2.201007	0.29501	2.201007	0.590042	2.201007	0.884734	2.201007	1.179513	2.201007	2.457032	1.972023	0.290378	1.972023	0.58092	1.972023	0.870702	1.972023	1.160603	1.972023	2.41749
2.194068	0.294893	2.194068	0.589812	2.194068	0.884379	2.194068	1.179035	2.194068	2.456035	1.965084	0.290206	1.965084	0.580582	1.965084	0.87018	1.965084	1.159902	1.965084	2.416023
2.18713	0.294777	2.18713	0.589581	2.18713	0.884025	2.18713	1.178557	2.18713	2.455037	1.958145	0.290033	1.958145	0.580243	1.958145	0.869659	1.958145	1.159201	1.958145	2.414555
2.180191	0.29466	2.180191	0.58935	2.180191	0.883671	2.180191	1.178079	2.180191	2.454039	1.951206	0.289858	1.951206	0.5799	1.951206	0.869129	1.951206	1.158489	1.951206	2.413067
2.173252	0.294528	2.173252	0.58909	2.173252	0.883271	2.173252	1.177539	2.173252	2.452911	1.944267	0.28969	1.944267	0.57957	1.944267	0.868621	1.944267	1.157804	1.944267	2.411634
2.166313	0.294395	2.166313	0.588826	2.166313	0.882866	2.166313	1.176994	2.166313	2.45177	1.937328	0.289519	1.937328	0.579235	1.937328	0.868104	1.937328	1.157108	1.937328	2.410178

1.930389	0.289342	1.930389	0.578887	1.930389	0.867567	1.930389	1.156386	1.930389	2.408667	1.701404	0.282436	1.701404	0.565427	1.701404	0.846755	1.701404	1.128347	1.701404	2.350122
1.92345	0.289146	1.92345	0.578504	1.92345	0.866974	1.92345	1.155587	1.92345	2.406997	1.694465	0.282223	1.694465	0.565013	1.694465	0.846114	1.694465	1.127482	1.694465	2.348318
1.916511	0.28895	1.916511	0.57812	1.916511	0.866381	1.916511	1.154788	1.916511	2.405327	1.687526	0.282007	1.687526	0.564593	1.687526	0.845465	1.687526	1.126608	1.687526	2.346495
1.909572	0.288753	1.909572	0.577736	1.909572	0.865788	1.909572	1.153989	1.909572	2.403657	1.680587	0.281792	1.680587	0.564174	1.680587	0.844816	1.680587	1.125734	1.680587	2.344671
1.902633	0.288557	1.902633	0.577352	1.902633	0.865195	1.902633	1.153191	1.902633	2.401987	1.673648	0.281575	1.673648	0.563754	1.673648	0.844166	1.673648	1.124858	1.673648	2.342845
1.895694	0.288361	1.895694	0.576968	1.895694	0.864602	1.895694	1.152392	1.895694	2.400316	1.666709	0.281324	1.666709	0.563267	1.666709	0.843411	1.666709	1.123841	1.666709	2.340721
1.888755	0.288165	1.888755	0.576584	1.888755	0.864008	1.888755	1.151593	1.888755	2.398647	1.65977	0.281083	1.65977	0.562798	1.65977	0.842685	1.65977	1.122862	1.65977	2.338675
1.881816	0.287969	1.881816	0.5762	1.881816	0.863415	1.881816	1.150794	1.881816	2.396976	1.652832	0.28085	1.652832	0.562344	1.652832	0.841982	1.652832	1.121915	1.652832	2.336694
1.874877	0.287772	1.874877	0.575816	1.874877	0.862822	1.874877	1.149995	1.874877	2.395306	1.645893	0.280616	1.645893	0.56189	1.645893	0.841279	1.645893	1.120967	1.645893	2.334712
1.867939	0.287576	1.867939	0.575432	1.867939	0.862229	1.867939	1.149196	1.867939	2.393636	1.638954	0.280383	1.638954	0.561436	1.638954	0.840576	1.638954	1.12002	1.638954	2.332731
1.861	0.28738	1.861	0.575048	1.861	0.861636	1.861	1.148397	1.861	2.391966	1.632015	0.28015	1.632015	0.560982	1.632015	0.839873	1.632015	1.119072	1.632015	2.33075
1.854061	0.287184	1.854061	0.574664	1.854061	0.861043	1.854061	1.147598	1.854061	2.390296	1.625076	0.279916	1.625076	0.560528	1.625076	0.83917	1.625076	1.118125	1.625076	2.328768
1.847122	0.286988	1.847122	0.574281	1.847122	0.86045	1.847122	1.146799	1.847122	2.388625	1.618137	0.279656	1.618137	0.560023	1.618137	0.838387	1.618137	1.11707	1.618137	2.326564
1.840183	0.286796	1.840183	0.573905	1.840183	0.85987	1.840183	1.146019	1.840183	2.386995	1.611198	0.279371	1.611198	0.559473	1.611198	0.837533	1.611198	1.115921	1.611198	2.324162
1.833244	0.286605	1.833244	0.573533	1.833244	0.859295	1.833244	1.145245	1.833244	2.385378	1.604259	0.279087	1.604259	0.558922	1.604259	0.836679	1.604259	1.114771	1.604259	2.321759
1.826305	0.286415	1.826305	0.573161	1.826305	0.85872	1.826305	1.144471	1.826305	2.383762	1.59732	0.278802	1.59732	0.558372	1.59732	0.835826	1.59732	1.113621	1.59732	2.319356
1.819366	0.286225	1.819366	0.572789	1.819366	0.858146	1.819366	1.143697	1.819366	2.382145	1.590381	0.278512	1.590381	0.557811	1.590381	0.834954	1.590381	1.112448	1.590381	2.316903
1.812427	0.286012	1.812427	0.572375	1.812427	0.857505	1.812427	1.142834	1.812427	2.380345	1.583442	0.278216	1.583442	0.557237	1.583442	0.834064	1.583442	1.111248	1.583442	2.314392
1.805488	0.285789	1.805488	0.571941	1.805488	0.856834	1.805488	1.141929	1.805488	2.378456	1.576503	0.27792	1.576503	0.556663	1.576503	0.833173	1.576503	1.110048	1.576503	2.311881
1.798549	0.285565	1.798549	0.571507	1.798549	0.856162	1.798549	1.141024	1.798549	2.376567	1.569564	0.277624	1.569564	0.556089	1.569564	0.832282	1.569564	1.108848	1.569564	2.30937
1.79161	0.285342	1.79161	0.571072	1.79161	0.85549	1.79161	1.140118	1.79161	2.374678	1.562625	0.277328	1.562625	0.555515	1.562625	0.831392	1.562625	1.107649	1.562625	2.306859
1.784671	0.285118	1.784671	0.570638	1.784671	0.854818	1.784671	1.139213	1.784671	2.372789	1.555686	0.277031	1.555686	0.554941	1.555686	0.830501	1.555686	1.106449	1.555686	2.304348
1.777732	0.284895	1.777732	0.570204	1.777732	0.854146	1.777732	1.138307	1.777732	2.3709	1.548748	0.276735	1.548748	0.554368	1.548748	0.82961	1.548748	1.105249	1.548748	2.301837
1.770793	0.284671	1.770793	0.56977	1.770793	0.853474	1.770793	1.137402	1.770793	2.369011	1.541809	0.276439	1.541809	0.553794	1.541809	0.82872	1.541809	1.104049	1.541809	2.299326
1.763855	0.284448	1.763855	0.569335	1.763855	0.852802	1.763855	1.136496	1.763855	2.367122	1.53487	0.276143	1.53487	0.55322	1.53487	0.827829	1.53487	1.102849	1.53487	2.296815
1.756916	0.284224	1.756916	0.568901	1.756916	0.85213	1.756916	1.135591	1.756916	2.365233	1.527931	0.275847	1.527931	0.552646	1.527931	0.826938	1.527931	1.10165	1.527931	2.294304
1.749977	0.284001	1.749977	0.568467	1.749977	0.851458	1.749977	1.134685	1.749977	2.363344	1.520992	0.27555	1.520992	0.552072	1.520992	0.826048	1.520992	1.10045	1.520992	2.291793
1.743038	0.283777	1.743038	0.568033	1.743038	0.850786	1.743038	1.13378	1.743038	2.361456	1.514053	0.275254	1.514053	0.551498	1.514053	0.825157	1.514053	1.09925	1.514053	2.289282
1.736099	0.283554	1.736099	0.567598	1.736099	0.850115	1.736099	1.132874	1.736099	2.359567	1.507114	0.274958	1.507114	0.550924	1.507114	0.824266	1.507114	1.09805	1.507114	2.286771
1.72916	0.28333	1.72916	0.567164	1.72916	0.849443	1.72916	1.131969	1.72916	2.357678	1.500175	0.274662	1.500175	0.55035	1.500175	0.823376	1.500175	1.09685	1.500175	2.28426
1.722221	0.283107	1.722221	0.56673	1.722221	0.848771	1.722221	1.131063	1.722221	2.355789	1.493236	0.274365	1.493236	0.549777	1.493236	0.822485	1.493236	1.095651	1.493236	2.281749
1.715282	0.282883	1.715282	0.566296	1.715282	0.848099	1.715282	1.130158	1.715282	2.3539	1.486297	0.274069	1.486297	0.549203	1.486297	0.821594	1.486297	1.094451	1.486297	2.279238
1.708343	0.28266	1.708343	0.565862	1.708343	0.847427	1.708343	1.129253	1.708343	2.352011	1.479358	0.273766	1.479358	0.548619	1.479358	0.820688	1.479358	1.093229	1.479358	2.276683

1.472419	0.273461	1.472419	0.548033	1.472419	0.819778	1.472419	1.092005	1.472419	2.274121	1.243434	0.262153	1.243434	0.526324	1.243434	0.785996	1.243434	1.046492	1.243434	2.17908
1.46548	0.273157	1.46548	0.547448	1.46548	0.818869	1.46548	1.09078	1.46548	2.271559	1.236495	0.261577	1.236495	0.525223	1.236495	0.78428	1.236495	1.044178	1.236495	2.174247
1.458541	0.272852	1.458541	0.546862	1.458541	0.817959	1.458541	1.089555	1.458541	2.268996	1.229557	0.261001	1.229557	0.524122	1.229557	0.782563	1.229557	1.041863	1.229557	2.169415
1.451602	0.272548	1.451602	0.546277	1.451602	0.817049	1.451602	1.08833	1.451602	2.266434	1.222618	0.260426	1.222618	0.523022	1.222618	0.780847	1.222618	1.039549	1.222618	2.164582
1.444664	0.272243	1.444664	0.545691	1.444664	0.81614	1.444664	1.087106	1.444664	2.263873	1.215679	0.25985	1.215679	0.521921	1.215679	0.779131	1.215679	1.037235	1.215679	2.159751
1.437725	0.271939	1.437725	0.545106	1.437725	0.815231	1.437725	1.085881	1.437725	2.261311	1.20874	0.259274	1.20874	0.52082	1.20874	0.777415	1.20874	1.03492	1.20874	2.154919
1.430786	0.271635	1.430786	0.544522	1.430786	0.814324	1.430786	1.08466	1.430786	2.258756	1.201801	0.258698	1.201801	0.51972	1.201801	0.775699	1.201801	1.032606	1.201801	2.150087
1.423847	0.271335	1.423847	0.543945	1.423847	0.813427	1.423847	1.083453	1.423847	2.256231	1.194862	0.258123	1.194862	0.518619	1.194862	0.773983	1.194862	1.030292	1.194862	2.145255
1.416908	0.271035	1.416908	0.543368	1.416908	0.81253	1.416908	1.082245	1.416908	2.253706	1.187923	0.257547	1.187923	0.517519	1.187923	0.772267	1.187923	1.027977	1.187923	2.140423
1.409969	0.270707	1.409969	0.542736	1.409969	0.811548	1.409969	1.080923	1.409969	2.250944	1.180984	0.256971	1.180984	0.516418	1.180984	0.770551	1.180984	1.025663	1.180984	2.135591
1.40303	0.270368	1.40303	0.542085	1.40303	0.810534	1.40303	1.079556	1.40303	2.248095	1.174045	0.256395	1.174045	0.515318	1.174045	0.768835	1.174045	1.023349	1.174045	2.130759
1.396091	0.27003	1.396091	0.541434	1.396091	0.80952	1.396091	1.07819	1.396091	2.245246	1.167106	0.25582	1.167106	0.514217	1.167106	0.767119	1.167106	1.021035	1.167106	2.125927
1.389152	0.269691	1.389152	0.540782	1.389152	0.808506	1.389152	1.076823	1.389152	2.242396	1.160167	0.255243	1.160167	0.513115	1.160167	0.7654	1.160167	1.018717	1.160167	2.121088
1.382213	0.269352	1.382213	0.540131	1.382213	0.807492	1.382213	1.075457	1.382213	2.239547	1.153228	0.2547	1.153228	0.512075	1.153228	0.763779	1.153228	1.016531	1.153228	2.116533
1.375274	0.269014	1.375274	0.53948	1.375274	0.806479	1.375274	1.074091	1.375274	2.236698	1.146289	0.254175	1.146289	0.511071	1.146289	0.762214	1.146289	1.014421	1.146289	2.112138
1.368335	0.268675	1.368335	0.538828	1.368335	0.805465	1.368335	1.072724	1.368335	2.233848	1.13935	0.25365	1.13935	0.510067	1.13935	0.760649	1.13935	1.012311	1.13935	2.107743
1.361396	0.268337	1.361396	0.538177	1.361396	0.804451	1.361396	1.071358	1.361396	2.230999	1.132411	0.253125	1.132411	0.509063	1.132411	0.759084	1.132411	1.010201	1.132411	2.103348
1.354457	0.267989	1.354457	0.537509	1.354457	0.803411	1.354457	1.069957	1.354457	2.228077	1.125473	0.252601	1.125473	0.508059	1.125473	0.757519	1.125473	1.008091	1.125473	2.098954
1.347518	0.26764	1.347518	0.53684	1.347518	0.802368	1.347518	1.068551	1.347518	2.225146	1.118534	0.252076	1.118534	0.507055	1.118534	0.755954	1.118534	1.00598	1.118534	2.094559
1.34058	0.267291	1.34058	0.53617	1.34058	0.801325	1.34058	1.067146	1.34058	2.222215	1.111595	0.251493	1.111595	0.505942	1.111595	0.754218	1.111595	1.00364	1.111595	2.089684
1.333641	0.266942	1.333641	0.5355	1.333641	0.800282	1.333641	1.06574	1.333641	2.219284	1.104656	0.250826	1.104656	0.504673	1.104656	0.75224	1.104656	1.000972	1.104656	2.084124
1.326702	0.266603	1.326702	0.53485	1.326702	0.79927	1.326702	1.064376	1.326702	2.216436	1.097717	0.250159	1.097717	0.503405	1.097717	0.750261	1.097717	0.998303	1.097717	2.078563
1.319763	0.266266	1.319763	0.534204	1.319763	0.798265	1.319763	1.063023	1.319763	2.21361	1.090778	0.249588	1.090778	0.502317	1.090778	0.748563	1.090778	0.996014	1.090778	2.073795
1.312824	0.26593	1.312824	0.533559	1.312824	0.797261	1.312824	1.06167	1.312824	2.210783	1.083839	0.249074	1.083839	0.501334	1.083839	0.747031	1.083839	0.993947	1.083839	2.06949
1.305885	0.265593	1.305885	0.532913	1.305885	0.796256	1.305885	1.060317	1.305885	2.207957	1.0769	0.248559	1.0769	0.500351	1.0769	0.745499	1.0769	0.99188	1.0769	2.065186
1.298946	0.265256	1.298946	0.532268	1.298946	0.795252	1.298946	1.058964	1.298946	2.205131	1.069961	0.248045	1.069961	0.499369	1.069961	0.743967	1.069961	0.989813	1.069961	2.060882
1.292007	0.26492	1.292007	0.531622	1.292007	0.794247	1.292007	1.057611	1.292007	2.202304	1.063022	0.24753	1.063022	0.498386	1.063022	0.742434	1.063022	0.987746	1.063022	2.056578
1.285068	0.264583	1.285068	0.530977	1.285068	0.793243	1.285068	1.056259	1.285068	2.199478	1.056083	0.247016	1.056083	0.497404	1.056083	0.740902	1.056083	0.985679	1.056083	2.052274
1.278129	0.264246	1.278129	0.530332	1.278129	0.792239	1.278129	1.054906	1.278129	2.196652	1.049144	0.246501	1.049144	0.496421	1.049144	0.73937	1.049144	0.983612	1.049144	2.04797
1.27119	0.26391	1.27119	0.529686	1.27119	0.791234	1.27119	1.053553	1.27119	2.193826	1.042205	0.245987	1.042205	0.495438	1.042205	0.737837	1.042205	0.981545	1.042205	2.043666
1.264251	0.263573	1.264251	0.529041	1.264251	0.79023	1.264251	1.0522	1.264251	2.191	1.035266	0.245473	1.035266	0.494456	1.035266	0.736305	1.035266	0.979479	1.035266	2.039362
1.257312	0.263237	1.257312	0.528395	1.257312	0.789226	1.257312	1.050847	1.257312	2.188174	1.028327	0.244958	1.028327	0.493473	1.028327	0.734773	1.028327	0.977412	1.028327	2.035059
1.250373	0.262729	1.250373	0.527424	1.250373	0.787712	1.250373	1.048807	1.250373	2.183912	1.021389	0.244444	1.021389	0.492491	1.021389	0.733241	1.021389	0.975345	1.021389	2.030755

1.01445	0.243929	1.01445	0.491508	1.01445	0.731709	1.01445	0.973278	1.01445	2.026451	0.785467	0.219409	0.785467	0.44485	0.785467	0.659098	0.785467	0.87544	0.785467	1.823519
1.007511	0.243415	1.007511	0.490526	1.007511	0.730176	1.007511	0.971211	1.007511	2.022147	0.778528	0.218583	0.778528	0.443277	0.778528	0.656652	0.778528	0.872145	0.778528	1.816702
1.000572	0.242901	1.000572	0.489543	1.000572	0.728644	1.000572	0.969145	1.000572	2.017844	0.771589	0.217574	0.771589	0.441355	0.771589	0.653669	0.771589	0.86813	0.771589	1.808364
0.993633	0.242386	0.993633	0.488561	0.993633	0.727112	0.993633	0.967078	0.993633	2.01354	0.76465	0.216497	0.76465	0.439301	0.76465	0.650483	0.76465	0.863843	0.76465	1.799454
0.986694	0.241778	0.986694	0.487402	0.986694	0.725307	0.986694	0.964644	0.986694	2.008478	0.757711	0.215419	0.757711	0.437247	0.757711	0.647297	0.757711	0.859556	0.757711	1.790545
0.979755	0.241059	0.979755	0.486034	0.979755	0.723178	0.979755	0.961776	0.979755	2.002519	0.750772	0.214342	0.750772	0.435192	0.750772	0.644111	0.750772	0.85527	0.750772	1.781635
0.972816	0.24034	0.972816	0.484666	0.972816	0.72105	0.972816	0.958908	0.972816	1.996561	0.743833	0.213264	0.743833	0.433138	0.743833	0.640925	0.743833	0.850983	0.743833	1.772726
0.965877	0.239621	0.965877	0.483299	0.965877	0.718921	0.965877	0.95604	0.965877	1.990602	0.736894	0.212187	0.736894	0.431084	0.736894	0.637739	0.736894	0.846697	0.736894	1.763817
0.958938	0.238902	0.958938	0.481931	0.958938	0.716793	0.958938	0.953172	0.958938	1.984643	0.729956	0.211096	0.729956	0.429006	0.729956	0.634515	0.729956	0.84236	0.729956	1.754784
0.952	0.238183	0.952	0.480563	0.952	0.714664	0.952	0.950305	0.952	1.978685	0.723017	0.210033	0.723017	0.42698	0.723017	0.631385	0.723017	0.838153	0.723017	1.74603
0.945061	0.237464	0.945061	0.479195	0.945061	0.712536	0.945061	0.947437	0.945061	1.972726	0.716078	0.208984	0.716078	0.424977	0.716078	0.628286	0.716078	0.833986	0.716078	1.737345
0.938122	0.236745	0.938122	0.477828	0.938122	0.710407	0.938122	0.944569	0.938122	1.966768	0.709139	0.207934	0.709139	0.422974	0.709139	0.625188	0.709139	0.829819	0.709139	1.728662
0.931183	0.236027	0.931183	0.47646	0.931183	0.708279	0.931183	0.941701	0.931183	1.96081	0.7022	0.206884	0.7022	0.420971	0.7022	0.622089	0.7022	0.825652	0.7022	1.719978
0.924244	0.235308	0.924244	0.475093	0.924244	0.70615	0.924244	0.938834	0.924244	1.954852	0.695261	0.205835	0.695261	0.418969	0.695261	0.618991	0.695261	0.821485	0.695261	1.711295
0.917305	0.234589	0.917305	0.473725	0.917305	0.704022	0.917305	0.935966	0.917305	1.948894	0.688322	0.204785	0.688322	0.416966	0.688322	0.615892	0.688322	0.817318	0.688322	1.702612
0.910366	0.233847	0.910366	0.472315	0.910366	0.701827	0.910366	0.933009	0.910366	1.942756	0.681383	0.203736	0.681383	0.414963	0.681383	0.612794	0.681383	0.813151	0.681383	1.693929
0.903427	0.233095	0.903427	0.470887	0.903427	0.699604	0.903427	0.930013	0.903427	1.93654	0.674445	0.202686	0.674445	0.41296	0.674445	0.609695	0.674445	0.808984	0.674445	1.685246
0.896489	0.232343	0.896489	0.469459	0.896489	0.69738	0.896489	0.927016	0.896489	1.930324	0.667506	0.201637	0.667506	0.410958	0.667506	0.606597	0.667506	0.804818	0.667506	1.676563
0.88955	0.231591	0.88955	0.468031	0.88955	0.695156	0.88955	0.92402	0.88955	1.924108	0.660567	0.200587	0.660567	0.408955	0.660567	0.603499	0.660567	0.800651	0.660567	1.667881
0.882611	0.23084	0.882611	0.466603	0.882611	0.692933	0.882611	0.921024	0.882611	1.917891	0.653628	0.199538	0.653628	0.406953	0.653628	0.600401	0.653628	0.796485	0.653628	1.659199
0.875672	0.230088	0.875672	0.465175	0.875672	0.690709	0.875672	0.918028	0.875672	1.911676	0.646689	0.198489	0.646689	0.40495	0.646689	0.597303	0.646689	0.792318	0.646689	1.650517
0.868733	0.229303	0.868733	0.463684	0.868733	0.688386	0.868733	0.914897	0.868733	1.905188	0.63975	0.197439	0.63975	0.402948	0.63975	0.594205	0.63975	0.788152	0.63975	1.641835
0.861794	0.228492	0.861794	0.462144	0.861794	0.685984	0.861794	0.911659	0.861794	1.898484	0.632811	0.196241	0.632811	0.400618	0.632811	0.590603	0.632811	0.783311	0.632811	1.631757
0.854855	0.227669	0.854855	0.460576	0.854855	0.683547	0.854855	0.908375	0.854855	1.891685	0.625872	0.194978	0.625872	0.39815	0.625872	0.586786	0.625872	0.778182	0.625872	1.621083
0.847916	0.226842	0.847916	0.459004	0.847916	0.681103	0.847916	0.905084	0.847916	1.88487	0.618934	0.193716	0.618934	0.395681	0.618934	0.58297	0.618934	0.773053	0.618934	1.610409
0.840978	0.226016	0.840978	0.457432	0.840978	0.678659	0.840978	0.901792	0.840978	1.878053	0.611995	0.192454	0.611995	0.393212	0.611995	0.579154	0.611995	0.767924	0.611995	1.599737
0.834039	0.22519	0.834039	0.455859	0.834039	0.676216	0.834039	0.898501	0.834039	1.871238	0.605056	0.191191	0.605056	0.390744	0.605056	0.575338	0.605056	0.762796	0.605056	1.589064
0.8271	0.224364	0.8271	0.454287	0.8271	0.673772	0.8271	0.895208	0.8271	1.864422	0.598117	0.189929	0.598117	0.388275	0.598117	0.571522	0.598117	0.757668	0.598117	1.578393
0.820161	0.223538	0.820161	0.452714	0.820161	0.671326	0.820161	0.891914	0.820161	1.857605	0.591178	0.188667	0.591178	0.385807	0.591178	0.567706	0.591178	0.75254	0.591178	1.567722
0.813222	0.222712	0.813222	0.451141	0.813222	0.66888	0.813222	0.888619	0.813222	1.850787	0.584239	0.187438	0.584239	0.383415	0.584239	0.564015	0.584239	0.747581	0.584239	1.557419
0.806283	0.221886	0.806283	0.449569	0.806283	0.666435	0.806283	0.885324	0.806283	1.84397	0.5773	0.186232	0.5773	0.381078	0.5773	0.560414	0.5773	0.742746	0.5773	1.547384
0.799344	0.221061	0.799344	0.447996	0.799344	0.663989	0.799344	0.882029	0.799344	1.837153	0.570361	0.185027	0.570361	0.378741	0.570361	0.556813	0.570361	0.737912	0.570361	1.537348
0.792405	0.220235	0.792405	0.446423	0.792405	0.661543	0.792405	0.878735	0.792405	1.830336	0.563423	0.183821	0.563423	0.376405	0.563423	0.553213	0.563423	0.733077	0.563423	1.527314

0.556484	0.182331	0.556484	0.373501	0.556484	0.548768	0.556484	0.727118	0.556484	1.514718	0.327501	0.120198	0.327501	0.250825	0.327501	0.363491	0.327501	0.479397	0.327501	0.995189
0.549545	0.180793	0.549545	0.370505	0.549545	0.544186	0.549545	0.720979	0.549545	1.501716	0.320562	0.11781	0.320562	0.245933	0.320562	0.356209	0.320562	0.469676	0.320562	0.97419
0.542606	0.179256	0.542606	0.367509	0.542606	0.539604	0.542606	0.714839	0.542606	1.488714	0.313623	0.115495	0.313623	0.241125	0.313623	0.34903	0.313623	0.460076	0.313623	0.953094
0.535667	0.177733	0.535667	0.364573	0.535667	0.535122	0.535667	0.708837	0.535667	1.476098	0.306684	0.113179	0.306684	0.236318	0.306684	0.341851	0.306684	0.450477	0.306684	0.931999
0.528728	0.176213	0.528728	0.361649	0.528728	0.53066	0.528728	0.702863	0.528728	1.463556	0.299745	0.110849	0.299745	0.231491	0.299745	0.334646	0.299745	0.440848	0.299745	0.910922
0.521789	0.174693	0.521789	0.358725	0.521789	0.526198	0.521789	0.696888	0.521789	1.451016	0.292807	0.108395	0.292807	0.2265	0.292807	0.327218	0.292807	0.430947	0.292807	0.890006
0.51485	0.173173	0.51485	0.355802	0.51485	0.521736	0.51485	0.690914	0.51485	1.438475	0.285868	0.105942	0.285868	0.221508	0.285868	0.319789	0.285868	0.421048	0.285868	0.869091
0.507912	0.171653	0.507912	0.352878	0.507912	0.517274	0.507912	0.68494	0.507912	1.425934	0.278929	0.102272	0.278929	0.213733	0.278929	0.308219	0.278929	0.405526	0.278929	0.836035
0.500973	0.170133	0.500973	0.349954	0.500973	0.512812	0.500973	0.678966	0.500973	1.413394	0.27199	0.098628	0.27199	0.206056	0.27199	0.296805	0.27199	0.390229	0.27199	0.804064
0.494034	0.168614	0.494034	0.347031	0.494034	0.50835	0.494034	0.672991	0.494034	1.400854	0.265051	0.095157	0.265051	0.198902	0.265051	0.286311	0.265051	0.376275	0.265051	0.775058
0.487095	0.167094	0.487095	0.344107	0.487095	0.503888	0.487095	0.667017	0.487095	1.388314	0.258112	0.09172	0.258112	0.191857	0.258112	0.276035	0.258112	0.362652	0.258112	0.746551
0.480156	0.165371	0.480156	0.34073	0.480156	0.498761	0.480156	0.660151	0.480156	1.373729	0.251173	0.088352	0.251173	0.184953	0.251173	0.265913	0.251173	0.34923	0.251173	0.719062
0.473217	0.163623	0.473217	0.337295	0.473217	0.49355	0.473217	0.65317	0.473217	1.358883	0.244234	0.084694	0.244234	0.177487	0.244234	0.255153	0.244234	0.335095	0.244234	0.689154
0.466278	0.161875	0.466278	0.33386	0.466278	0.48834	0.466278	0.64619	0.466278	1.344038	0.237296	0.081097	0.237296	0.169964	0.237296	0.244225	0.237296	0.320677	0.237296	0.65912
0.459339	0.160127	0.459339	0.330425	0.459339	0.483129	0.459339	0.63921	0.459339	1.329194	0.230357	0.077501	0.230357	0.162441	0.230357	0.2333	0.230357	0.306263	0.230357	0.629092
0.452401	0.15838	0.452401	0.326991	0.452401	0.47792	0.452401	0.632231	0.452401	1.314351	0.223418	0.074029	0.223418	0.155193	0.223418	0.22275	0.223418	0.292312	0.223418	0.600069
0.445462	0.156632	0.445462	0.323557	0.445462	0.47271	0.445462	0.625252	0.445462	1.299508	0.216479	0.070467	0.216479	0.147772	0.216479	0.21198	0.216479	0.278095	0.216479	0.570567
0.438523	0.154845	0.438523	0.320065	0.438523	0.467408	0.438523	0.618163	0.438523	1.284636	0.20954	0.066289	0.20954	0.139071	0.20954	0.199502	0.20954	0.261797	0.20954	0.536793
0.431584	0.153073	0.431584	0.316584	0.431584	0.462109	0.431584	0.611089	0.431584	1.269978	0.202601	0.062111	0.202601	0.130371	0.202601	0.187024	0.202601	0.245499	0.202601	0.503021
0.424645	0.151301	0.424645	0.313103	0.424645	0.456811	0.424645	0.604015	0.424645	1.255321	0.195662	0.05793	0.195662	0.121659	0.195662	0.174516	0.195662	0.22915	0.195662	0.469084
0.417706	0.149373	0.417706	0.309281	0.417706	0.451023	0.417706	0.596276	0.417706	1.239137	0.188723	0.053495	0.188723	0.112474	0.188723	0.161395	0.188723	0.21201	0.188723	0.433916
0.410767	0.14731	0.410767	0.305167	0.410767	0.444814	0.410767	0.587966	0.410767	1.22164	0.181785	0.049012	0.181785	0.103228	0.181785	0.148205	0.181785	0.194775	0.181785	0.398799
0.403829	0.145247	0.403829	0.301054	0.403829	0.438606	0.403829	0.579656	0.403829	1.204144	0.174846	0.044529	0.174846	0.093982	0.174846	0.135017	0.174846	0.177542	0.174846	0.363683
0.39689	0.143185	0.39689	0.29694	0.39689	0.432397	0.39689	0.571346	0.39689	1.186649	0.167907	0.039904	0.167907	0.084435	0.167907	0.121429	0.167907	0.159827	0.167907	0.327625
0.389951	0.141108	0.389951	0.292813	0.389951	0.426177	0.389951	0.563023	0.389951	1.169166	0.160968	0.034668	0.160968	0.073603	0.160968	0.106135	0.160968	0.140031	0.160968	0.287701
0.383012	0.138985	0.383012	0.288645	0.383012	0.419925	0.383012	0.554672	0.383012	1.151792	0.154029	0.028894	0.154029	0.061681	0.154029	0.089416	0.154029	0.11847	0.154029	0.244924
0.376073	0.136962	0.376073	0.284637	0.376073	0.413893	0.376073	0.546621	0.376073	1.135218	0.14709	0.023133	0.14709	0.049751	0.14709	0.072662	0.14709	0.096837	0.14709	0.201921
0.369134	0.134911	0.369134	0.28058	0.369134	0.407783	0.369134	0.538471	0.369134	1.118436	0.140151	0.017668	0.140151	0.038255	0.140151	0.056307	0.140151	0.075487	0.140151	0.158756
0.362195	0.132499	0.362195	0.275664	0.362195	0.400435	0.362195	0.528655	0.362195	1.097903	0.133212	0.012886	0.133212	0.028116	0.133212	0.041915	0.133212	0.05666	0.133212	0.119401
0.355256	0.130067	0.355256	0.270693	0.355256	0.393015	0.355256	0.518746	0.355256	1.077108	0.126274	0.008028	0.126274	0.017706	0.126274	0.027135	0.126274	0.037287	0.126274	0.078606
0.348318	0.127687	0.348318	0.265841	0.348318	0.385776	0.348318	0.509083	0.348318	1.056813	0.119335	0.002821	0.119335	0.006224	0.119335	0.009362	0.119335	0.012803	0.119335	0.026707
0.341379	0.125206	0.341379	0.260855	0.341379	0.378372	0.341379	0.499218	0.341379	1.036303	0.112396	0	0.112396	0	0.112396	0	0.112396	0	0.112396	0
0.33444	0.122702	0.33444	0.25584	0.33444	0.370931	0.33444	0.489307	0.33444	1.015746	0.105457	0.00E+00	0.105457	0.00E+00	0.105457	0.00E+00	0.105457	0.00E+00	0.105457	0.00E+00

undef	undef	undef	undef	undef	undef	undef	undef	undef	undef	-0.28312	0.049939	-0.28312	0.051025	-0.28312	0.089931	-0.28312	0.167328	-0.28312	0.354065
-0.06108	0.00E+00	-0.06108	0.00E+00	-0.06108	0.00E+00	-0.06108	0	-0.06108	0	-0.29006	0.050375	-0.29006	0.051798	-0.29006	0.091982	-0.29006	0.171548	-0.29006	0.35688
-0.06802	0	-0.06802	0	-0.06802	0	-0.06802	0	-0.06802	0	-0.297	0.050569	-0.297	0.052333	-0.297	0.093792	-0.297	0.175751	-0.297	0.359076
-0.07495	5.65E-06	-0.07495	3.47E-06	-0.07495	3.16E-06	-0.07495	3.12E-05	-0.07495	2.36E-04	-0.30394	0.050979	-0.30394	0.053042	-0.30394	0.095759	-0.30394	0.179729	-0.30394	0.361139
-0.08189	0	-0.08189	0	-0.08189	0	-0.08189	0	-0.08189	0	-0.31088	0.051144	-0.31088	0.053558	-0.31088	0.097591	-0.31088	0.183615	-0.31088	0.362536
-0.08883	8.58E-04	-0.08883	5.48E-04	-0.08883	8.51E-04	-0.08883	0.001801	-0.08883	0.010276	-0.31781	0.051283	-0.31781	0.054056	-0.31781	0.09941	-0.31781	0.187441	-0.31781	0.363667
-0.09577	0.003409	-0.09577	0.003464	-0.09577	0.005009	-0.09577	0.008381	-0.09577	0.033795	-0.32475	0.051509	-0.32475	0.054629	-0.32475	0.101286	-0.32475	0.191128	-0.32475	0.364424
-0.10271	0.007296	-0.10271	0.006788	-0.10271	0.009794	-0.10271	0.015656	-0.10271	0.061861	-0.33169	0.051682	-0.33169	0.05516	-0.33169	0.103156	-0.33169	0.194816	-0.33169	0.365219
-0.10965	0.011595	-0.10965	0.010044	-0.10965	0.014685	-0.10965	0.023151	-0.10965	0.091468	-0.33863	0.051529	-0.33863	0.055442	-0.33863	0.104987	-0.33863	0.198503	-0.33863	0.366008
-0.11659	0.015417	-0.11659	0.012839	-0.11659	0.019103	-0.11659	0.030002	-0.11659	0.118669	-0.34557	0.051405	-0.34557	0.055747	-0.34557	0.106825	-0.34557	0.202126	-0.34557	0.366467
-0.12353	0.01907	-0.12353	0.015552	-0.12353	0.023548	-0.12353	0.036952	-0.12353	0.14572	-0.35251	0.051349	-0.35251	0.056105	-0.35251	0.108681	-0.35251	0.205591	-0.35251	0.366129
-0.13046	0.022223	-0.13046	0.018029	-0.13046	0.027741	-0.13046	0.043613	-0.13046	0.170124	-0.35945	0.051294	-0.35945	0.056463	-0.35945	0.110536	-0.35945	0.209056	-0.35945	0.365836
-0.1374	0.024616	-0.1374	0.020009	-0.1374	0.031145	-0.1374	0.049121	-0.1374	0.189126	-0.36639	0.051074	-0.36639	0.05666	-0.36639	0.112187	-0.36639	0.21202	-0.36639	0.364572
-0.14434	0.027254	-0.14434	0.022407	-0.14434	0.035279	-0.14434	0.056068	-0.14434	0.209767	-0.37333	0.050847	-0.37333	0.056848	-0.37333	0.113827	-0.37333	0.21496	-0.37333	0.363285
-0.15128	0.029727	-0.15128	0.024758	-0.15128	0.039342	-0.15128	0.063081	-0.15128	0.228702	-0.38026	0.050632	-0.38026	0.057038	-0.38026	0.115435	-0.38026	0.21781	-0.38026	0.361366
-0.15822	0.031677	-0.15822	0.026784	-0.15822	0.042855	-0.15822	0.069535	-0.15822	0.241991	-0.3872	0.050423	-0.3872	0.057229	-0.3872	0.117028	-0.3872	0.220618	-0.3872	0.359174
-0.16516	0.033448	-0.16516	0.028707	-0.16516	0.046189	-0.16516	0.075791	-0.16516	0.253574	-0.39414	0.050005	-0.39414	0.057186	-0.39414	0.118153	-0.39414	0.222141	-0.39414	0.356518
-0.1721	0.035083	-0.1721	0.030533	-0.1721	0.049318	-0.1721	0.081782	-0.1721	0.263719	-0.40108	0.049523	-0.40108	0.057069	-0.40108	0.119162	-0.40108	0.22341	-0.40108	0.353496
-0.17904	0.036637	-0.17904	0.032398	-0.17904	0.052496	-0.17904	0.088186	-0.17904	0.272734	-0.40802	0.049052	-0.40802	0.056962	-0.40802	0.120216	-0.40802	0.224869	-0.40802	0.35036
-0.18598	0.038071	-0.18598	0.034143	-0.18598	0.055478	-0.18598	0.094239	-0.18598	0.28148	-0.41496	0.048581	-0.41496	0.056855	-0.41496	0.121271	-0.41496	0.226327	-0.41496	0.347318
-0.19291	0.039223	-0.19291	0.035595	-0.19291	0.057994	-0.19291	0.099478	-0.19291	0.288248	-0.4219	0.048111	-0.4219	0.056749	-0.4219	0.122326	-0.4219	0.227786	-0.4219	0.344374
-0.19985	0.040337	-0.19985	0.037034	-0.19985	0.060497	-0.19985	0.104743	-0.19985	0.29469	-0.42884	0.0475	-0.42884	0.056528	-0.42884	0.123211	-0.42884	0.228904	-0.42884	0.340971
-0.20679	0.041451	-0.20679	0.03847	-0.20679	0.062995	-0.20679	0.109998	-0.20679	0.301477	-0.43578	0.046617	-0.43578	0.056085	-0.43578	0.123767	-0.43578	0.229368	-0.43578	0.336578
-0.21373	0.042683	-0.21373	0.040078	-0.21373	0.06595	-0.21373	0.116121	-0.21373	0.309355	-0.44271	0.045735	-0.44271	0.055642	-0.44271	0.124324	-0.44271	0.229847	-0.44271	0.33228
-0.22067	0.043878	-0.22067	0.041646	-0.22067	0.068844	-0.22067	0.122138	-0.22067	0.317171	-0.44965	0.044832	-0.44965	0.055181	-0.44965	0.124938	-0.44965	0.230571	-0.44965	0.328068
-0.22761	0.044882	-0.22761	0.043007	-0.22761	0.071423	-0.22761	0.127632	-0.22761	0.32274	-0.45659	0.043899	-0.45659	0.054696	-0.45659	0.125632	-0.45659	0.231627	-0.45659	0.323894
-0.23455	0.045709	-0.23455	0.044227	-0.23455	0.073957	-0.23455	0.133041	-0.23455	0.327363	-0.46353	0.042664	-0.46353	0.053867	-0.46353	0.1256	-0.46353	0.231369	-0.46353	0.319881
-0.24149	0.0465	-0.24149	0.045419	-0.24149	0.076482	-0.24149	0.138434	-0.24149	0.33182	-0.47047	0.041199	-0.47047	0.05278	-0.47047	0.125019	-0.47047	0.230126	-0.47047	0.316084
-0.24843	0.047319	-0.24843	0.046608	-0.24843	0.078979	-0.24843	0.143674	-0.24843	0.336513	-0.47741	0.039735	-0.47741	0.051694	-0.47741	0.124441	-0.47741	0.228902	-0.47741	0.312445
-0.25536	0.048067	-0.25536	0.047689	-0.25536	0.081354	-0.25536	0.148647	-0.25536	0.340913	-0.48435	0.038273	-0.48435	0.050608	-0.48435	0.123865	-0.48435	0.227696	-0.48435	0.308968
-0.2623	0.048672	-0.2623	0.048645	-0.2623	0.083638	-0.2623	0.153608	-0.2623	0.344535	-0.49129	0.036813	-0.49129	0.049524	-0.49129	0.123291	-0.49129	0.226509	-0.49129	0.305659
-0.26924	0.049074	-0.26924	0.049426	-0.26924	0.085732	-0.26924	0.15832	-0.26924	0.347761	-0.49823	0.035355	-0.49823	0.048442	-0.49823	0.12272	-0.49823	0.225342	-0.49823	0.302524
-0.27618	0.049435	-0.27618	0.050172	-0.27618	0.087789	-0.27618	0.162984	-0.27618	0.350925	-0.50516	0.033918	-0.50516	0.047382	-0.50516	0.122198	-0.50516	0.224248	-0.50516	0.299681

-0.5121	0.032516	-0.5121	0.046304	-0.5121	0.121567	-0.5121	0.222831	-0.5121	0.296623
-0.51904	0.031461	-0.51904	0.04529	-0.51904	0.119673	-0.51904	0.218246	-0.51904	0.290703
-0.52598	0.030438	-0.52598	0.044311	-0.52598	0.117855	-0.52598	0.213737	-0.52598	0.284614
-0.53292	0.029416	-0.53292	0.043332	-0.53292	0.116037	-0.53292	0.209236	-0.53292	0.278541
-0.53986	0.028394	-0.53986	0.042353	-0.53986	0.114222	-0.53986	0.204743	-0.53986	0.272485
-0.5468	0.027373	-0.5468	0.041374	-0.5468	0.112407	-0.5468	0.200258	-0.5468	0.266446
-0.55374	0.026352	-0.55374	0.040395	-0.55374	0.110595	-0.55374	0.195782	-0.55374	0.260427
-0.56068	0.025332	-0.56068	0.039417	-0.56068	0.108784	-0.56068	0.191316	-0.56068	0.254428
-0.56761	0.024312	-0.56761	0.038439	-0.56761	0.106975	-0.56761	0.186861	-0.56761	0.248451
-0.57455	0.023293	-0.57455	0.037461	-0.57455	0.105168	-0.57455	0.182416	-0.57455	0.242498
-0.58149	0.022045	-0.58149	0.036141	-0.58149	0.102447	-0.58149	0.176543	-0.58149	0.236344
-0.58843	0.020724	-0.58843	0.034712	-0.58843	0.099438	-0.58843	0.170224	-0.58843	0.230324
-0.59537	0.01933	-0.59537	0.033011	-0.59537	0.095617	-0.59537	0.163173	-0.59537	0.22477
-0.60231	0.01791	-0.60231	0.03121	-0.60231	0.091503	-0.60231	0.155855	-0.60231	0.219467
-0.60925	0.01649	-0.60925	0.029411	-0.60925	0.087398	-0.60925	0.14854	-0.60925	0.214332
-0.61619	0.015172	-0.61619	0.027655	-0.61619	0.082912	-0.61619	0.140904	-0.61619	0.209458
-0.62313	0.013863	-0.62313	0.025904	-0.62313	0.078409	-0.62313	0.133302	-0.62313	0.204836
-0.63006	0.012554	-0.63006	0.024156	-0.63006	0.073928	-0.63006	0.125777	-0.63006	0.200479
-0.637	0.011245	-0.637	0.022411	-0.637	0.069471	-0.637	0.118342	-0.637	0.196404
-0.64394	0.010014	-0.64394	0.020687	-0.64394	0.064821	-0.64394	0.110476	-0.64394	0.19251
-0.65088	0.008892	-0.65088	0.018987	-0.65088	0.059932	-0.65088	0.102031	-0.65088	0.188845
-0.65782	0.007792	-0.65782	0.017288	-0.65782	0.055093	-0.65782	0.093691	-0.65782	0.185603
-0.66476	0.006726	-0.66476	0.015592	-0.66476	0.050319	-0.66476	0.085484	-0.66476	0.182808
-0.6717	0.005713	-0.6717	0.013936	-0.6717	0.04559	-0.6717	0.077306	-0.6717	0.18085
-0.67864	0.004841	-0.67864	0.012405	-0.67864	0.040923	-0.67864	0.069357	-0.67864	0.173636
-0.68557	0.004235	-0.68557	0.010947	-0.68557	0.036612	-0.68557	0.062606	-0.68557	0.148968
-0.69251	0.003675	-0.69251	0.009518	-0.69251	0.032129	-0.69251	0.055413	-0.69251	0.12695

Appendix F. Data points of impulse response

On all PID controllers, data points were exported directly from simulation result to data analysis software.

Table F-15. Values of time domain rolling moment on M2-C during downwash.

Time(s)	cl	Time(s)	cl	Time(s)	cl	Time(s)	cl	Time(s)	cl
IFFT of cl	0.3 m/s	IFFT of cl	0.6 m/s	IFFT of cl	0.9 m/s	IFFT of cl	1.2 m/s	IFFT of cl	2.5 m/s
1	7.91E-06	1	-4.92E-05	1	-8.03E-05	1	-1.49E-04	1	-5.37E-04
2	7.41E-06	2	-6.21E-05	2	-9.73E-05	2	-1.77E-04	2	-7.64E-04
3	7.15E-06	3	-6.32E-05	3	-1.08E-04	3	-2.27E-04	3	-4.12E-04
4	6.60E-06	4	-3.46E-05	4	-1.02E-04	4	-1.50E-04	4	-4.84E-04
5	6.56E-06	5	-5.79E-05	5	-9.95E-05	5	-1.45E-04	5	-5.79E-04
6	6.72E-06	6	-5.53E-05	6	-9.20E-05	6	-1.65E-04	6	-6.13E-04
7	6.73E-06	7	-5.44E-05	7	-8.66E-05	7	-1.64E-04	7	-6.28E-04
8	6.50E-06	8	-5.30E-05	8	-8.56E-05	8	-1.64E-04	8	-6.01E-04
9	6.28E-06	9	-5.10E-05	9	-8.49E-05	9	-1.70E-04	9	-5.72E-04
10	6.37E-06	10	-5.02E-05	10	-8.45E-05	10	-1.55E-04	10	-5.48E-04
11	5.84E-06	11	-4.36E-05	11	-8.42E-05	11	-1.66E-04	11	-5.97E-04
12	5.18E-06	12	-4.67E-05	12	-8.75E-05	12	-1.55E-04	12	-6.81E-04
13	4.55E-06	13	-4.37E-05	13	-7.93E-05	13	-1.59E-04	13	-6.20E-04
14	3.93E-06	14	-4.34E-05	14	-7.86E-05	14	-1.57E-04	14	-5.94E-04
15	3.27E-06	15	-4.29E-05	15	-7.83E-05	15	-1.54E-04	15	-5.65E-04
16	2.68E-06	16	-4.26E-05	16	-7.74E-05	16	-1.48E-04	16	-5.23E-04
17	2.54E-06	17	-4.14E-05	17	-8.12E-05	17	-1.55E-04	17	-5.37E-04
18	2.42E-06	18	-4.11E-05	18	-8.05E-05	18	-1.57E-04	18	-5.61E-04
19	2.73E-06	19	-4.06E-05	19	-7.96E-05	19	-1.58E-04	19	-6.95E-04
20	2.98E-06	20	-4.07E-05	20	-7.95E-05	20	-1.57E-04	20	-6.83E-04
21	2.22E-06	21	-3.99E-05	21	-7.61E-05	21	-1.40E-04	21	-6.06E-04
22	1.28E-06	22	-3.93E-05	22	-7.61E-05	22	-1.46E-04	22	-6.16E-04
23	1.30E-09	23	-3.90E-05	23	-7.55E-05	23	-1.50E-04	23	-6.15E-04

24	-5.33E-07	24	-3.81E-05	24	-7.43E-05	24	-1.66E-04	24	-6.48E-04
25	-1.43E-06	25	-3.72E-05	25	-7.43E-05	25	-1.64E-04	25	-6.45E-04
26	-1.86E-06	26	-3.72E-05	26	-7.56E-05	26	-1.47E-04	26	-6.36E-04
27	-1.96E-06	27	-3.70E-05	27	-7.90E-05	27	-1.50E-04	27	-5.69E-04
28	-1.77E-06	28	-3.67E-05	28	-7.90E-05	28	-1.50E-04	28	-6.04E-04
29	-1.18E-06	29	-3.63E-05	29	-7.92E-05	29	-1.63E-04	29	-6.31E-04
30	-2.51E-07	30	-3.65E-05	30	-7.65E-05	30	-1.65E-04	30	-7.11E-04
31	-5.53E-07	31	-3.54E-05	31	-6.42E-05	31	-1.63E-04	31	-6.29E-04
32	-1.64E-06	32	-3.51E-05	32	-6.77E-05	32	-1.62E-04	32	-6.77E-04
33	-2.83E-06	33	-3.43E-05	33	-7.31E-05	33	-1.56E-04	33	-6.70E-04
34	-3.93E-06	34	-3.29E-05	34	-8.60E-05	34	-1.50E-04	34	-6.23E-04
35	-4.83E-06	35	-3.28E-05	35	-8.52E-05	35	-1.53E-04	35	-6.44E-04
36	-5.33E-06	36	-3.50E-05	36	-7.72E-05	36	-1.64E-04	36	-6.13E-04
37	-5.24E-06	37	-3.50E-05	37	-7.75E-05	37	-1.63E-04	37	-5.64E-04
38	-4.77E-06	38	-3.46E-05	38	-7.83E-05	38	-1.59E-04	38	-6.06E-04
39	-3.94E-06	39	-3.44E-05	39	-7.72E-05	39	-1.48E-04	39	-6.31E-04
40	-3.03E-06	40	-3.41E-05	40	-7.01E-05	40	-1.56E-04	40	-6.07E-04
41	-3.44E-06	41	-2.80E-05	41	-8.63E-05	41	-1.71E-04	41	-5.20E-04
42	-4.60E-06	42	-2.81E-05	42	-8.36E-05	42	-1.71E-04	42	-5.40E-04
43	-6.22E-06	43	-2.76E-05	43	-8.00E-05	43	-1.63E-04	43	-4.64E-04
44	-6.90E-06	44	-2.90E-05	44	-6.74E-05	44	-1.38E-04	44	-4.02E-04
45	-7.80E-06	45	-2.93E-05	45	-6.95E-05	45	-1.41E-04	45	-4.07E-04
46	-7.91E-06	46	-3.25E-05	46	-5.77E-05	46	-1.45E-04	46	-4.67E-04
47	-7.63E-06	47	-3.28E-05	47	-6.56E-05	47	-1.59E-04	47	-4.73E-04
48	-7.00E-06	48	-3.28E-05	48	-7.20E-05	48	-1.57E-04	48	-4.85E-04
49	-6.40E-06	49	-3.24E-05	49	-7.68E-05	49	-1.50E-04	49	-4.26E-04
50	-5.41E-06	50	-3.17E-05	50	-7.88E-05	50	-1.38E-04	50	-2.89E-04
51	-5.42E-06	51	-2.56E-05	51	-7.28E-05	51	-1.25E-04	51	-3.32E-04
52	-6.58E-06	52	-2.47E-05	52	-7.13E-05	52	-1.25E-04	52	-3.27E-04
53	-7.86E-06	53	-2.44E-05	53	-6.48E-05	53	-1.24E-04	53	-2.21E-04
54	-8.10E-06	54	-2.51E-05	54	-6.61E-05	54	-1.18E-04	54	-1.94E-04
55	-9.09E-06	55	-2.52E-05	55	-7.12E-05	55	-1.11E-04	55	-3.18E-04
56	-9.45E-06	56	-2.61E-05	56	-7.49E-05	56	-1.15E-04	56	-3.53E-04

57	-9.47E-06	57	-2.59E-05	57	-6.92E-05	57	-1.20E-04	57	-3.55E-04
58	-9.01E-06	58	-3.08E-05	58	-6.86E-05	58	-1.21E-04	58	-3.05E-04
59	-8.30E-06	59	-3.02E-05	59	-6.30E-05	59	-1.12E-04	59	-8.28E-05
60	-7.39E-06	60	-2.92E-05	60	-5.78E-05	60	-7.56E-05	60	1.18E-04
61	-7.47E-06	61	-2.57E-05	61	-5.03E-05	61	-1.16E-04	61	5.75E-05
62	-7.75E-06	62	-2.42E-05	62	-5.28E-05	62	-1.02E-04	62	-3.84E-05
63	-8.40E-06	63	-2.09E-05	63	-5.60E-05	63	-8.54E-05	63	-6.69E-05
64	-8.95E-06	64	-1.85E-05	64	-5.51E-05	64	-6.79E-05	64	-1.60E-04
65	-9.75E-06	65	-1.78E-05	65	-7.19E-05	65	-4.04E-05	65	2.35E-05
66	-9.82E-06	66	-1.96E-05	66	-6.77E-05	66	-5.14E-05	66	-9.31E-05
67	-9.68E-06	67	-2.04E-05	67	-6.22E-05	67	-6.84E-05	67	-8.27E-05
68	-9.09E-06	68	-2.12E-05	68	-5.20E-05	68	-6.12E-05	68	-7.83E-05
69	-8.30E-06	69	-2.12E-05	69	-4.25E-05	69	-4.23E-05	69	7.09E-06
70	-7.32E-06	70	-2.06E-05	70	-3.31E-05	70	-2.14E-05	70	8.36E-05
71	-7.55E-06	71	-1.89E-05	71	-5.14E-05	71	-3.75E-05	71	2.90E-04
72	-7.81E-06	72	-1.64E-05	72	-3.90E-05	72	-3.44E-05	72	4.33E-04
73	-9.06E-06	73	-1.55E-05	73	-2.91E-05	73	-2.74E-05	73	7.00E-05
74	-9.72E-06	74	-1.32E-05	74	-2.57E-05	74	-8.99E-06	74	4.60E-05
75	-1.07E-05	75	-1.14E-05	75	-2.83E-05	75	2.12E-05	75	1.33E-04
76	-1.04E-05	76	-1.27E-05	76	-3.36E-05	76	5.01E-05	76	1.35E-04
77	-9.85E-06	77	-1.62E-05	77	-3.25E-05	77	3.82E-05	77	2.61E-04
78	-8.84E-06	78	-2.05E-05	78	-2.63E-05	78	3.06E-05	78	3.45E-04
79	-7.58E-06	79	-2.14E-05	79	-1.39E-05	79	3.02E-05	79	4.94E-04
80	-6.47E-06	80	-2.08E-05	80	-4.07E-06	80	4.00E-05	80	5.74E-04
81	-6.33E-06	81	-1.12E-05	81	1.14E-05	81	4.57E-05	81	5.77E-04
82	-6.64E-06	82	-5.59E-06	82	1.85E-06	82	1.85E-05	82	6.47E-04
83	-7.29E-06	83	-2.31E-07	83	-7.60E-06	83	3.17E-05	83	6.27E-04
84	-7.65E-06	84	4.77E-06	84	-8.82E-06	84	6.38E-05	84	5.29E-04
85	-7.64E-06	85	5.92E-06	85	-1.19E-06	85	9.45E-05	85	4.39E-04
86	-8.12E-06	86	1.64E-06	86	-1.76E-05	86	1.23E-04	86	3.94E-04
87	-7.89E-06	87	-4.16E-06	87	-1.67E-05	87	1.10E-04	87	3.36E-04
88	-7.20E-06	88	-6.59E-06	88	-6.95E-06	88	1.03E-04	88	3.09E-04
89	-6.22E-06	89	-8.13E-06	89	6.21E-06	89	1.06E-04	89	3.21E-04

90	-5.19E-06	90	-7.54E-06	90	1.73E-05	90	1.22E-04	90	3.60E-04
91	-5.05E-06	91	6.17E-07	91	3.36E-05	91	1.28E-04	91	4.35E-04
92	-5.92E-06	92	-6.75E-07	92	4.55E-05	92	1.52E-04	92	4.67E-04
93	-6.30E-06	93	-1.95E-07	93	4.69E-05	93	1.53E-04	93	4.95E-04
94	-6.86E-06	94	5.59E-06	94	5.27E-05	94	1.55E-04	94	4.79E-04
95	-6.69E-06	95	7.14E-06	95	5.07E-05	95	1.54E-04	95	4.74E-04
96	-6.04E-06	96	6.57E-06	96	5.10E-05	96	1.45E-04	96	4.17E-04
97	-5.07E-06	97	5.88E-06	97	5.26E-05	97	1.61E-04	97	4.17E-04
98	-3.98E-06	98	4.62E-06	98	5.29E-05	98	1.70E-04	98	3.80E-04
99	-3.25E-06	99	4.91E-06	99	5.47E-05	99	1.69E-04	99	4.01E-04
100	-2.52E-06	100	4.73E-06	100	6.49E-05	100	1.84E-04	100	3.56E-04
101	-2.76E-06	101	9.05E-06	101	7.55E-05	101	2.02E-04	101	3.88E-04
102	-3.40E-06	102	1.45E-05	102	9.25E-05	102	2.03E-04	102	3.46E-04
103	-3.78E-06	103	1.38E-05	103	9.41E-05	103	1.90E-04	103	3.22E-04
104	-4.03E-06	104	1.31E-05	104	9.13E-05	104	1.96E-04	104	2.36E-04
105	-3.67E-06	105	1.37E-05	105	8.99E-05	105	2.02E-04	105	2.44E-04
106	-3.03E-06	106	1.61E-05	106	8.41E-05	106	2.04E-04	106	1.71E-04
107	-2.18E-06	107	1.80E-05	107	8.20E-05	107	2.05E-04	107	1.40E-04
108	-1.09E-06	108	2.26E-05	108	8.39E-05	108	2.09E-04	108	1.23E-04
109	-2.97E-07	109	2.46E-05	109	8.74E-05	109	2.12E-04	109	1.40E-04
110	4.51E-07	110	2.51E-05	110	9.32E-05	110	2.20E-04	110	1.28E-04
111	2.32E-07	111	2.47E-05	111	1.00E-04	111	2.22E-04	111	1.45E-04
112	6.68E-07	112	2.94E-05	112	1.06E-04	112	2.21E-04	112	5.44E-05
113	3.64E-07	113	3.04E-05	113	1.08E-04	113	2.17E-04	113	5.99E-05
114	5.39E-07	114	3.26E-05	114	1.11E-04	114	2.20E-04	114	-3.30E-05
115	1.16E-06	115	3.30E-05	115	1.13E-04	115	2.09E-04	115	-5.99E-05
116	1.92E-06	116	3.63E-05	116	1.15E-04	116	2.11E-04	116	-1.40E-04
117	2.77E-06	117	3.85E-05	117	1.21E-04	117	2.08E-04	117	-1.55E-04
118	3.62E-06	118	4.15E-05	118	1.21E-04	118	2.13E-04	118	-2.09E-04
119	4.40E-06	119	4.29E-05	119	1.22E-04	119	2.07E-04	119	-1.57E-04
120	4.92E-06	120	4.45E-05	120	1.24E-04	120	2.11E-04	120	-1.55E-04
121	4.86E-06	121	4.81E-05	121	1.24E-04	121	2.03E-04	121	-1.12E-04
122	5.27E-06	122	5.20E-05	122	1.22E-04	122	2.03E-04	122	-1.22E-04

123	4.93E-06	123	5.24E-05	123	1.21E-04	123	1.82E-04	123	-6.37E-05
124	5.39E-06	124	5.38E-05	124	1.17E-04	124	1.65E-04	124	-3.85E-05
125	5.98E-06	125	5.37E-05	125	1.16E-04	125	1.55E-04	125	5.27E-05
126	6.98E-06	126	5.48E-05	126	1.16E-04	126	1.45E-04	126	7.21E-05
127	7.86E-06	127	5.55E-05	127	1.17E-04	127	1.31E-04	127	1.51E-04
128	8.60E-06	128	5.67E-05	128	1.20E-04	128	1.32E-04	128	1.78E-04
129	9.22E-06	129	5.87E-05	129	1.23E-04	129	1.28E-04	129	2.38E-04
130	9.68E-06	130	6.01E-05	130	1.24E-04	130	1.28E-04	130	2.64E-04
131	1.00E-05	131	6.19E-05	131	1.23E-04	131	1.18E-04	131	3.57E-04
132	9.88E-06	132	6.48E-05	132	1.17E-04	132	1.06E-04	132	4.03E-04
133	9.63E-06	133	6.81E-05	133	1.13E-04	133	9.20E-05	133	5.37E-04
134	1.05E-05	134	7.12E-05	134	1.08E-04	134	7.88E-05	134	6.17E-04
135	1.16E-05	135	7.34E-05	135	1.03E-04	135	6.29E-05	135	7.30E-04
136	1.29E-05	136	7.38E-05	136	9.59E-05	136	5.86E-05	136	7.82E-04
137	1.41E-05	137	7.50E-05	137	9.39E-05	137	5.36E-05	137	8.71E-04
138	1.49E-05	138	7.57E-05	138	9.48E-05	138	5.75E-05	138	8.73E-04
139	1.54E-05	139	7.61E-05	139	9.62E-05	139	5.97E-05	139	9.37E-04
140	1.55E-05	140	7.69E-05	140	9.87E-05	140	6.49E-05	140	9.34E-04
141	1.56E-05	141	7.69E-05	141	9.48E-05	141	6.72E-05	141	9.75E-04
142	1.59E-05	142	7.89E-05	142	8.73E-05	142	6.69E-05	142	9.78E-04
143	1.65E-05	143	7.97E-05	143	8.13E-05	143	6.07E-05	143	0.001051
144	1.72E-05	144	8.08E-05	144	7.43E-05	144	5.12E-05	144	0.001056
145	1.82E-05	145	8.21E-05	145	6.55E-05	145	4.77E-05	145	0.001122
146	1.91E-05	146	8.39E-05	146	6.33E-05	146	5.50E-05	146	0.001071
147	2.02E-05	147	8.54E-05	147	6.59E-05	147	6.46E-05	147	0.001124
148	2.11E-05	148	8.69E-05	148	6.92E-05	148	7.77E-05	148	0.001104
149	2.17E-05	149	8.78E-05	149	7.23E-05	149	9.07E-05	149	0.001105
150	2.20E-05	150	8.91E-05	150	7.65E-05	150	1.04E-04	150	0.001058